SYNTHESIS OF MESOSTRUCTURED METAL SULFIDES USING TRANSITION METAL SALTS:PLURONIC LIQUID CRYSTALLINE MESOPHASES

A THESIS
SUBMITTED TO THE DEPARTMENT OF CHEMISTRY AND THE INSTITUTE OF ENGINEERING AND SCIENCES OF BİLKENT UNIVERSITY
IN PARTIAL FULFILLMENT OF THE REQUIREMENTS FOR THE DEGREE
OF
MASTER OF SCIENCE

by

YURDANUR TÜRKER

JULY 2007

I certify that I have read this thesis and in my opinion it is fully adequate, in scope and quality, as a thesis of the degree of Master of Science

_____

Prof. Dr. Ömer DAĞ

I certify that I have read this thesis and in my opinion it is fully adequate, in scope and quality, as a thesis of the degree of Master of Science

_____

Prof. Dr. Şefik SÜZER

I certify that I have read this thesis and in my opinion it is fully adequate, in scope and quality, as a thesis of the degree of Master of Science

_____

Assoc. Prof. Dr. Margarita KANTCHEVA

I certify that I have read this thesis and in my opinion it is fully adequate, in scope and quality, as a thesis of the degree of Master of Science

_____

Prof. Dr. Ahmet ORAL

I certify that I have read this thesis and in my opinion it is fully adequate, in scope and quality, as a thesis of the degree of Master of Science

_____

Assoc. Prof. Dr. Nihal AYDOĞAN

Approved for the Institute of Engineering and Sciences

_____

Prof. Dr. Mehmet BARAY

Director of Institute of Engineering and Sciences

ABSTRACT

SYNTHESIS OF MESOSTRUCTURED METAL SULFIDES USING TRANSITION METAL SALTS:PLURONIC LIQUID CRYSTALLINE MESOPHASES

YURDANUR TÜRKER

M.S. in Chemistry
Supervisor: Prof. Dr. Ömer DAĞ
July 2007

The Liquid Crystalline Templating (LCT) approach has been extensively used to produce mesostructured Metal Sulfides (MS) powders by using nonionic surfactants (C_nEO_m). The aim in this work is to synthesize larger pore size mesostructured MS at high salt concentrations by mixing Pluronics ($PEO_xPPO_yPEO_x$, EO = $-OCH_2CH_2-$, PO = $-OCH(CH_3)CH_2-$) with transition metal salts (TMS) $[M(H_2O)_4](NO_3)_2$ in a dilute media. This enables to synthesize thin films of mesostructured MS. In this thesis, the MS (M= Cd, Zn, $Cd_{1-x}Zn_x$, $Cd_{1-x}Co_x$ and $Cd_{1-x}Mn_x$) were synthesized by the LCT approach using Pluronic P85 ($(PEO)_{26}(PPO)_{40}(PEO)_{26}$) and TMS. The P85 and salts can be dissolved in various solvents to obtain clear solution that enables one to increase the salt to pluronic mole ratio up to 30:1. However, the LC mesophases form in the

$[Cd(H_2O)_4](NO_3)_2$:P85 mole ratio range of 3:1 to 11:1 with a 3D hexagonal structure and *P6₃/mmc* space group having unit cell parameters of ***a*** = 99.5 Å and ***c*** = 162.5 Å with a ***c/a*** ratio of 1.633.

The CdS thin film samples, obtained by exposing the $[Cd(H_2O)_4](NO_3)_2$:P85 LC phase to H_2S gas, could retain the mesostructure of the LC mesophase in the mole ratio range of 3:1 to 11:1. The film samples that consist of 50-100 nm mesostructured CdS and free surfactant molecules are uniform and soft in early stages of the H_2S reaction. However, in time, the free surfactant molecules diffuse out of the mesostructured CdS and form dendritic structures, producing CdS thin films with huge domains. The CdS thin film samples consist of 4.3 nm CdS nanoparticles that emit orange light under UV irradiation. Well homogenized LC mesophases produce cracked well structured film samples upon H_2S reaction.

This method can be used to fine tune both the composition (between x=0.0 and 1.0) and the optical band-gap of $Cd_{1-x}Zn_xS$ nanocrystallites between 2.60 eV and 4.00 eV. The Zn(II) and Cd(II) ions are homogenously doped throughout the mesostructure and nanocrystallites synthesized by this approach are slightly larger in every composition compared to the ones synthesized in the mesostructured silica channels. Also both Co(II) and Mn(II) ions could be incorporated into the CdS lattice with $x \leq 0.15$ for stable $Cd_{1-x}Co_xS$ and $Cd_{1-x}Mn_xS$ film samples, respectively. The Co(II) ions occupy the isolated tetrahedral holes in the CdS lattice until x = 0.15 for stable samples.

In this thesis, the structure and structural changes in the LC mesophase during the synthesis of MS and particle size analysis of the nanocrystallites were investigated using diffraction (XRD), spectroscopy (FT-IR, micro-Raman and UV-Vis absorption) and microscopy (OM and SEM) techniques.

Keywords: Liquid Crystal Templating, Pluronics, Transition Metal Complexes, Mesostructured Metal Sulfides, Doping CdS, Mesostructured Thin Films, Nanocrystallites.

ÖZET

GEÇİŞ METAL TUZLARI:PLURONİK SIVI KRİSTAL MEZOFAZLARI KULLANARAK MEZOYAPILI METAL SÜLFÜRLERİN SENTEZLENMESİ

YURDANUR TÜRKER

Kimya Bölümü Yüksek Lisans Tezi

Tez Yöneticisi: Prof. Dr. Ömer Dağ

Temmuz 2007

Sıvı Kristal Kalıplama (SKK) yaklaşımı iyonik olmayan yüzey aktifler (C_nEO_m) kullanılarak mezoyapılı Metal Sülfür (MS) tozları üretmek için kullanılmıştır. Bu çalışmadaki amaç pluronikleri ($PEO_xPPO_yPEO_x$, EO = $-OCH_2CH_2-$, PO = $-OCH(CH_3)CH_2-$) geçiş metal tuzlarıyla $[M(H_2O)_4](NO_3)_2$ (GMT) seyreltik ortamda karıştırarak daha geniş gözenekli mezoyapılı metal sülfürler sentezlemektir. Bu mezoyapılı metal sülfürlerin ince filmlerinin sentezlenmesini sağlar. Bu tezde, Pluronik P85 ($(PEO)_{26}(PPO)_{40}(PEO)_{26}$) ve GMT, kullanılarak SKK yaklaşımıyla MS ler (M = Cd, Zn, $Cd_{1-x}Zn_x$, $Cd_{1-x}Co_x$ ve $Cd_{1-x}Mn_x$) sentezlenmiştir. P85 ve tuzlar, tuz pluronik mol oranının 30:1 e kadar yükselmesini sağlayan farklı çözeltilerde çözülerek homojen çözeltileri elde edilebilir. SK mezofazları 3:1 ile 11:1 $[Cd(H_2O)_4](NO_3)_2$:P85 mol oranı aralığında 3B hekzagonal yapıda ve *P6₃/mmc* grubu ile olup, birim hücre parametreleri ***a*** = 99,5 Å ve ***c*** = 162,5 Å ve ***c/a*** = 1,633.

$[Cd(H_2O)_4](NO_3)_2$:P85 SK fazın H_2S ile tepkimesi sonucu elde edilen CdS ince film numuneleri, 3:1 ile 11:1 mol oranı aralığında SK fazının mezoyapısını koruyabilmektedir. 50-100 nm mezoyapılı CdS ve fazlalık yüzeyaktif molekülleri içeren film numuneleri, H_2S tepkimesinin erken dönemlerinde düzenli ve yumuşaktır. Fakat, zaman içerisinde, fazla olan yüzey aktif molekülleri mezoyapılı CdS den dışarı çıkarak dendritik yapılar oluşturup CdS ince filmlerini büyük parçalar halinde üretirler. CdS ince film numuneleri UV altında turuncu ışık yayan 4,3 nm büyüklüğünde CdS nanokristalleri içermektedir. İyi homojenize olmuş SK mezofazları H_2S tepkimesi üzerine çatlak düzenli yapıda film numuneleri üretmektedirler.

Ayrıca bu yöntemin, $Cd_{1-x}Zn_xS$ nanokristallerinin kompozisyonunu (x = 0,0 ve 1,0 arasında) ve optik bant aralığının 2,60 eV ve 4,00 eV arasında ayarlanmasında kullanılabildiğini gösterildi ve Zn(II) ve Cd(II) iyonları mezoyapı boyunca homojen olarak katkılandırıldı. Bu yaklaşımla sentezlenen nanokristaller her bir kompozisyonda, mezoyapılı silika kanalları içerisinde sentezlenenlerden biraz daha büyüktürler. Ayrıca, Co(II) ve Mn(II) iyonlarının, sırasıyla kararlı $Cd_{1-x}Co_xS$ ve $Cd_{1-x}Mn_xS$ numuneleri için CdS örgüsüne x = 0,0 ve 0,15 arasında katkılandırılmasında kullanılabileceğini tespit ettik. Co(II) iyonları kararlı numuneler için x = 0,15 e kadar, CdS örgüsünde izole edilmiş tetrahedral boşluklara yerleşmektedirler.

Bu tezde, MS`lerin yapısı ve sentezi esnasında SK mezofazda gerçekleşen yapısal değişiklikler ve parçacık boyut analizi difraksiyon (XRD), spektroskopi (FT-IR, mikro-Raman ve UV-Vis emilimi) ve mikroskop (OM ve SEM) teknikleri kullanılarak incelenmiştir.

Anahtar Kelimeler: Sıvı Kristal Kalıplama, Pluronikler, Geçiş Metal Kompleksleri, Mezoyapılı Metal Sülfürler, CdS Katkılandırılması, Mezoyapılı İnce Filmler, Nanokristaller.

ACKNOWLEDGEMENT

I would like to extend my gratitude to;

... Prof. Dr. Ömer DAĞ for his encouragement and supervision throughout my studies…

…my family and Cenk, for their continuous support and help…

... my group members Cemal Albayrak, Altuğ Poyraz and Halil Okur for their helps in the laboratory…

... Past and present members of Chemistry Department; where I learned a lot and made great friends during last 6 years...

…the Scientific and Technical Research Council of Turkey (TÜBİTAK) for the financial support in the framework of the project 105T224 and the National Scholarship for Master of Science…

TABLE OF CONTENTS

LIST OF TABLES

LIST OF FIGURES

INTRODUCTION

1.1. Mesoporous Inorganic Materials

Porous inorganic solids find wide application in technology such as heterogeneous catalysis, adsorption and molecular separation [1-5] due to their microstructures. This enables them to obtain high surface area materials compared to many inorganic solids. Over the last three decades, there has been a great attention on the synthesis of porous materials to tailor the pore size and shape, characterization and applications of porous inorganic materials. According to IUPAC definition [6] inorganic solids with pore diameters in the range of 20 to 500 Å are called *mesoporous materials*. Some examples of mesoporous materials such as aerogels, pillared layered clays and M41S type silica are given in Table 1.1. [7]

Table 1.1 Nomenclature of Porous Inorganic Materials according to their pore sizes.

Pore Size	Definition	Example	Actual size range
Macroporous	> 500 Å	Glasses	> 500 Å
Mesoporous	20-500 Å	Aerogels	> 100 Å
		Pillared layered clays	10 Å, 100 Å
		M41S	16-100 Å
Microporous	< 20 Å	Zeolites, zeotypes	< 14.2 Å
		Activated carbon	6 Å

Since the discovery of aluminophosphate molecular sieves by Flanigen et. al. [8-9], there have been various numbers of explorations of the many transition- and main- group elements for novel *microporous* materials because of their industrial applications in the fields of catalysis, ionic exchange, molecular sieves, gas separation, etc. This class of solids was initially categorized as zeolites (aluminosilicates), however in the last decades, a new series of porous crystalline materials, including phosphates, sulfides, borates, and nitrides, were discovered.[10] For example, in the field of microporous membranes, Gavalas`s group prepared a microporous silica membrane within the pores of Vycor tubes by silane oxidation.[11-12] However, instead of microporous membranes, the mesoporous membranes with more uniform pores are preferred for high-performance applications. The conventional membranes such as SiO_2 and TiO_2 synthesized by the sol-gel method have wide pore size distributions. [13]

There have been a vast number of reports demonstrating the synthesis of ordered porous materials with pore sizes beyond 30 nm (*macroporous*) using colloidal templates, for example, polystyrene latex spheres in a colloidal solution,[14-15] and oil droplets in an oil-in-water emulsion,[16] polymer gels,[17] vesicles,[18] foams,[19] and bacteria[20] as templates. However, the macroporous materials have low surface area. In order to be used effectively in a variety of applications such as catalytic supports, optics, electronics, adsorbents, slow drug delivery, electrode materials, introduction of porosity on two or three different length scales in an ordered fashion with interconnectivity between the pores and with high surface area would be more convenient.

On the other hand, frameworks of mesoporous molecular sieves accommodate internal channels and cavities[21] which supply extremely high surface areas (> 1000 m^2g^{-1}) and an advantage of precise tuning of pore sizes. For that reason, the internal channels and cavities of mesoporous materials enable to serve as "nanosized *chemical laboratories*". [4] Considerable efforts have been focused on the design and synthesis of various framework structures.[22] The mesoporous materials are much more convenient to be used in catalysis, gas sensing, sorption, optics and photovoltaics. [22]

The first report on the synthesis of mesoporous materials by means of surfactant templating was made by a research group of Mobil Oil Company in 1992 (MCM-41).[23] Since then, research in this field has steadily grown. Many new methods, such as monolayer depositions of thiols,[24] synthesis of optical materials[25-27] etc., have been discovered to produce a great variety of new functional mesoporous materials with a controllable shape and pore size. A different strategy was employed by Roggenbuck and Tiemann who used a carbon template to synthesize thermally stable MgO, which contains a periodic array of 4-8 nm pores in diameter.[28] Zhou et. al. synthesized a mesoporous germanium oxide with crystalline pore walls and its chiral derivative with a primitive cell volume of 67 640 $Å^3$ by using the standard hydrothermal methods without using surfactants, but with an organic amine as the structure-directing agent.[29] This is similar to conventional zeolite synthesis. It was also shown that mesoporous GeO_2 could be produced by a surfactant templating method with a thermal stability.[30] Chiral mesoporous oxides are particularly desirable for enantioselective sorption and catalysis.[31]

In 1995, Attard et. al. synthesized mesoporous silica by using the true liquid crystalline (TLC) templating approach that uses non-ionic surfactants, C_nEO_m, in their lyotropic liquid crystalline mesophase both as a template and silica polymerization reaction media. [32] The resulting silica phase, with pores of ~ 3 nm diameter, was the cast of the organic mesophase. Then, in 1996, mesoporous silica was synthesized as thin (0.2 – 1 μm) ordered films on freshly cleaved mica substrates.[33] From a technological point of view, the preparation of such materials in the form of mesoporous thin films is desirable. By using different methods, those mesoporous silica films have been used as a template to produce nanostructured materials in the channels of mesostructured silica films and monoliths, for example, CdS, ZnS.[34-37]

On the other hand, the mesoporous CdS, ZnS nanowires and nanoparticles have also been synthesized by using TLC templating approach.[38-41] By this approach, instead of preparing the mesoporous nanoparticles in the channels of silica as a template, the synthesized materials could form the channels themselves. However, in all of these studies, the LC phase was formed using water as a second

component of the lyotropic liquid crystalline (LLC) phase and then the metal salt was added in the mixture as a third component, (ternary system). As it will be mentioned in detail in section 1.2, this causes a problem at high salt concentrations; the LC phase is not stable and converts into disordered non – structured phase. Therefore, these nanostructured material syntheses were carried in solutions of the LC phase containing very low metal ion concentrations; ~ 0.1 M. Here the growth of inorganic phase occurs in the already formed organic mesophase as in the case of synthesis of mesostructured silica.

However, we aim to form an organic mesophase directly with the inorganic as organic – inorganic hybrid mesophase. Previously, it was shown that such kind of organic – inorganic hybrid mesophase can be successfully used to obtain CdS and ZnS. [42] Besides, so far, all mesoporous CdS, ZnS or similar mesoporous materials were synthesized as powders and there has been no study in the literature showing the preparation of thin films of those mesoporous inorganic materials, which may advance many applications. In this thesis, we performed synthesis of mesostructured materials, CdS, by using thin film samples of LC mesophase as a template formed by mixing TMS, $[Cd(H_2O)_4](NO_3)_2$ and pluronic, P85. The prepared nano – CdS as a nanocrystalline semiconductor has an optical band gap in the visible region of the electromagnetic spectrum. Upon exposing the samples to H_2S gas, the $Cd(H_2O)_4^{2+}$ ions immediately react with H_2S gas to produce mesostructured CdS, according to reaction below;

$$[Cd(H_2O)_4](NO_3)_2 + H_2S \rightarrow CdS + 2HNO_3 + 4H_2O$$

1.2. Liquid Crystalline Mesophases

The liquid crystalline (LC) state is the fourth state of matter that is intermediate between the amorphous liquid and crystalline solid. Liquids have neither positional nor orientational order, but LC phases have small degree of orientational order which gives them anisotropic nature.[43]

The LC can be divided into two main groups, the thermotropic liquid crystals and lyotropic liquid crystals, (LLC). The thermotropic ones are made up of rod like, disc like or polymeric molecules. The temperature determines which phases will exist. The LLCs form depending on both temperature and concentration of mesogen in an appropriate solvent but concentration is far more important in the LLC systems.[43-44] Throughout this work, only the LLCs are investigated. For that reason, only the LLC phases will be explained in detail.

It has been well known that surfactants (amphiphilic molecules) form LLC mesophase with different mesostructures depending on surfactant concentration in water (as a solvent).[43-44] Surfactants are bifunctional molecules that contain a solvent-loving (hydrophilic) head group and a solvent-hating (hydrophobic) tail (i.e. they are amphiphiles).[45] There are various kinds of surfactants, which can be classified as anionic, cationic, amphoteric and non-ionic because of their head groups. In this work, a non-ionic pluronic, poly(ethylene oxide) – poly(propylene oxide) – poly(ethylene oxide) triblock copolymer, P85 has been used (Fig. 1.2.1).

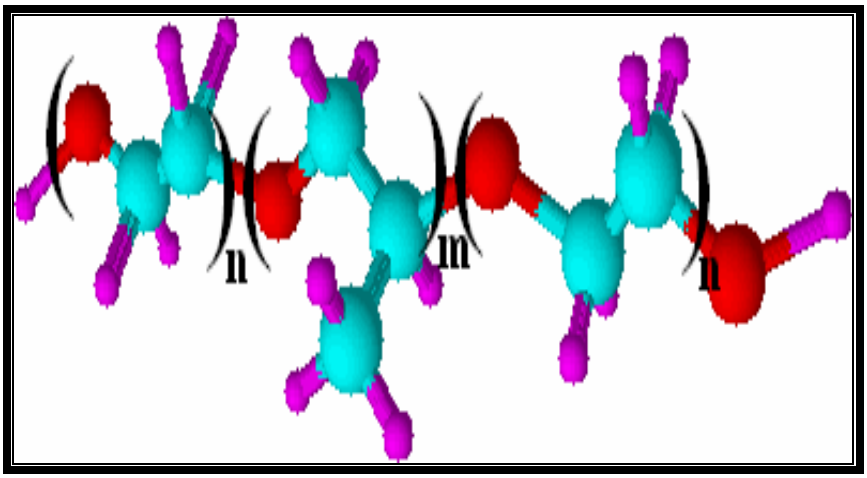

Figure 1.2.1: Non ionic Pluronics, $(PEO)_n(PPO)_m(PEO)_n$. (Cyan: Carbon, Red: Oxygen, Magenta: Hydrogen)

Pluronic P85, difunctional block copolymer surfactant terminating in primary hydroxyl groups, is a nonionic surfactant that is 100% active and relatively nontoxic. The structure of P85 is poly(ethylene oxide)$_{26}$-poly(propylene oxide)$_{40}$-poly(etyhlene oxide)$_{26}$, $(PEO)_{26}(PPO)_{40}(PEO)_{26}$. Its molecular weight is approximately 4600 g/mol. According to nomenclature of The Chemical Company BASF, "P" stands for paste that is its physical form at RT. The first digit (two digits in a three-digit number) in the numerical designation, multiplied by 300, indicates the approximate molecular weight of the hydrophobic part that means the molecular weight of polypropylene oxide part is approximately 2400 (8x300). The last digit, when multiplied by 10, indicates the approximate ethylene oxide content so the hydrophile represents approximately (5x10) 50% of the molecule, by weight.

1.2.a. LC phases: surfactant and water

The LC phase occurs as a result of hydrophobic and hydrophilic interactions of surfactants with water. Basically, oil – like group of the surfactant tends to minimize the interaction with water and forms micelles in diluted water solutions while the polar ethylene oxide (EO) groups tend to stay outside the micelles. The extent of micellization, the shape of micelles into liquid crystals depends on the surfactant concentration. A schematic phase diagram for a cationic surfactant, C_{16}TMABr, in water is shown in Figure 1.2.a.1. At very low concentration, the surfactant is present as free molecules dissolved in solution. At concentrations higher than critical micelle concentrations (CMC1), the individual surfactant molecules form micelles and at concentrations higher than CMC2, spherical micelles form elongated cylindrical micelles. Therefore, it is possible to get different kinds of mesophases and mesostructures like hexagonal, cubic or lamellar by changing the surfactant concentration and/or temperature. [46]

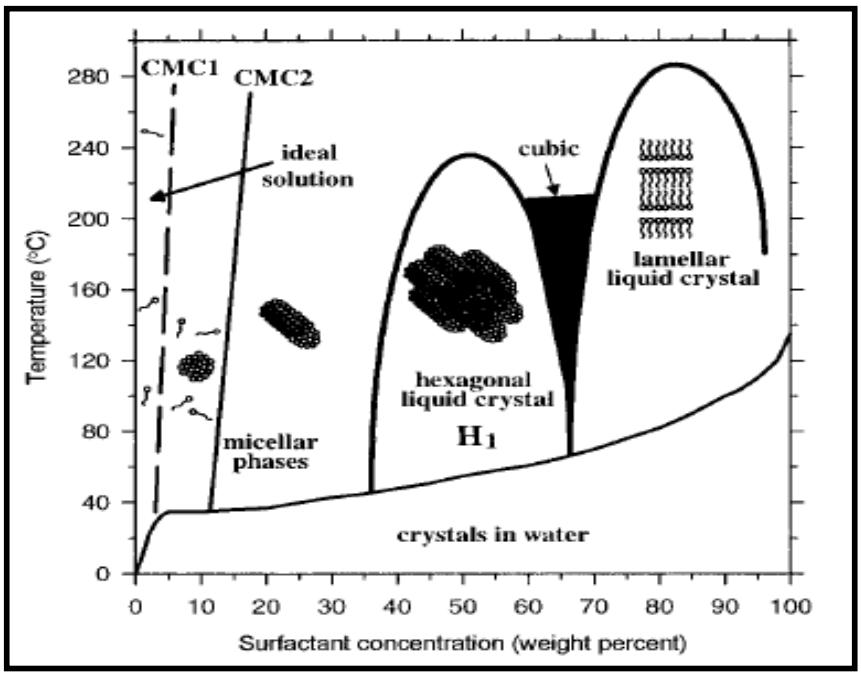

Figure 1.2.a.1: Schematic phase diagram for C_{16}TMABr, a cationic surfactant, in water.[46]

The homopolymer non-ionic surfactants, C_nEO_m, also form a variety of LLC mesophases depending on the temperature of the solution and concentration of the surfactant. They form stable casts for the synthesis of mesostructured and mesoporous materials. The non-ionic surfactants have some considerable advantages over the ionic surfactants such as thicker inorganic walls, easy tuning of pore diameter, and easy removal of surfactant molecules. [47-48]

The phase behaviour of hexaoxyethylene n-dodecyl ether ($C_{12}E_6$ or $C_{12}EO_6$) in water was studied thermodynamically in detail. [49] The phase diagram [50], given in Figure 1.2.a.2, demonstrates three LC mesophases at concentrations higher than 35 wt % of $C_{12}E_6$: hexagonal (HI), cubic (VI) and lamellar (Lα) structures.

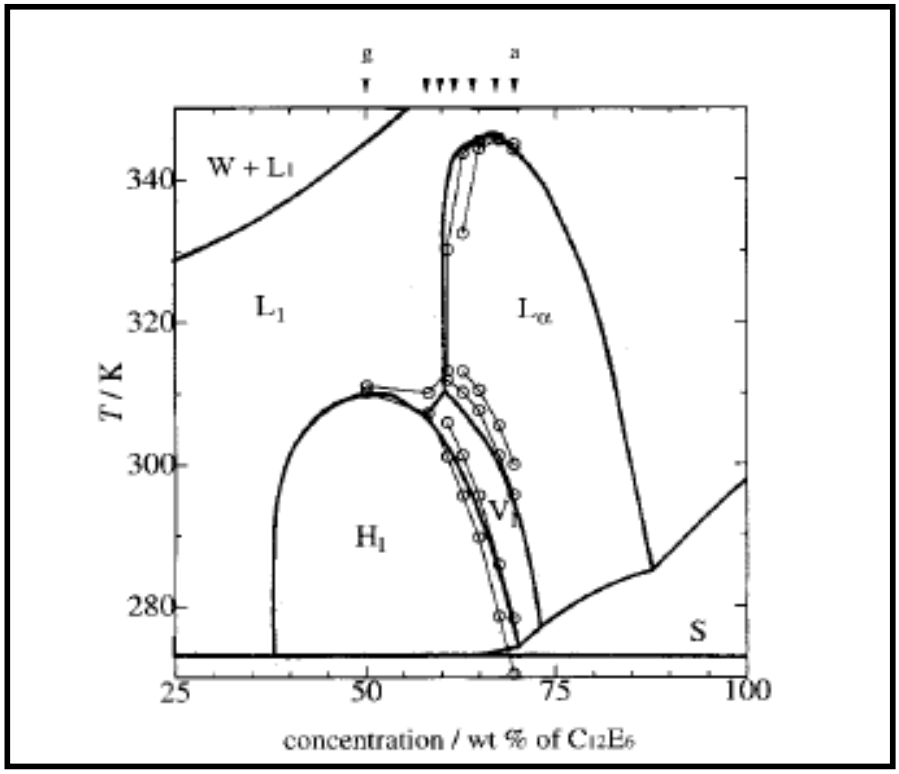

Figure 1.2.a.2: Phase diagram of the $C_{12}E_6$-water system. L_α, lamellar phase; VI, normal bicontinuous cubic phase; HI, normal hexagonal phase; L1, aqueous surfactant solution; W, very dilute surfactant solution; S, solid surfactant.[50]

In 1995, Attard et. al. [32] introduced the new method, the liquid crystalline templating (LCT) approach that uses homopolymer non-ionic surfactants, C_nEO_m, in their LLC mesophase to template the synthesis of mesoporous silica. They showed the predictability of the structure of the synthesized mesoporous materials according to the mesophase of LC template by using the phase diagram of homopolymer non-ionic surfactant/water alone. [50] Since the phase diagram of the surfactant/silica/water system at high surfactant concentration is similar to the phase diagram of the non-ionic surfactant/water alone. With 50 wt % non-ionic surfactant (C_nEO_m) in water, a hexagonal LLC phase forms as shown in Figure 1.2.a.2. Adding tetramethoxysilane (TMOS) as a silica source to these phases and removing evolved methanol results in MCM-41 type hexagonal silica arrays, with pores of ~ 3 nm in diameter. In this case the surfactant array appears to act as a cast or mold in which the inorganic network polymerizes throughout the aqueous domains of the LC mesophase, and formation of the ordered mesophase is effectively independent of surfactant:silicate interfacial interactions.

It should be emphasized that the templating step is crucial in order to be able to make materials with desired shape and size. In template based synthesis, inorganic materials copy the shape and size of the organic template.[51] The nature of interaction between the template and embedding matrix, the ability of the matrix to conform the template and relative sizes of the template, and primary units used to construct the matrix are factors to consider for mimicking the template.[46] The surfactant molecules form the ordered organic template in the appropriate conditions and this organic template directs the structure of the added inorganic material during the synthesis by forming a network. When optimum conditions are provided to carry the polymerization and condensation reactions of the inorganic precursors in the hydrophilic domains of the organic template, it allows mimicking the shape and size of the organic building blocks so that the inorganic material with the same structure can be synthesized. When the organic template is removed from the inorganic matrix, porous inorganic material with controlled shape and pore size can be obtained.

In 1996, it was reported that mesoporous silica could be synthesized as thin (0.2 – 1 μm) ordered films on freshly cleaved mica substrates by using a cationic

surfactant to form the LCT and tetraetyhlorthosilicate (TEOS) as a silica source under inactive aqueous acidic conditions.[52] The cationic surfactant had the hexagonal mesophase in the appropriate concentration range as expected from the cationic surfactant/water phase diagram given in Figure 1.2.a.1. Hence, the material obtained from this LCT had the hexagonal symmetry channel structure of the mesoporous MCM-41 type silica film. From a technological point of view, preparation of such materials in the form of mesoporous thin films is desirable.

Göltner et. al.[53] used non-ionic amphihilic copolymers with a polyethylene oxide head group and a polystyrene tail group as LCT at higher polymer concentrations to create crack-free mesoporous silica monoliths, by using a larger size template to obtain mesoporous materials with larger pores and thicker walls.

It has been found out that the three block copolymers consisting of poly(ethylene oxide)$_n$-poly(propylene oxide)$_m$-poly(ethylene oxide)$_n$, $(PEO)_n(PPO)_m(PEO)_n$, form the richest variety of mesostructures in solution phase ever observed in other surfactants such as homopolymer non-ionic surfactants or cationic surfactants.[54] As shown in the phase diagram given in Figure 1.2.a.3, the $(EO)_{19}(PO)_{43}(EO)_{19}$-$2H_2O$-*p*-xylene (oil) system exhibits nine different phases that all are thermodynamically stable at the same temperature (25 °C): normal micellar cubic, normal hexagonal, normal bicontinuous cubic, lamellar, reverse bicontinuous cubic, reverse hexagonal, and reverse micellar cubic lyotropic liquid crystalline phases, as well as water-rich and water-lean micellar solutions. Also the total number of phases would be 10 if the solvent free $(EO)_{19}(PO)_{43}(EO)_{19}$ copolymer, a lamellar state, was added.

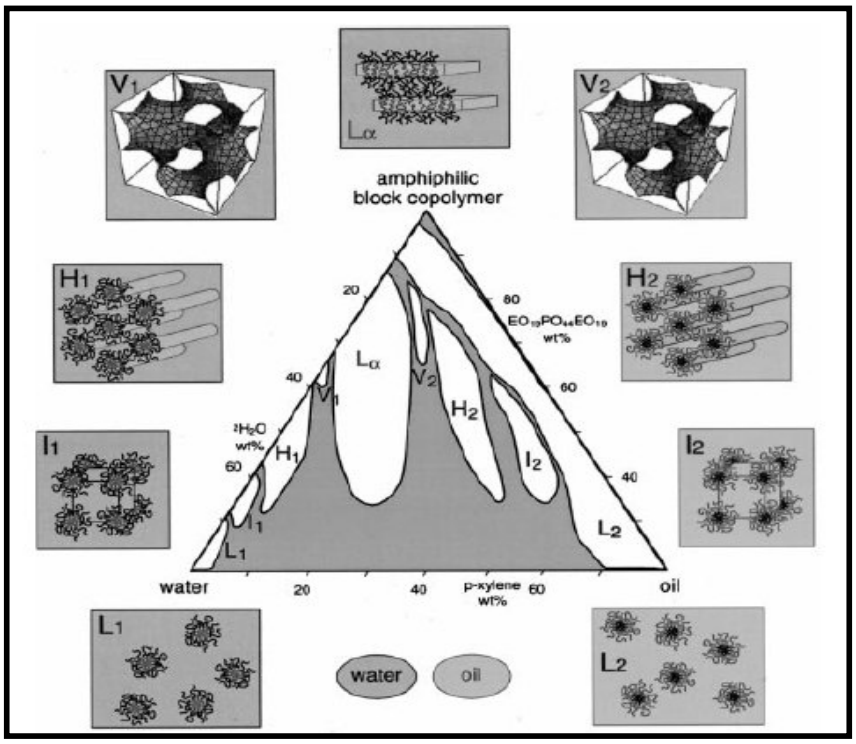

Figure 1.2.a.3: Phase diagram of the $(EO)_{19}(PO)_{43}(EO)_{19}$-water-oil ternary system at RT. The phase boundaries of the one-phase regions are drawn with solid lines. I_1, H_1, V_1, L_α, V_2, H_2, and I_2, denote normal (oil-in-water) micellar cubic, normal hexagonal, normal bicontinuous cubic, lamellar, reverse (water-in-oil) bicontinuous cubic, reverse hexagonal, and reverse micellar cubic lyotropic liquid crystalline phases, respectively, while L_1 and L_2 denote water-rich (normal micellar) and water-lean/oil-rich (reverse micellar) solutions.[54]

The large-pore, around 63 Å, mesoporous silica fibers [55] and the continuous mesoporous silica films with highly ordered large pore structures [56] have been synthesized by using $(PEO)_n(PPO)_m(PEO)_n$ triblock copolymers as structure-directing agents. It has also been shown that it is possible to extend the pore size up to 30 nm [57] and get various type of mesoporous structure [58] by changing the type of the copolymer.

1.2.b LC phases: surfactant + water + metal salt

Non-ionic surfactants, such as oligoethylene oxides (C_nEO_m) and pluronics form LC mesophases with water at various mole ratios. Generally, metal salts have been added to the media as a third component of the mixture in order to create materials with desirable functions and structures. In such systems, the LC phase is obtained by using water and it is generally accepted that metal salts dissolve in the water (polar) region. The fundamental goal has been to control and organize the surfactant molecules into various mesostructures. With the current interest in nanoscience and, in particular, nanostructured materials, LLC assemblies are especially attractive for the design of nanoscale systems for targeted materials applications. The only limitation with LLC phases is that they are inherently fluidic, and hence lack the robustness required from any materials applications.

Attard and his co-workers later showed that metals, such as platinum, tin [59-61] and their alloys [62], having a well-defined periodic mesoporous nanostructure could be obtained by the LCT approach. The metal salts were dissolved in the aqueous domains of the liquid crystalline phases of the oligoethylene oxide surfactant, a homopolymer non-ionic surfactant. In these structured reaction systems, the metal is formed between the surfactant supramolecular assemblies that constitute the building blocks of the phases. That means the metal ions are distributed into the LC mesophase as in the order of that mesophase. Also highly ordered mesoporous Ni particles [63] and mesostructured Ni-Co alloys [64] were prepared by electroless deposition from LLC as structure-directing agent formed in the presence of a homopolymer non-ionic surfactant, $C_{16}(EO)_n$.

Stucky et. al. [65] reported a simple and versatile procedure for the synthesis of thermally stable, ordered, large-pore (up to 140 Å) mesoporous metal oxides, including TiO_2, ZrO_2, Al_2O_3, Nb_2O_5, Ta_2O_5, WO_3, HfO_2, SnO_2, and mixed oxides $SiAlO_{3.5}$, $SiTiO_4$, $ZrTiO_4$, Al_2TiO_5 and ZrW_2O_8 by the LCT approach. The

hexagonal mesoporous metal oxides were synthesized from the LC phase formed by dissolving triblock copolymer, P123, in 10.0 mL ethanol and then, adding the respective inorganic chloride precursor at very low concentration, 0.01 mol. The surfactants were later removed by calcining the samples at 400° C.

Stupp et al. also used the LCT approach to synthesize the nanostructured semiconductors CdS, CdSe and ZnS.[38-40] The LC phase was formed by mixing non-ionic oligo ethylene oxide type surfactant with different types of metal salts at very low concentration, ~0.01 mol. The nanocomposite material, semiconductor CdS, templated directly by the hexagonal LC mesophase had the superlattice with the matching symmetry and periodicity to the LC mesophase as shown in Figure 1.2.b.1. Effects of the counteranion to the LCT of nanostructured CdS were studied. [40] It was shown that the type of counteranion defines the mesostructure of LC phase and so, the mesostructure of synthesized CdS nanoparticles since they mimic the LC template.

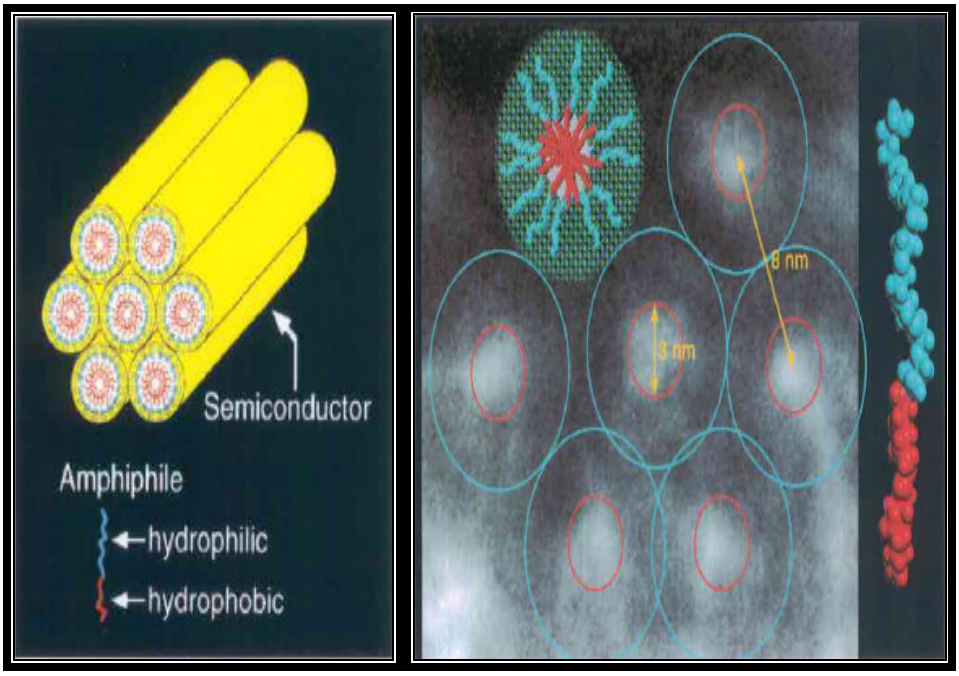

Figure 1.2.b.1: Left; schematic represantation of an ordered nanocomposite solid semiconductor, yellow regions, in which the organic phase consists of hexagonally close-packed tubules of self-assembled amphihiles. Right; high-magnification electron micrograph of the semiconductor CdS super lattice.[38]

On the other hand, for a long time, it had been presumed that in order to synthesize the mesostructured and/or nanostructured metal sulfides, the LC mesophase must be formed in high water (50% w/w water: surfactant) and low salt (on average 0.1 M salt $Cd(NO_3)_2$ solutions) concentrations and H_2S gas as a sulphur source.[38, 41, 66] Such LC systems had the disadvantage that the LC phase is only stable at low salt: surfactant ratios, typically up to around 0.1 M salt concentration, and they are liquid at higher salt concentrations.That means there is no mesophase at all. However, in 2001, Dag`s group found out how to overcome this disadvantage.[67] In their work, they have demonstrated the construction of a LC phase directly from metal aqua complexes. The coordinated water molecules mediate the formation of the LC phase. It can be seen that the presence of coordinated water molecules, ($M\text{-}OH_2$), in the self- assembly processes is very important for organizing the surfactant molecules into metallotropic mesophases through hydrogen – bonding interactions. Here, the EO chain of the oligo(ethylene oxide) surfactant forms hydrogen bonds with metal aqua complexes. As shown in the Figure 1.2.b.2, this interaction may organize the surfactant molecules into hexagonally ordered rods which build the LC hexagonal structures [67] or maybe into any other LC structure.

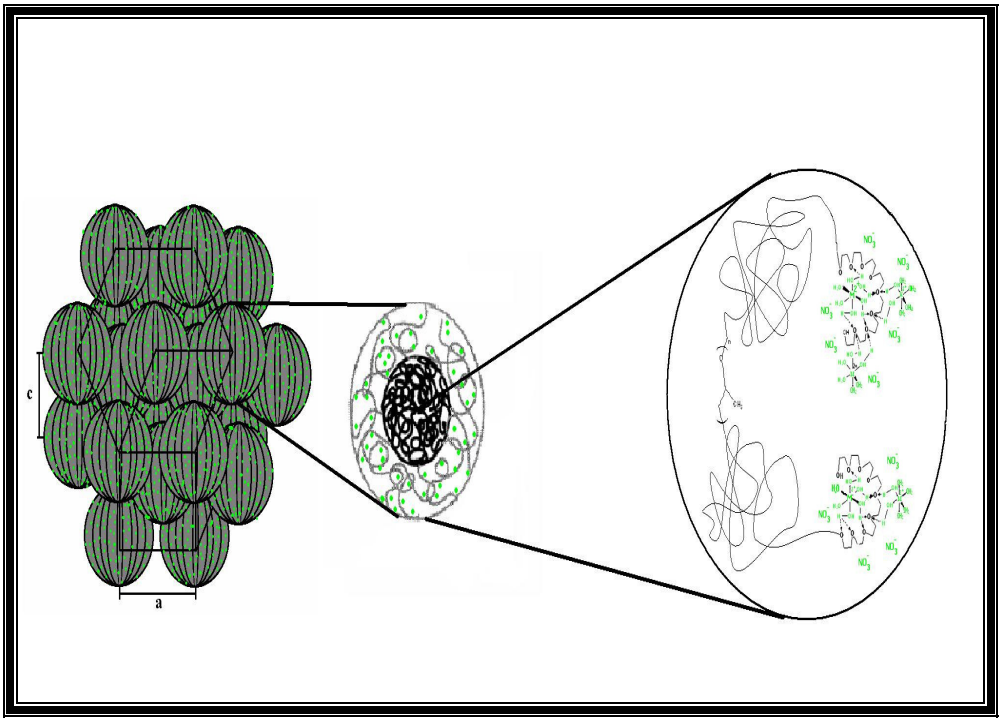

Figure 1.2.b.2: Representation of the structure of the LC phase formed directly with metal aqua complexes by the help of hydrogen bonding

This new LC system has been widely investigated to explore the properties of LC systems formed in a variety of transition metal salts and in oligo type and pluronic type surfactants.[42, 68-70] Then, it was shown that one-pot synthesis of CdS nanoparticles in the channels of mesostructured silica films and monoliths could be realized collectively using the new LC system and the TLC approach, so that large quantities of transition metal complex ions could be incorporated into mesoporous materials.[36] By this approach, solid solutions of $Cd_{1-x}Zn_xS$ and CdS, ZnS, nanocrystals were synthesized in the channels of mesostructured silica films.[37]

We have studied the LC phase behavior of a transition metal aqua complex $[Cd(H_2O)_4](NO_3)_2$ with the $(PEO)_{26}(PPO)_{40}(PEO)_{26}$ triblock copolymer, Pluronic P85 in the absence, and the presence of different amounts of free water and

different solvents like ethanol, acetone in the media, at different temperatures. The phase behavior was investigated in a range of transition metal salt (TMS) to pluronic mole ratio from 1:1 to 20:1 by means of diffraction and spectroscopic techniques to elucidate the structural and templating properties. Mixing of $[Cd(H_2O)_4](NO_3)_2$ salt with P85 has produced a new phase depending on the concentration range. The aim of varying the amount and type of the solvent, temperature, time of mixing solutions and mole ratio of TMS to surfactant was to optimize the conditions for the preparation of homogenized and ordered mesostructured LC samples. The challenges on obtaining optimum conditions and reasons of choosing these conditions will be discussed in the section 3.1.

Type and concentration of metal salts and collective interactions of metal aqua complex ion–surfactant and metal ion–counteranion are the central factors that influence the self–assembly of mesophases.[42, 67-70] The *Hofmeister`s* series;

$$\mathbf{(SO_4^{2-} > HPO_4^{2-} > CrO_4^{-} > CO_3^{2-} > Cl^{-} > Br^{-} > NO_3^{-} > I^{-} > ClO_4^{-} > SCN^{-})}$$

for anions has been known since 1888. According to that series, anions on the left hand side of the series are lyotropic and make the surfactant molecules more hydrophobic, which reduces the solubility of the salts in the salt: surfactant media and those on the right – hand side are hydrotropic and make surfactant molecules more hydrophilic. For that reason, the metal salts of anions on the right – hand side are expected to be more soluble.[71-72] Therefore, perchlorate ions could be expected to make the surfactant molecules more hydrophilic than a nitrate ion in water: surfactant LC system.[73] However, it has been shown that it is not so easy to dissolve the perchlorate transition metal salts (TMS) compared to nitrate TMS in a TMS: surfactant LC system.[74] Here, one of the essential factors to take into account is that the coordination interaction of a nitrate counteranion with a metal ion reduces the ion density (ionic strength) of the LC medium, hence, improves the solubility, so that it can avoid crystallization of nitrate salts in the LC medium. Therefore, it was reasonable to choose the NO_3^- anion as the counteranion in such a new LC system formed by the pluronics.

It has been shown that an equilibrium ligand exchange reaction occurs between the coordinated water molecules and the nitrate ions while excess water evaporating.[68] In the presence of the excess water in the LC media, nitrate ions are in the liquid and/or LC mesophase and the water molecules coordinate the Cd^{2+} metal ions, forming the $[Cd(H_2O)_4]^{2+}$ complex ions. Upon evaporation of the excess water, the nitrate ions tend to coordinate to the metal center and produce the +1 charged complex ion, $[Cd(H_2O)_2(O_2NO)]^+$ (eq 1.2.b.1). The water molecules still coordinated to that metal complex keep mediating the LC mesophase by means of hydrogen bonding.

$$\mathbf{[Cd(H_2O)_4]^{2+} + 2NO_3^- \leftrightarrow [Cd(H_2O)_2(O_2NO)]^+ + NO_3^- + 2H_2O} \qquad \mathbf{(eq\ 1.2.b.1)}$$

It was confirmed that the pluronics show LC behavior in the presence of transition metal salts [69] and when the transition metal aqua complexes dissolve in the triblock Pluronic copolymers. The interactions of the coordinated water molecules and ethoxy groups of the PEO units ($M–OH_2$--OCH_2CH_2-), through hydrogen bonding, so acting as structure – directing agents, and nitrate ion with the metal ion ($M\text{-}O_2NO$), through coordination, provide the stabilization of the LC mesophase into a different structure type. In our LC system, we also used metal aqua complex, salt $[Cd(H_2O)_4](NO_3)_2$,. Hence, the same principle was valid in the formation of the LC mesophase from $[Cd(H_2O)_4](NO_3)_2$ salt and pluronic, P85 and we showed that mixing the $[Cd(H_2O)_4](NO_3)_2$ with P85 in the absence or the presence of free water, or in different amount of free water or even in different types of solvents like ethanol and acetone did not change the structure of the LC phase at the same concentration of TMS and temperature. For that reason, we can certainly conclude that since the coordinated water molecules of $[Cd(H_2O)_4](NO_3)_2$ are used to mediate the formation of LC phase and the solvent, water or ethanol or acetone, would already evaporate while preparing the thin films of those LCs. Hence, it can be supported that the solvent is needed to make the homogenisation process easier and provide the advantage that we could form the ordered LC phases up to the salt to surfactant mole ratio 11:1.

1.3. $Cd_{1-x}Zn_xS$ Nanoparticles

Binary metal chalcogenides of group IIB have been the most studied semiconductor materials among the various semiconductors due to their potential applications. They have nonlinear optical and luminescence properties,[75-82] quantum size effect, (QSE) [75-85] and other important physical and chemical properties.[86-89] For example; nanocrystalline thin films of CdS and ZnS are attractive materials in photoconducting cells and optoelectronic devices such as solar cells and photodetectors. [90-91]

Similarly, $Cd_{1-x}Zn_xS$ are direct band gap semiconductors which are important optical materials, for use as high density optical recording, as blue or even UV laser diodes.[92-93] The band gap can be tuned by changing x in the composition such that the gap of $Cd_{1-x}Zn_xS$ displays an almost linear dependence on the amount of CdS and ZnS components of the resulting materials.[94-95] However, the particle size of these nanocrystallites has also an important impact on the band-gap of those materials due to quantum confinement effect (QCE).[78] Previous works carried out in our group showed that the $Cd_{1-x}Zn_xS$ nanoparticles in the channels of mesostructured silica films can be synthesized by using the true liquid crystalline templating (TLCT) approach.[37] In this work, we investigate that LLC system in order to control the particle size and the band-gap in mesostructured $Cd_{1-x}Zn_xS$ (x= 0.0- 1.0) films. In this contribution, the structure and particle size of the $Cd_{1-x}Zn_xS$ (x= 0.0- 1.0) materials were characterized by using XRD and UV-Vis absorption spectroscopy.

1.4. $Cd_{(1-x)}Co_xS$ and $Cd_{(1-x)}Mn_xS$ Nanoparticles

Diluted magnetic semiconductors (DMSs) can be formed upon random substitution of magnetic ions with host cations. Thus, it has received a great attention due to potential use as electronic materials. [96-98] However, to be integrable into electronic devices, DMSs are required to have low-dimensional structures like nanowires, nanocrystals or quantum dots (QDs), so that advantages provided by their spin can be used properly. So far, many nanosized DMS materials, manganese (Mn)-doped cadmium sulfide (CdMnS) [99-100], Mn-doped $Cd_{1-x}Mn_xS$ DMSs as nanostructured guest species in mesoporous thin-film silica host media, [101-102] cobalt (Co)-doped ZnSe DMS QDs [103-104] have been synthesized using various methods. In the DMS class of materials, the most-investigated materials are (II,Mn)VI semiconductors where a fraction *x* of the group II cations are substituted by Mn^{2+} ions. This results in a variety of interesting properties:

i) The ternary nature gives the possibility to tune the lattice constant and band gap parameters by varying the chemical composition of the material,

ii) The random distribution of magnetic ions throughout the cation sublattice leads to interesting magnetic effects, such as the formation of a spin-glass phase at low temperatures; the exchange interaction between spins of the band states and those of the localized d-electrons of Mn^{2+}, giving rise to the so called giant Zeeman splitting of band states; and antiferromagnetism at high Mn contents,

iii) The substitutional Mn atoms in the lattice of wide-gap II-VI semiconductors give rise to a highly efficient Mn $3d^5$- related luminescence, which makes these kinds of alloys interesting for applications in optical flat-panel displays.[105]

Here, we have studied LC mesophase $([Cd(H_2O)_4](NO_3)_2)_{1-x}(M(H_2O)_6](NO_3)_2)_x$: P85 (M is Co(II) and Mn(II)) in order to synthesize mesostructured $Cd_{1-x}Co_xS$ and $Cd_{1-x}Mn_xS$ magnetic films, respectively.

2. EXPERIMENTAL

2.1. Materials

All chemicals and solvents were reagent grade and used as received without any further treatment.

Surfactant used throughout this work, the triblock copolymer having a poly(ethylene oxide) – poly(propylene oxide) – poly(ethylene oxide) (EO-PO-EO) so called Pluronics, P85 ($PEO_{26}PPO_{40}PEO_{26}$), M_{av} = 4600 was generously donated by BASF Corp. and used without further treatment.

The other chemicals used are; Cadmium(II) nitrate tetrahydrate $[Cd(H_2O)_4](NO_3)_2$, 99%, Fluka, Poland), Zinc(II) nitrate hexahydrate $[Zn(H_2O)_6](NO_3)_2$, 98%, Aldrich, Germany), Cobalt(II) nitrate hexahydrate $[Co(H_2O)_6](NO_3)_2$, 98%, Aldrich, Germany), Manganese(II) nitrate tetrahydrate $[Mn(H_2O)_4](NO_3)_2$, 96%, Riedel-de Haën, Germany), hydrogen sulfide (H_2S, 99.5%, Aldrich, Germany), ethanol (C_2H_5OH, 99.9%, Merck, Germany), methanol (CH_3OH, 99.5%, Merck, Germany) and acetone (CH_3COCH_3, 99.8%, Merck, Germany).

2.2. Synthesis

2.2.1 Synthesis of Liquid Crystalline Phase of Inorganic Salts:P85

The liquid crystalline phase of TMS, $[Cd(H_2O)_4](NO_3)_2$ was prepared by stirring overnight at RT with 1.0 g P85 in the range of mole ratio of salt to pluronic, $[Cd(H_2O)_4](NO_3)_2$:P85, 1:1 – 20:1, in 10.0 mL ethanol. For example, in order to prepare n:1 mole ratio of $[Cd(H_2O)_4](NO_3)_2$:P85 solution, first, 1.0 g P85 is weighed in a vial and dissolved in 10.0 mL ethanol by stirring for half an hour over magnetic stirrer until the solution looks homogenized. Then, ((1/4600 (M.W. of

P85))*308.48(M.W. of $[Cd(H_2O)_4](NO_3)_2$)*n = m g) m g $[Cd(H_2O)_4](NO_3)_2$ is added to that mixture and let the solution mix overnight at RT. In order to prepare the n:1 mole ratio of (1-x)$[Cd(H_2O)_4](NO_3)_2$:x$[Zn(H_2O)_4](NO_3)_2$:P85 solution, after mixing the 1.0 g P85 in 10.0 mL ethanol in a vial at RT, ((1/4600 (M.W. of P85))*308.48(M.W. of $[Cd(H_2O)_4](NO_3)_2$)*n*(1-x) = a g) a g $[Cd(H_2O)_4](NO_3)_2$ and ((1/4600 (M.W. of P85))*297.49 (M.W. of $[Zn(H_2O)_6](NO_3)_2$)*n*x) = b g) $[Zn(H_2O)_6](NO_3)_2$ are added to that of P85 and ethanol mixture and let the solution mix overnight at RT. The solutions are quite stable for long periods.

The solutions were used to prepare the thin film samples by 2000 rpm spin coating and dip coating with a coating speed of 0.4 mm/s over a glass, quartz or silicon substrates for various measurements. In order to prepare thin films of LC mesophase, 2.0 mL sample is injected over the small sized substrates while it is spinning at 2000 rpm speed. The LC film samples are also stable for long periods.

2.2.2 Synthesis of CdS, $Cd_{1-x}Zn_xS$, $Cd_{1-x}Mn_xS$ and $Cd_{1-x}Co_xS$

Thin films of mesophases prepared as described above were reacted in an evacuated reaction chamber under 350 torrs of H_2S gas for 15 minutes at RT. There is no observed affect of letting the film samples outside before they are exposed to H_2S. This process produces stable transparent CdS, $Cd_{1-x}Zn_xS$, $Cd_{1-x}Mn_xS$ and $Cd_{1-x}Co_xS$ materials with yellow color in the Cd(II) rich samples, colorless in the Zn(II) rich samples, black in the Co(II) rich samples and colorless in the Mn(II) rich samples upon exposing LC thin films of $[Cd(H_2O)_4](NO_3)_2$:P85,
(1-x)$[Cd(H_2O)_4](NO_3)_2$:x$[Zn(H_2O)_4](NO_3)_2$:P85,
(1-x)$[Cd(H_2O)_4](NO_3)_2$:x$[Mn(H_2O)_4](NO_3)_2$:P85 and
(1-x)$[Cd(H_2O)_4](NO_3)_2$:x$[Co(H_2O)_6](NO_3)_2$:P85 to H_2S atmosphere, respectively.

2.3. Instrumentation

2.3.1 X-Ray Diffraction

The X-Ray diffraction (XRD) patterns were obtained on a Rigaku Miniflex diffractometer using a high power $Cu_{K\alpha}$ source operating at 30 kV/15 mA. The XRD patterns of samples prepared on glass and silicon substrates were recorded both at small and high angle regions. The small angle diffraction patterns were recorded in 0.4 – 5, 2θ range with a scan rate of 0.10^{o}/minute. The high angle diffraction patterns were recorded in 15-45, 2θ range with a scan rate of 5.0^{o}/minute.

2.3.2 FT-IR Spectroscopy

FT-IR spectra were recorded with a Bruker Tensor 27 model FTIR spectrometer. A DigiTectTM DLATGS detector was used with a resolution of 4 cm^{-1} and 256 scans in the 400-4000 cm^{-1} range for all samples. The FTIR spectra were recorded in transmittance mode as thin films on single Si (100) wafers.

2.3.3 UV-Vis Spectroscopy

UV-Vis absorption spectroscopy was used for characterization and also to obtain information about the electronic properties of the mesostructured CdS, $Cd_{1-x}Zn_xS$, $Cd_{1-x}Co_xS$, and $Cd_{1-x}Mn_xS$. The UV-VIS Spectra were recorded using a Varian Cary 5 double beam spectrophotometer with a 20 nm/min speed and a resolution of 2 nm over a wavelength range, from 800 to 200 nm. The absorption spectra were obtained from the thin film samples of CdS, $Cd_{1-x}Zn_xS$, $Cd_{1-x}Co_xS$, and $Cd_{1-x}Mn_xS$ materials over glass and/or quartz slides.

2.3.4 Raman Spectroscopy

The micro Raman spectra were recorded on a LabRam Monel confocal Raman microscope with a 300 mm focal length. The spectrometer is equipped with a HeNe laser operated at 20 mW, polarized 500/1 with a wavelength of 632.817 nm, and a 1024 x 256 element CCD camera. The signal collected was transmitted through a fiber optic cable into a spectrometer with a 600 g/mm grating. The Raman spectra were collected by manually placing the probe tip near the desired point of the sample on the silicon wafer. The same systems were also used to record the confocal microscopy images.

2.3.5 Scanning Electron Microscopy (SEM) and Energy Dispersive X-Ray Spectroscopy (EDS)

The SEM images were recorded on a ZEISS EVO – 40 operating at 15 kV. The samples were prepared on silicon wafers that were attached to aluminum sample holders using conductive carbon adhesive tabs. EDS data and EDS maps were collected using the same SEM using a Bruker AXS XFlash detector 4010.

3. RESULTS AND DISCUSSION

3.1. The $[Cd(H_2O)_4](NO_3)_2$: P85 LC system

During optimization of conditions for preparation of homogenous LC mesophase, the first attempt was to form LC phase by mixing TMS, $[Cd(H_2O)_4](NO_3)_2$, with pluronic, P85, as a binary system, at different salt to pluronic mole ratios. In order to make the solutions homogenized, they needed to be shake at 50°C for a week. The thick film samples were prepared by spreading the above mixture over the surfaces of glass substrates. Those thick films did not give well ordered, intense small angle diffraction lines as depicted in Fig. 3.1.1.A, even though those film samples were forced to be oriented through one direction by an applied shear force. The high angle diffraction patterns of the film samples as given in Fig. 3.1.1.B indicated us that the mixtures of salt – pluronic were not well homogenized. Until salt concentration of 5 (salt/P85 mole ratio), the film samples gave intense high angle diffraction lines similar to pure P85. That means, salt and pluronic did not mix well and free surfactant crystallites dominate the mixture. The higher salt concentration, 7, did not give high angle diffraction lines since there were enough salt ions to mix with the surfactant molecules and to organize them into LC mesophases. However, this doesn't mean that those mixtures were homogenized since their thick film samples were crystallized by producing salt and P85 crystals in one week time. Therefore, this method was a time consuming process to prepare the mixtures in the absence of a solvent (water) and it is even harder for the mixtures of higher salt concentrations. Besides, since the mixtures were gel like, it was impossible to prepare transparent, thickness controlled films.

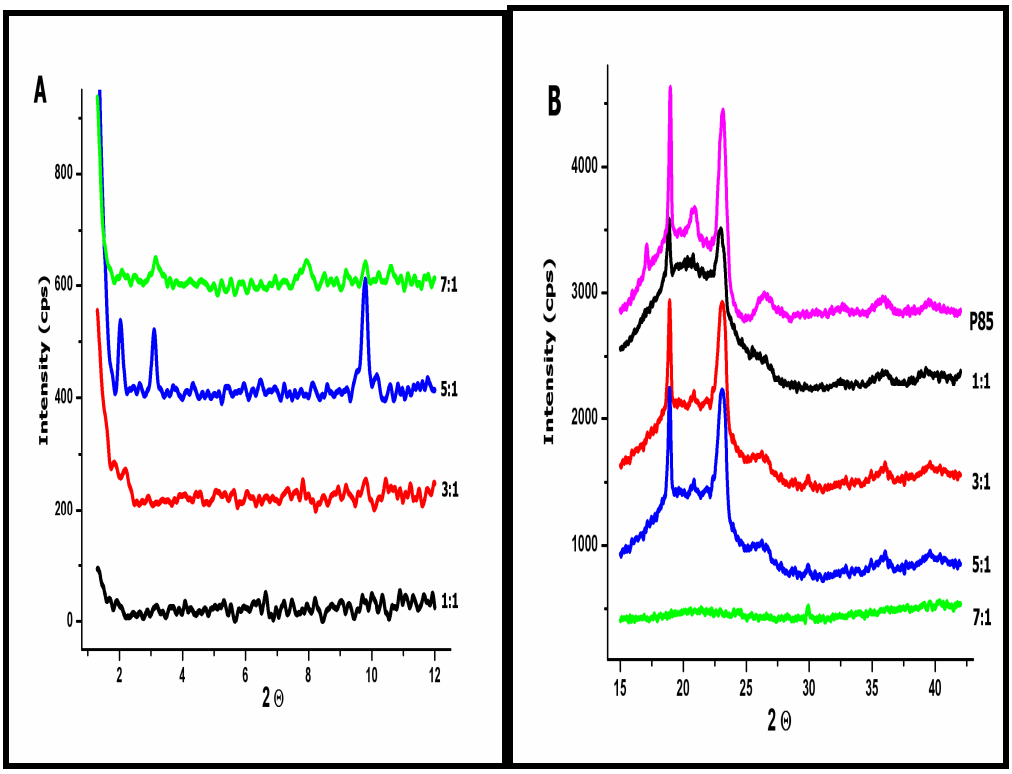

Figure 3.1.1: The XRD patterns of the $[Cd(H_2O)_4](NO_3)_2$:P85 film samples formed in the absence of free water at salt to surfactant mole ratios of; 1:1, 3:1, 5:1 and 7:1 **A)** small angle diffraction, **B)** high angle diffraction and P85.

To understand better if the high angle diffraction pattern is due to orientation of dominant free surfactant molecules or orientation of a LC mesophase, the thick film samples, prepared from the binary mixtures, were heated to around 50° C and cooled back to RT for several times to ensure homogenization. After several heating and cooling cycles, the high angle diffraction lines disappeared (Fig. 3.1.2). For that reason, we could conclude that the binary mixtures were not homogenized and the high angle diffraction lines originated from the prevailing free surfactant molecules in the mixture. If the high angle diffraction lines remained upon heating-cooling cycles, it would be reasonable to think that the diffraction lines were originated from the LC phase.

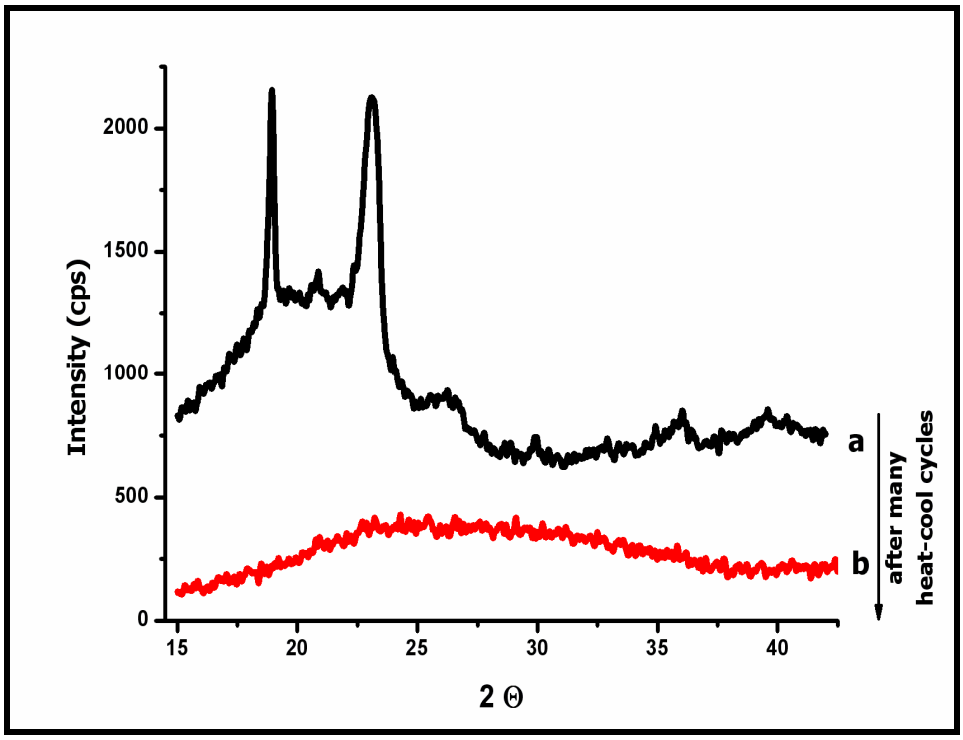

Figure 3.1.2: The XRD patterns of the $[Cd(H_2O)_4](NO_3)_2$:P85 film sample formed in the absence of free water at salt to surfactant mole ratio of 3:1 **a)** fresh sample, **b)** after many heat and cool cycles

In order to make the homogenization process easier, we first dissolved the TMS, $[Cd(H_2O)_4](NO_3)_2$, in 0.2 g distilled water and then, mixed with P85 and simply shaked at 50° C for a few days. Ternary system (water:salt:P85) provided homogenization process taking less time. The thick film samples prepared from those mixtures gave more intense small angle X- ray diffractions, showing us the presence of more oriented samples (Fig. 3.1.3.A). However, the high angle XRD pattern (Fig. 3.1.3.B) still had the intense diffraction lines which mean that the mixtures were still not homogenized enough in the presence of 0.2 g free water. In addition, it was still problematic to prepare transparent, thickness controlled films because the mixtures were still gel – like solutions.

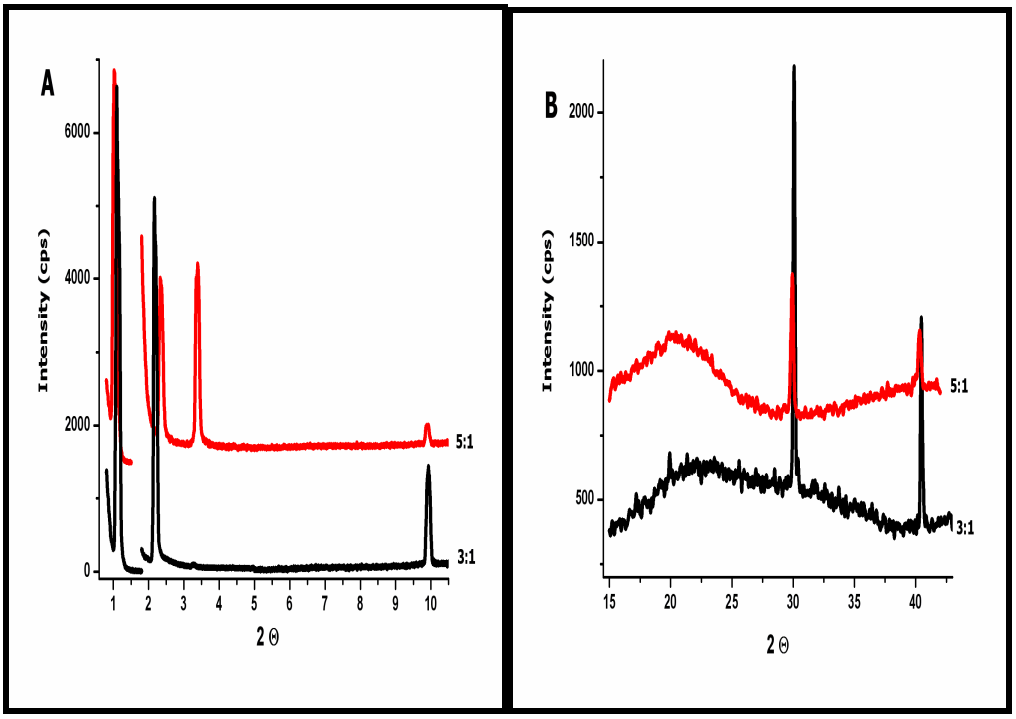

Figure 3.1.3: The XRD patterns of the $[Cd(H_2O)_4](NO_3)_2$:P85 film samples formed in the presence of 0.2g water at 50° C at salt to surfactant mole ratio of 3:1 and 5:1 **A)** small angle diffraction, **B)** high angle diffraction

Therefore, we increased the amount of solvent from 0.20 g distilled water up to 10.0 g distilled water to dissolve the salt and pluronic. By the addition of 10.0 g water as a solvent, it was sufficient to stir the solutions by a magnetic stirrer at RT for two days. The thin film samples could easily be prepared from those clear solutions by dip coating or spin coating on glass slides at different speeds of coating or by casting on the glass slides depending on the desired thickness. That means it was easier to prepare the transparent, more oriented, thickness controlled films from those liquid like ternary mixtures. Those films gave more intense small angle XRD pattern (Fig. 3.1.4.A) and no high angle XRD line (Fig. 3.1.4.B) showing the homogeneity of the mixtures. Increasing the amount of solvent provided shortening the time of homogenization process and avoiding heating samples at 50° C for days. For the time being, it is reasonable to avoid the mixtures from heating over RT, because their phase diagrams haven` t been established yet in contrast to the case of

many oligo(.ethylene oxide) – type surfactants. Note that the LLC properties and the phase diagrams of many oligo(ethylene oxide) – type surfactants, have been found out in water [50,106] and in the presence of alkali metal salts. [107-108]

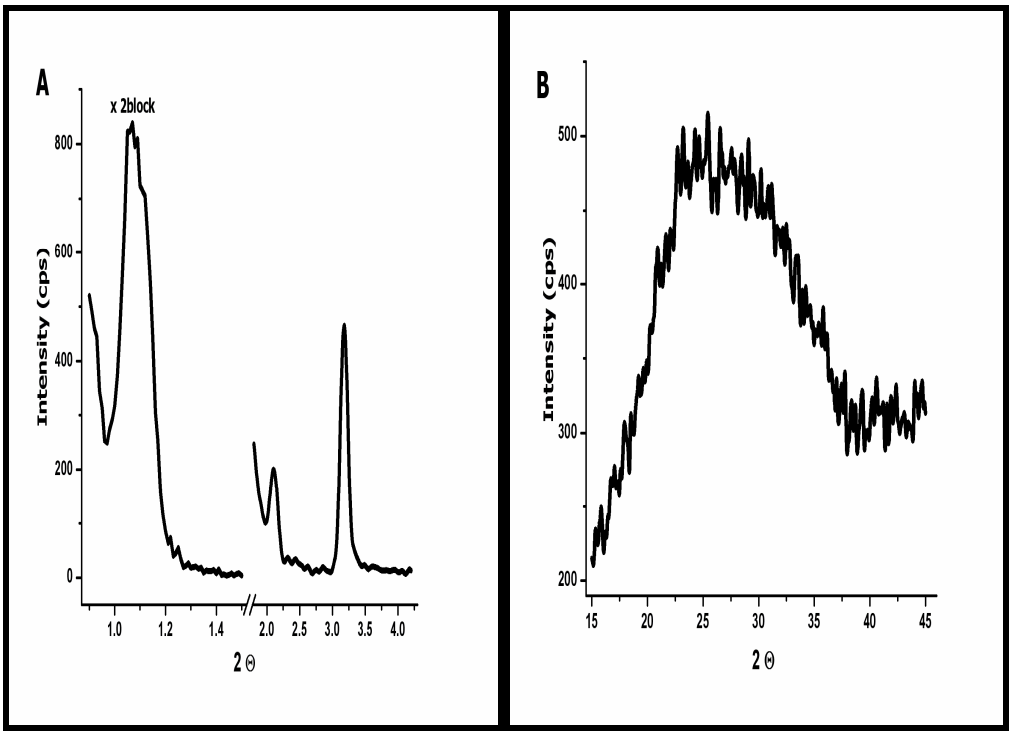

Figure 3.1.4: The XRD pattern of $[Cd(H_2O)_4](NO_3)_2$:P85 thin film sample formed in the presence of 10.0 mL of distilled water at RT at the mole ratio of salt to surfactant 7:1 **A)** small angle diffraction, **B)** high angle diffraction

As explained above, formation of LC phase is mediated by the coordinated water molecules of TMS through hydrogen bonding with the polar regions of pluronics. Hence, a solvent is required just to make the homogenization process easier. The solvent molecules (H_2O) evaporate when the thin films are formed. For that reason, we could change the solvent from water to ethanol or to acetone. Instead of distilled water, when we used 10.0 mL ethanol as a solvent, overnight stirring with a magnetic stirrer was enough to homogenize the ternary mixtures at RT instead of two days of stirring. The solutions prepared in the range of mole ratio

of salt to pluronic, $[Cd(H_2O)_4](NO_3)_2$:P85, 1:1 – 20:1, in 10.0 mL ethanol stirred at RT with a magnetic stirrer overnight were used to prepare the thin film samples by 2000 rpm spin coating and dip coating with a coating speed of 0.4 mm/s over a glass, quartz or silicon substrates for various measurements. Figure 3.1.5 shows the XRD patterns of the thin film samples of the LC $[Cd(H_2O)_4](NO_3)_2$:P85 mesophases in the salt to pluronic mole ratio range of 3:1 to 20:1 prepared by dip coating method over glass substrates. As seen, the mesophase appears at a $[Cd(H_2O)_4](NO_3)_2$ to P85 mole ratio of around 3 and stable up to a mole ratio of around 11, at higher mole ratios of salt there is no LC mesophase observed in the XRD pattern. The XRD pattern of those thin film samples didn't show any shift to higher or lower angles (not shown), that means the LC mesophases are stable for months.

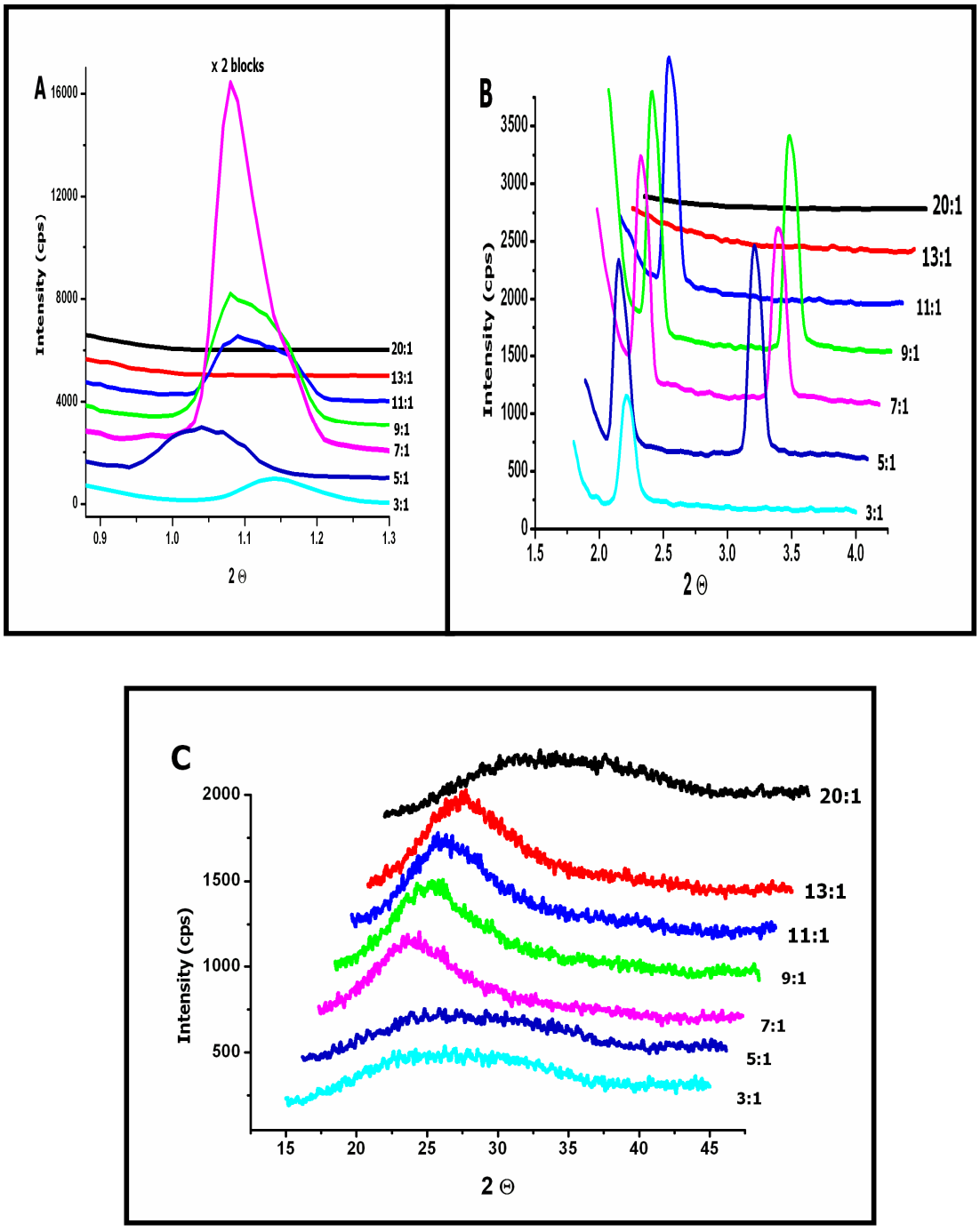

Figure 3.1.5: The XRD pattern of the $[Cd(H_2O)_4](NO_3)_2$:P85 thin film samples formed in the presence of 10.0 mL of pure ethanol at RT in the mole ratio range of salt: surfactant; 3:1 – 20:1 **A)** small angle diffraction (with ~100 times lower intensity), **B)** small angle diffraction, **C)** high angle diffraction.

X–ray diffraction (XRD) method has been used mainly to identify the structure and degree of order of the LC mesophases. The XRD method is a powerful technique in analyzing the structure of mesophases. The principle is that the X – rays are reflected from the parallel lattice planes having d – spacing, so a diffraction line is the result of constructive interferences of the reflected beams as formulated by Bragg` s law given below;

$$n\lambda = 2d \sin \Theta$$

In general, the LC mesophases have diffraction line at small angles, between 1° and 10°, 2Θ and they mostly have 2D or 3D hexagonal and lamellar type structures. The LC mesophases studied in this work have a 3D hexagonal structure. For the 3D hexagonal structure, the d spacing and (*hkl*) planes (h, k, l are the reflection indices) are related with the following formula:

$$\mathbf{1/d^2 = 4/3(h^2 + hk + k^2)/a^2 + l^2/c^2}$$

That could be reduced to;

$$\mathbf{d = (8a/ (10.667(h^2 + hk + k^2) + 3l^2)^{1/2}}$$

by taking a *c/a* ratio of 1.633. The *d* spacing versus $(8/ (10.667(h^2 + hk + k^2) + 3l^2)^{1/2}$ plot has a linear correlation and slope of this plot gives ***a*** parameter with a zero intercept. Figure 3.1.6 displays a plot of relation between d spacing values of the diffraction lines which can be indexed as the (100), (002), (101), (112) , (114), (300) and (400) reflections of $P6_3/mmc$ space group of the 3D hexagonal mesophase with unit cell parameters of ***a*** is 99.5 Å and ***c*** is
162.5 Å.

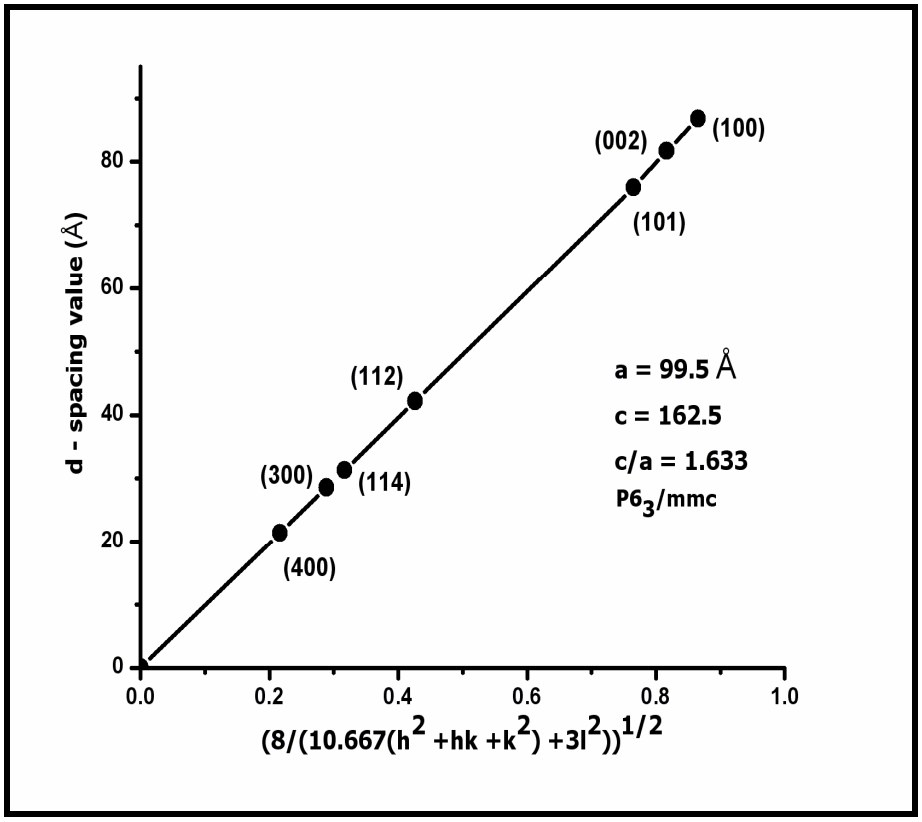

Figure 3.1.6: A plot of linear relation between *d*-spacing and $(8/ (10.667(h^2 + hk + k^2)/a^2 + 3l^2)^{1/2}$ of the LC $[Cd(H_2O)_4](NO_3)_2$:P85 thin film sample with a 7.0 mole ratio.

Figure 3.1.7 shows a characteristic 3D hexagonal XRD pattern with 7 diffraction lines between 1.0 and 5.0, 2Θ range, indexed to (100), (002), (101), (112), (300) and (400) lines at 86.8, 81.7, 76, 42.2, 31.3, 28.6 and 21.5 Å d spacings, respectively. This film was prepared from the mixture of $[Cd(H_2O)_4](NO_3)_2$ and P85 with a mole ratio of 7.0 by stirring on a magnetic stirrer in 10.0 mL acetone at RT for one hour. Then, the film was prepared by spin coating method on a glass substrate at 2000 rpm. Even though the films prepared with 10.0 mL water or ethanol, as described above, had the 3D hexagonal mesophase, their films gave the XRD patterns with some diffraction lines missing due to less order of the sample. Therefore, we can conclude that preparation conditions such as type and amount of solvent, duration of stirring, spinning rate of the film, thickness of the film, seriously influence the order of the thin films. The optimum conditions that

we defined so far are those stirring the mixture of $[Cd(H_2O)_4](NO_3)_2$ and P85 in 10.0 mL acetone for an hour at RT, then coating the substrates by ~2.0 mL solution at 2000 rpm for 30 seconds. The film samples prepared at those conditions usually form highly ordered LC mesophases.

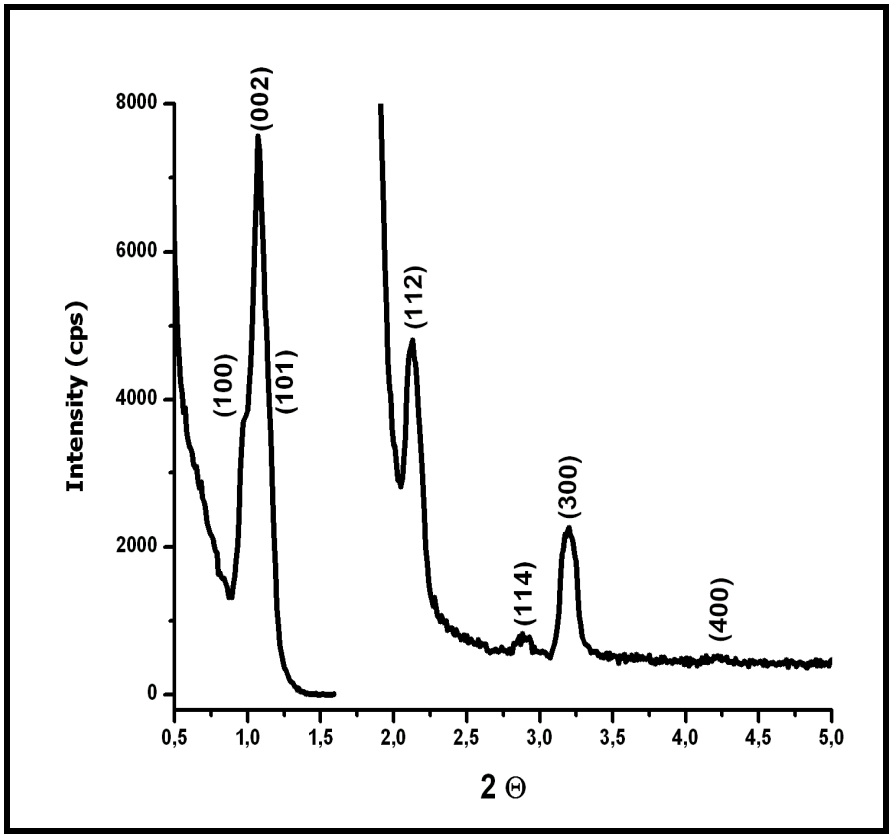

Figure 3.1.7: The XRD pattern of the LC $[Cd(H_2O)_4](NO_3)_2$:P85 thin film sample with salt to surfactant mole ratio of 7.0.

3.2. Synthesis of Mesostructured CdS Films

The small and high angle XRD patterns of CdS samples are given in Figure 3.2.1. These samples were prepared from the thin films of LC phase formed at mole ratios of $[Cd(H_2O)_4](NO_3)_2$: P85 in the range of 5:1 to 20:1. The thin films of the LC phase were prepared by dip coating method over glass substrates, Figure 3.1.5. The CdS samples were prepared upon exposing those thin films to 350 – 400 torrs H_2S gas in an evacuated reaction chamber for 15 minutes. Reaction of $[Cd(H_2O)_4]^{2+}$ ions with H_2S gas is too fast so that the thin films turn yellow as soon as they are exposed to H_2S gas. However, we leave the films to react with H_2S gas at least for 15 minutes to ensure that all $[Cd(H_2O)_4]^{2+}$ ions are converted into CdS. As we see in Figure 3.2.1, the CdS samples obtained from samples of 5, 7, 9 and 11:1 salt:P85 mole ratios give broad and weak diffraction line at around 1 – 1.5 °, 2Θ; however, those with 13 and 20 mole ratios don` t give any diffraction line. Note that the thin films with 5, 7, 9 and 11 mole ratios have highly ordered hexagonal mesostructure before H_2S reaction. During CdS formation, they somehow retain the structure but since the CdS samples are very thin and the mesostructured structure is still not ordered enough, they give weak and broad diffraction line. On the other hand, the CdS samples obtained from the samples with 13 and 20 mole ratios don` t have ordered structure as expected because at those concentrations, there is no mesostructure formation in the LC phase at all.

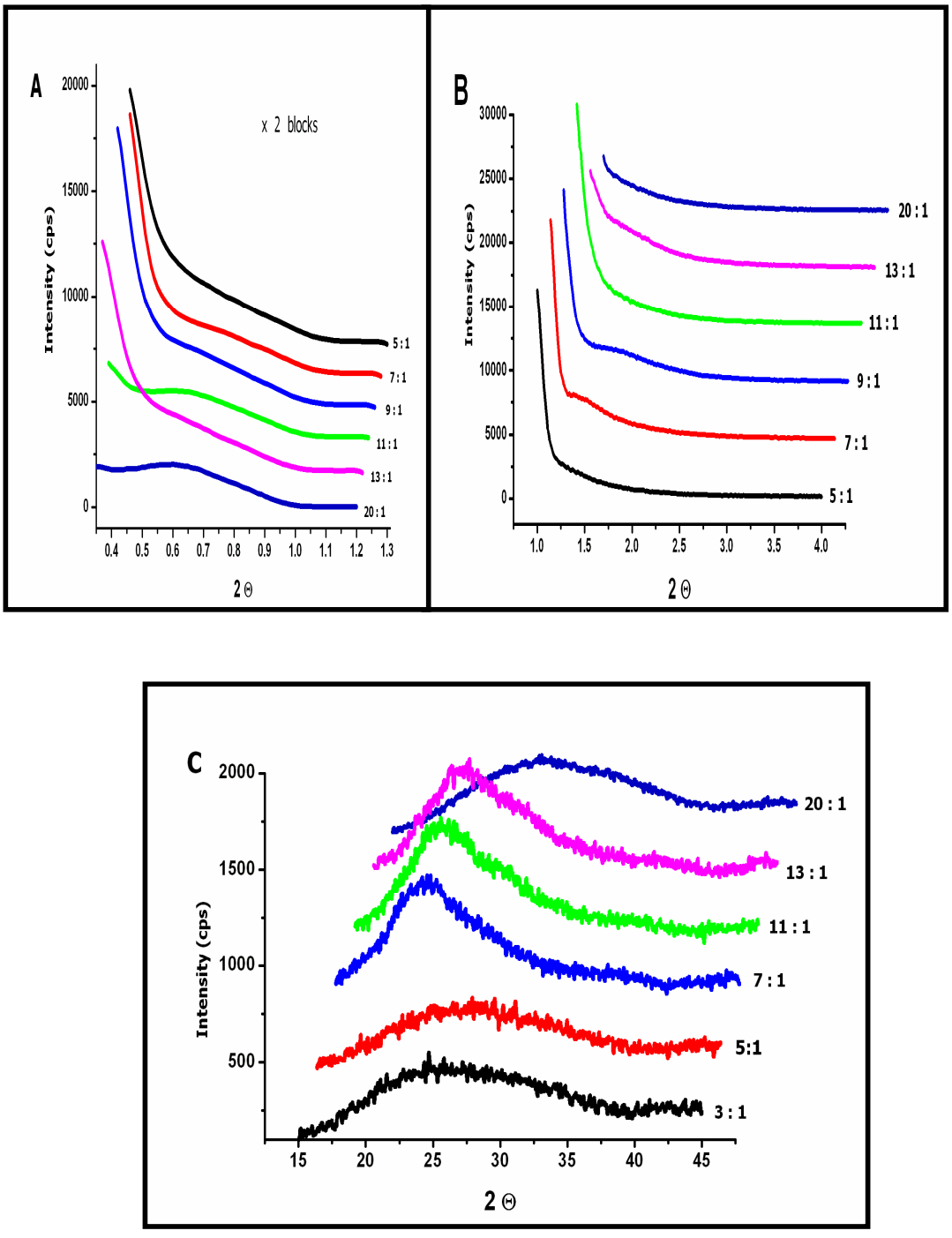

Figure 3.2.1: The XRD pattern of the fresh CdS samples prepared from the LC thin film samples at $[Cd(H_2O)_4](NO_3)_2$: P85 mole ratios of 3, 5, 7, 9, 11, 13 and 20:1. **A)** small angle diffraction (with ~100 times lower intensity), **B)** small angle diffraction, **C)**high angle diffraction.

The high angle XRD pattern of the CdS sample synthesized from the thin film of $[Cd(H_2O)_4](NO_3)_2$: P85 with 20:1 mole ratio was recorded in order to obtain structure and unit cell parameters of the CdS nanocrystals (Fig. 3.2.2). The relatively thicker film was prepared on silicon (Si) wafer so that the diffraction lines could be observed clearly by improving signal to noise ratio. The Si(200) diffraction line detected at 32.96°, 2Θ, is used as a reference to obtain the correct diffraction angles. The diffraction lines due to (111), (220) and (311) planes of CdS are observed at 26.02°, 43.31°, and 51.45°, respectively. All the diffraction lines index well with *zinc blend* structure. The unit cell parameter ***a*** calculated is around **5.91 Å** using all diffraction lines and the following equation (eq. 3.2.1);

$$1/d^2 = (h^2 + k^2 + l^2)/a^2 \qquad \text{(eq.3.2.1)}$$

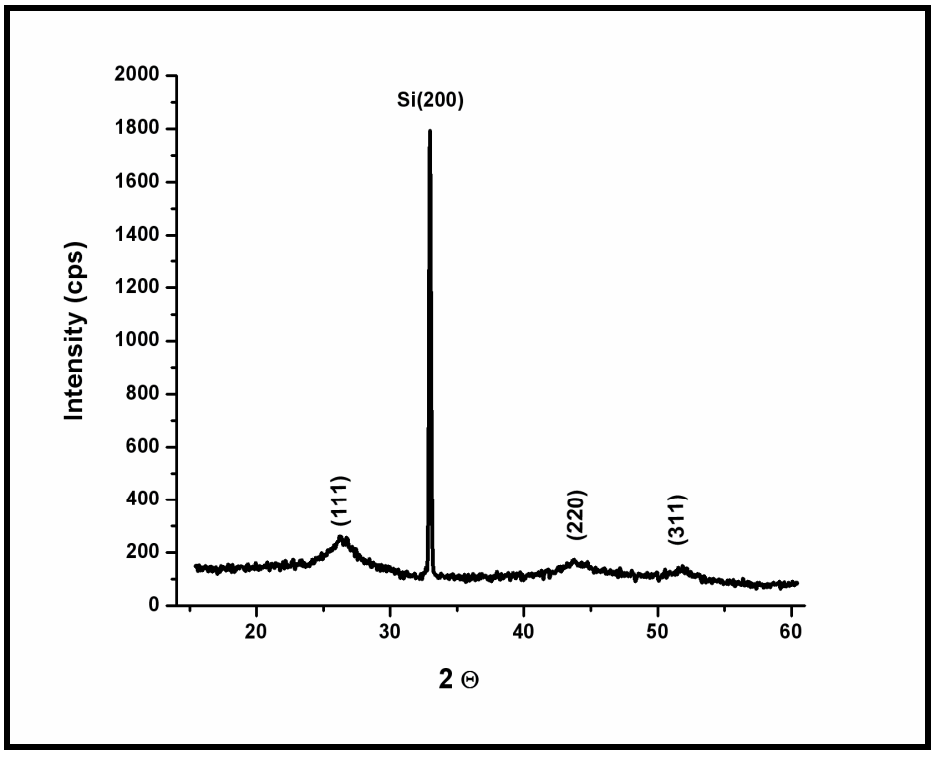

Figure 3.2.2: The high angle XRD pattern of CdS nanocrystals prepared from thin film of LC at $[Cd(H_2O)_4](NO_3)_2$: P85 mole ratio of 20: 1.

The XRD data also provides the particle size of the nanocrystals using the *Scherrer` s* formula,

$$\mathbf{D = 0.9\ \lambda / B\ cos\Theta}$$

where D is the diameter of the particles in Å, λ is wavelength of X – ray source, 1.54078 Å, B is the corrected full width at half maximum in radian, and Θ is half of the angle of diffraction of the (111) plane. The particle size of CdS nanocrystals obtained from *Scherrer` s* formula is around **4.3 nm**.

UV-Vis absorption spectroscopy is one of the most sensitive techniques to determine the optical band gaps of the semiconductor nanoparticles so that their size and changes in size can be calculated. The band gap values of semiconductor nanocrystalline materials are higher than semiconductor bulk values due to quantum confinement effect. The electronic absorption spectra of the H_2S treated samples in the mole ratio range of 1: 1 to 20: 1 were recorded in transmittance mode using thin films on quartz substrates (Figure 3.2.3). The UV-Vis absorption edge blue shifts in all samples compared to the bulk CdS absorption edge. Note that the bulk optical band gap of CdS is 2.42 eV at RT.[94] The blue-shift of the band gap is a clear indication that the mesostructured CdS is made of nanoparticles. Besides, the sharp absorption edge indicates that CdS nanoparticles have uniform size distribution. The band gaps for each sample were evaluated using the linear fit of the absorption edge after plotting the spectra against $(A^* h\upsilon)^2$ versus hυ given in Figure 3.2.4.[109] This relation is valid for direct band gap materials. Note that CdS is a direct-band gap semiconductor.

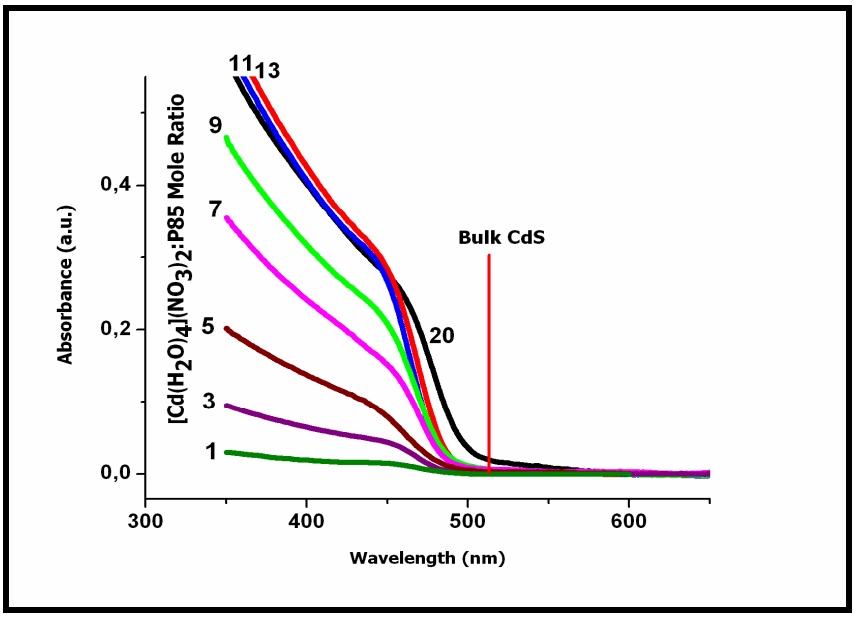

Figure 3.2.3: The UV-Vis absorption spectra of CdS thin films synthesized from the $[Cd(H_2O)_4](NO_3)_2$:P85 at mole ratios of 1, 3, 5, 7, 9, 11, 13 and 20 (stated on the spectra) samples.

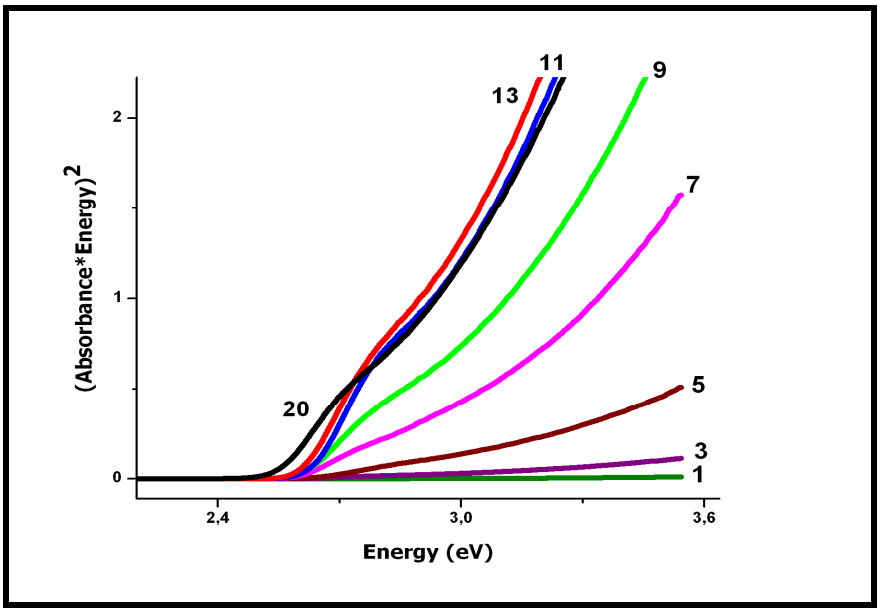

Figure 3.2.4: $(A*h\upsilon)^2$ versus $h\upsilon$ plots of the spectra of CdS thin films synthesized from the $[Cd(H_2O)_4](NO_3)_2$:P85 at mole ratios of 1, 3, 5, 7, 9, 11, 13 and 20 (stated on the spectra) samples.

There are different approaches to calculate the nanoparticle size from the band gap values.[110-112] We have used *Sarma* et.al.`s approach [111-112] to calculate the particle size of CdS, because this method has several advantages over other models, so that it provides a considerable enhancement in the accuracy of the results. Sapra and Sarma used the tight-binding (TB) model to evaluate the electronic structure of II-VI semiconductors in real space developed for the bulk II-VI semiconductors. Equation (3.2.2) has been obtained from the TB model that uses cation-anion and anion-anion interactions and experimental data points by Sarma et al. [112]

$$\Delta E_g = a_1 e^{-d/b1} + a_2 e^{-d/b2} \qquad \text{(eq. 3.2.2)}$$

The variation in the band gap difference ΔE_g between the bulk crystals and nanocrystals with the diameter (d) of the nanocrystals can be calculated from the empirical formula (3.2.2). The values of the parameters a and b used in equation 3.2.2 for all the $A^{II}B^{VI}$ semiconductors studied by tight-binding model were tabulated in Table 3.2.1. [112]

Table 3.2.1: Parameters of a and b used in equation (3.2.1) for ZnS, ZnSe, ZnTe, CdS, CdSe,and CdTe in tight-binding model.[112]

	ZnS	**ZnSe**	**ZnTe**	**CdS**	**CdSe**	**CdTe**
a_1	7.44	2.65	5.10	2.83	7.62	5.77
b_1	2.35	7.61	10.35	8.22	6.63	8.45
a_2	3.04	1.90	1.05	1.96	2.07	1.33
b_2	15.30	23.50	97.93	18.07	28.88	43.73

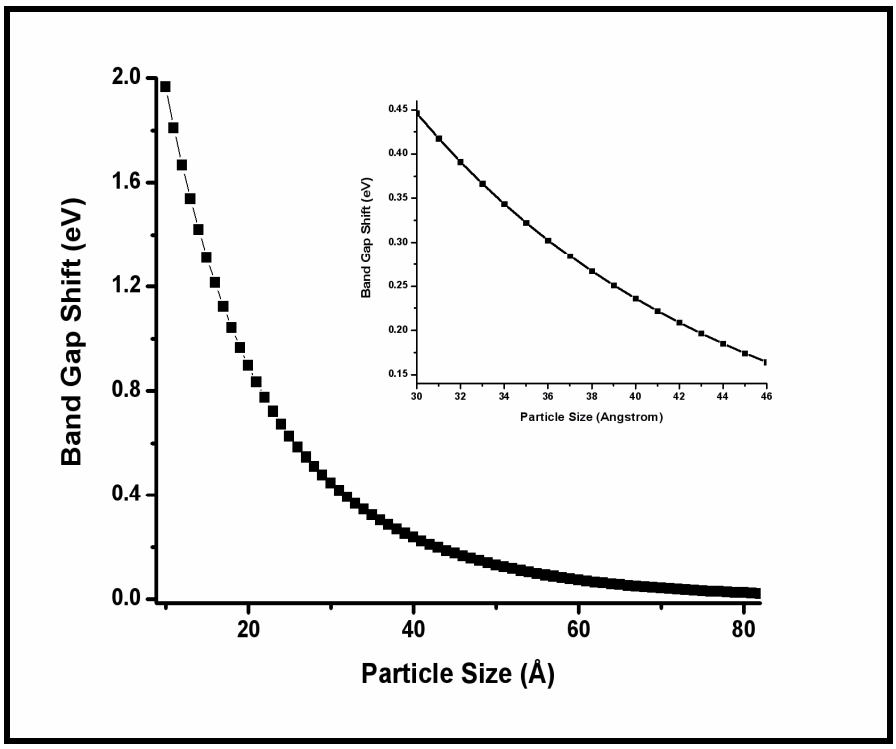

Figure 3.2.5: Plot of band-gap shift (ΔE_g) of CdS, obtained from empirical formula of equation (3.2.1), versus particle size (Å). The inset is the same plot showing the regions used in this work. [112]

The equation (3.2.2) provides band gap difference between the bulk and nanosized semiconductors of ZnS, ZnSe, ZnTe, CdS, CdSe and CdTe in the diameter (*d*) range of 5 to 80 Å. Figure 3.2.5 shows a plot of the band gap shift versus particle size, in a range of 5 to 80 Å by using *a* and *b* parameters of CdS in Table 3.2.1. Above 8-10 nm, the nanoparticles behave like bulk materials. The inset in Figure 3.2.5 shows the interval of 0.15-0.45 eV, in which all band gap differences from our samples are located. Using the plot, we calculated the particle size of the CdS nanoparticles as around 4.1- 4.4 nm (Table 3.2.2). Given in the table 3.2.2, in the $[Cd(H_2O)_4](NO_3)_2$: P85 mole ratio range of 1:1-13:1, CdS nanoparticles formed almost the same size, but, at higher concentrations like 20 were larger.

Table 3.2.2: Band gap (eV) and particle size (nm) values of CdS at mole ratio $[Cd(H_2O)_4](NO_3)_2$: P85 range of 1:1 to 20:1. Calculated from absorption spectra using *Sarma` s* approach.

$[Cd(H_2O)_4](NO_3)_2$: P85 mole ratio	**Band Gap (eV)**	**Particle Size (nm)**
1	2.60	4.4
3	2.63	4.3
5	2.64	4.1
7	2.61	4.3
9	2.60	4.4
11	2.62	4.3
13	2.60	4.4
20	2.56	5.0

The intensities at 438 nm versus mole ratio plot of the CdS films obtained from the $[Cd(H_2O)_4](NO_3)_2$: P85 mole ratio between 1:1 and 20:1 is given in Figure 3.2.6. The plot showed an s – shape deviation. The absorbance of CdS thin films linearly increase depending on the salt to pluronic mole ratio in the range of 3:1 to 11:1. However, at mole ratios below 3:1 and above 11:1, there are deviations from linearity. The intensity deviate 3.5% at 1:1 mole ratio, 5.4% at 13:1 mole ratio and 30% at 20:1 mole ratio. Notice that, in the regions where the plot deviates from linearity, there is no LC mesophase and the ions are in a disordered media.

The CdS films emit light under UV irradiation. Under 320 nm wavelength, films emit weakly orange at mole ratios 1, 3, 5, 11, 13, 20 and strongly orange at

mole ratios 7, 9. Under 280 nm wavelength, they emit weakly white at mole ratios 1, 3, 5, 11, 13, 20 and strongly orange at mole ratios 7, 9.

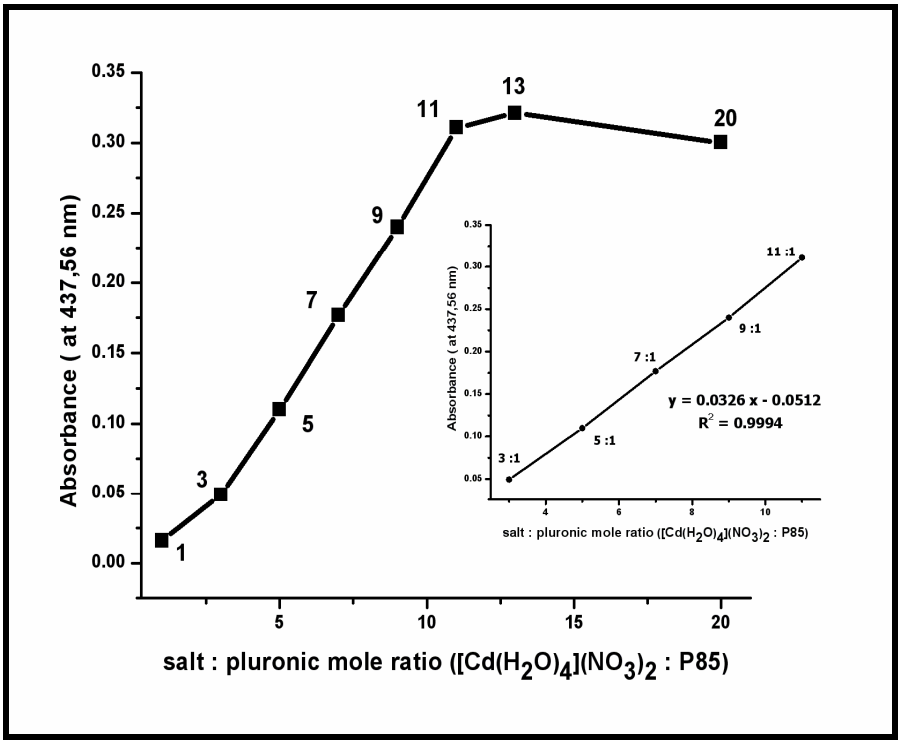

Figure 3.2.6: Absorbance values of CdS films at 437.56 nm in the $[Cd(H_2O)_4](NO_3)_2$:P85 mole ratio range of 1:1 to 20:1. The inset shows the linear dependence of absorbance of CdS films on mole ratio in the range of 3:1 to 11:1.

From the absorption spectra of CdS film samples, it was determined that the mesostructured CdS films are made of nanoparticles with almost same size at all mole ratios and those nanoparticles are organized into a mesostructure except at mole ratios higher than 13:1. Furthermore, there is a linear dependence of the absorbance in the $[Cd(H_2O)_4](NO_3)_2$: P85 mole ratio range of 3:1 to 11:1 and the XRD pattern of their LC phase in that range show that there is mesostructure in this region with the same structure. Therefore, this is a clear indication that in the mole ratio range of 3:1 to 11:1, the mesostructure is retained somehow during CdS formation and only the amount of $[Cd(H_2O)_4]^{2+}$ increases as the salt concentration increases with no effect on the structure.

3.3. Mesostructured Cracked and Dendritic CdS Thin Films

Our data support the idea that if the CdS particles are formed in the LC phase prepared from the metal aqua complex $[Cd(H_2O)_4](NO_3)_2$ and pluronic P85, there is more chance to prepare thin films of the mesostructured CdS.

In Figure 3.3.1, optical images of mesostructured CdS thin films prepared from $[Cd(H_2O)_4](NO_3)_2$: P85 LC phase at 7: 1 mole ratio are given. Observed cracks and wrinkles form upon reaction of H_2S gas with LC phase and they are significant evidence of formation of thin films. Note that the formation of thin films causes the release of stress which results in the form of cracks or wrinkles as a response.

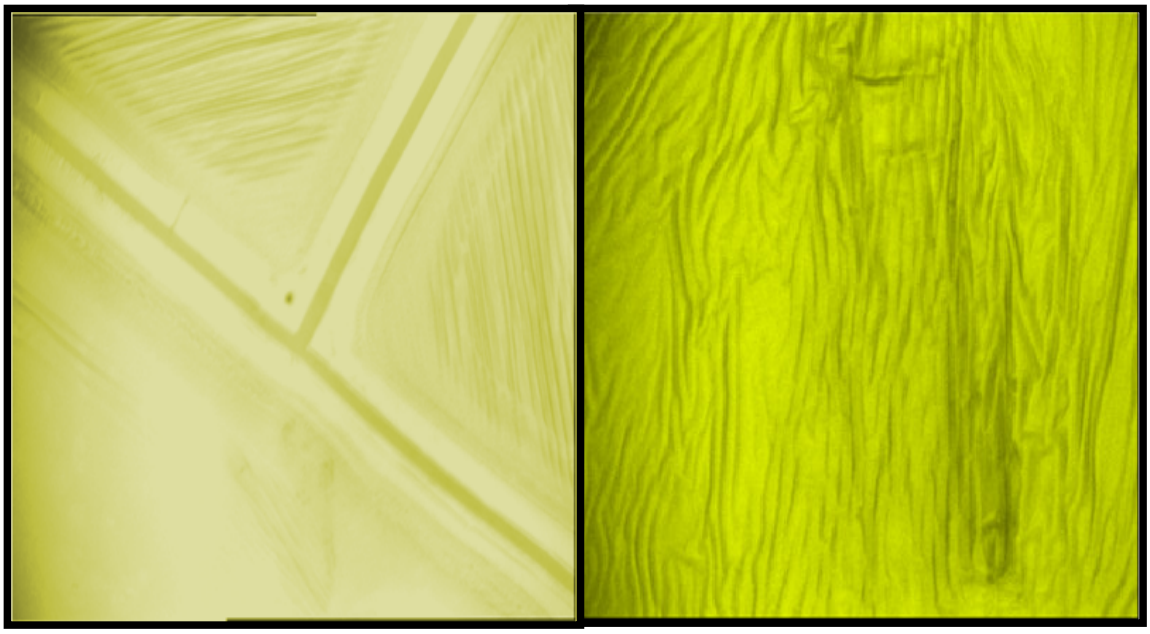

Figure 3.3.1: Optical microscopy images of cracked CdS thin films prepared from thin films of $[Cd(H_2O)_4](NO_3)_2$:P85 at mole ratio of 7: 1.

It seems that the thin films, around 100 nm thicknesses, could retain the order of LC phase during H_2S gas reaction as seen from their XRD patterns given in Figure 3.3.2. Formation of cracks and high order XRD pattern are the strong evidences of formation of the thin films of mesostructured CdS. Besides, they are very stable and retain their diffraction pattern for a month without any decrease in their intensity. However, we couldn't yet success in optimizing conditions for formation of well ordered CdS thin films. Further work is needed to find out the experimental conditions in detail. On the other hand, normal CdS samples which don't have cracks give broad and weak diffraction line at around 1–1.5°, 2Θ compared to the XRD patterns of those cracked CdS thin film samples. They still might form the CdS thin films, however, since they are very thin and not so well ordered as cracked films, the XRD analysis might not be enough to verify what they are. Therefore, we need Transmission Electron Microscopy (TEM) images or AFM or SEM images with nanometer resolution.

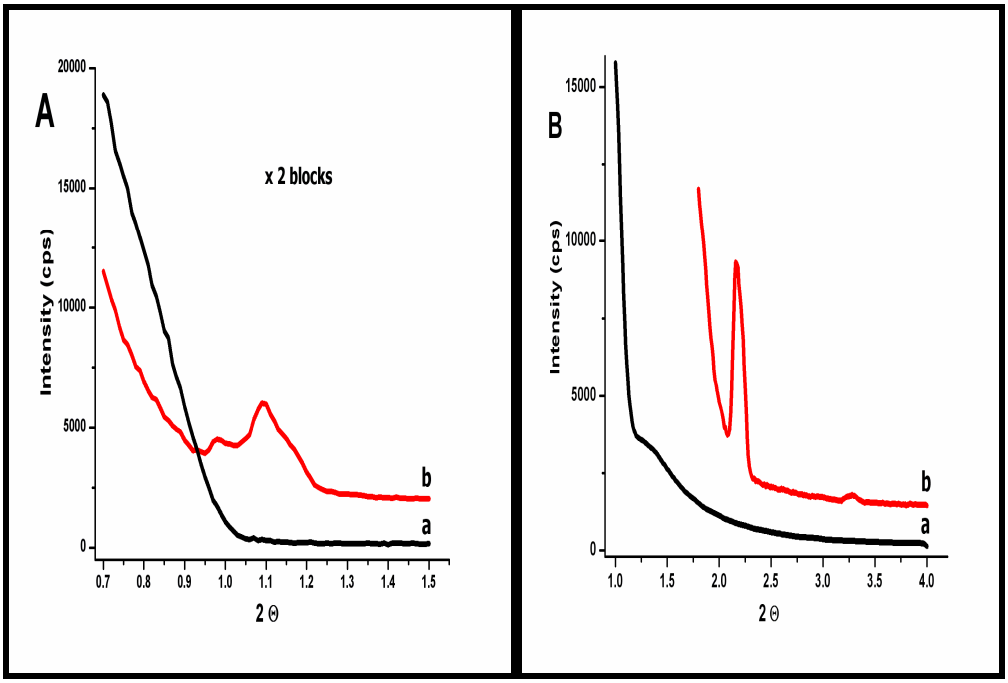

Figure 3.3.2: The XRD pattern of relatively less ordered CdS thin film and more ordered cracked CdS thin film **A)** small angle diffraction (with ~100 times lower intensity) **B)** small angle diffraction of **a)** normal thin film of CdS **b)** cracked thin film of CdS. Synthesized from $[Cd(H_2O)_4](NO_3)_2$: P85 at 7:1 mole ratio.

FT – IR and Micro –Raman spectra were obtained in order to determine structural changes in the LC phase before and after H_2S gas exposure. Effect of the formation of CdS on the LC phase is shown in Figure 3.3.3. The splitted NO_3^- signals at around 1300 – 1460 cm^{-1} loses its intensity. This indicates that during the reaction of the Cd(II) ions with H_2S gas, NO_3^- counter ion becomes free and solvated due to the free water produced. In addition, NO_3^- signal at around 810 cm^{-1} loses its intensity as well. In addition, in micro – Raman spectra given in Figure 3.3.3.B, the NO_3^- signal at around 1030 cm^{-1} loses its intensity when the Cd(II) ion reacts with H_2S gas for formation of both normal and cracked CdS thin films. Those show that NO_3^- counter ion loses the ion pair interaction with the metal complex and becomes a free ion. From all these results, we can be at least sure that $[Cd(H_2O)_4]^{2+}$ ions are converted to CdS and the coordinated NO_3^- counter ions become free and don`t coordinate back to the Cd^{2+} ions for a long time as observed from FT-IR and micro – Raman spectrum obtained (not shown) after 1 day for cracked thin films of mesostructured CdS as for normal thin films. Therefore, it can be concluded that the high order observed by XRD in the cracked thin films of mesostructured CdS is not due to any unreacted LC phase. Rather, it results from the ordered mesostructured CdS films.

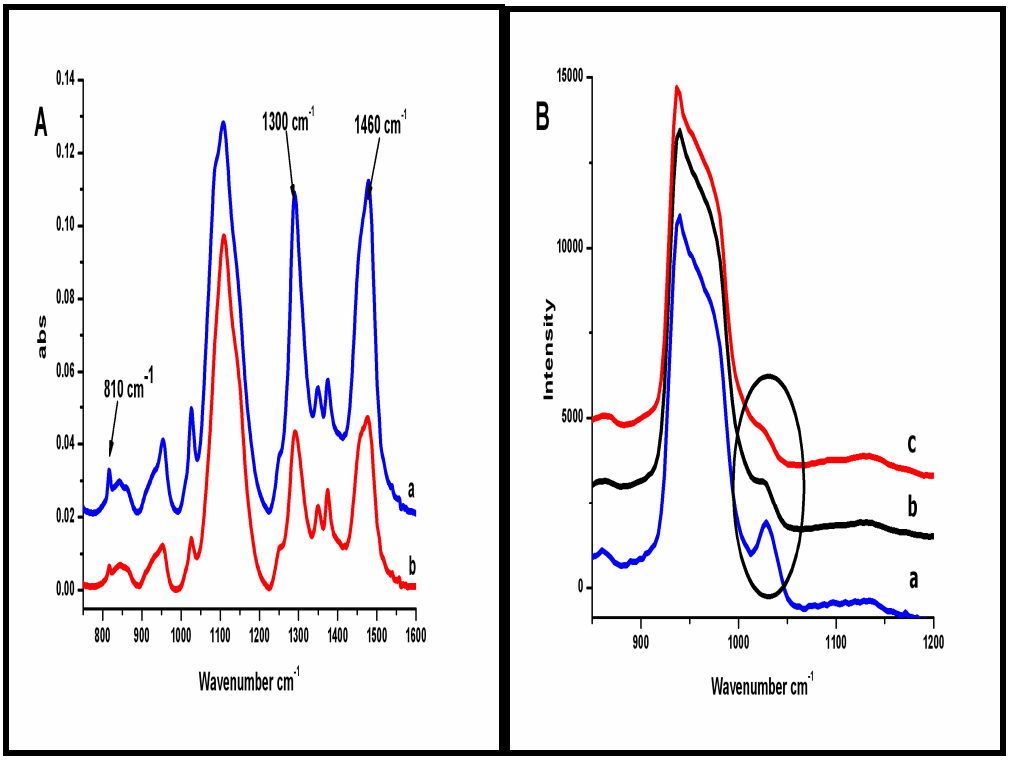

Figure 3.3.3: A) FT – IR spectra; **B)** Micro – Raman spectra of **a)** thin film of LC phase at 7: 1 mole ratio of $[Cd(H_2O)_4](NO_3)_2$:P85, **b)** the cracked thin film of the mesostructured CdS, **c)** the normal thin film of the mesostructured CdS.

The band-gap values of the CdS in normal and cracked thin films were evaluated to be between 2.53 and 2.62 eV. Figure 3.3.4 shows the absorption spectra of normal and cracked thin films of CdS that display a red shift in the absorption edge going from normal film to cracked film of CdS. This trend indicates that CdS nanoparticles grow further while cracked thin films form.

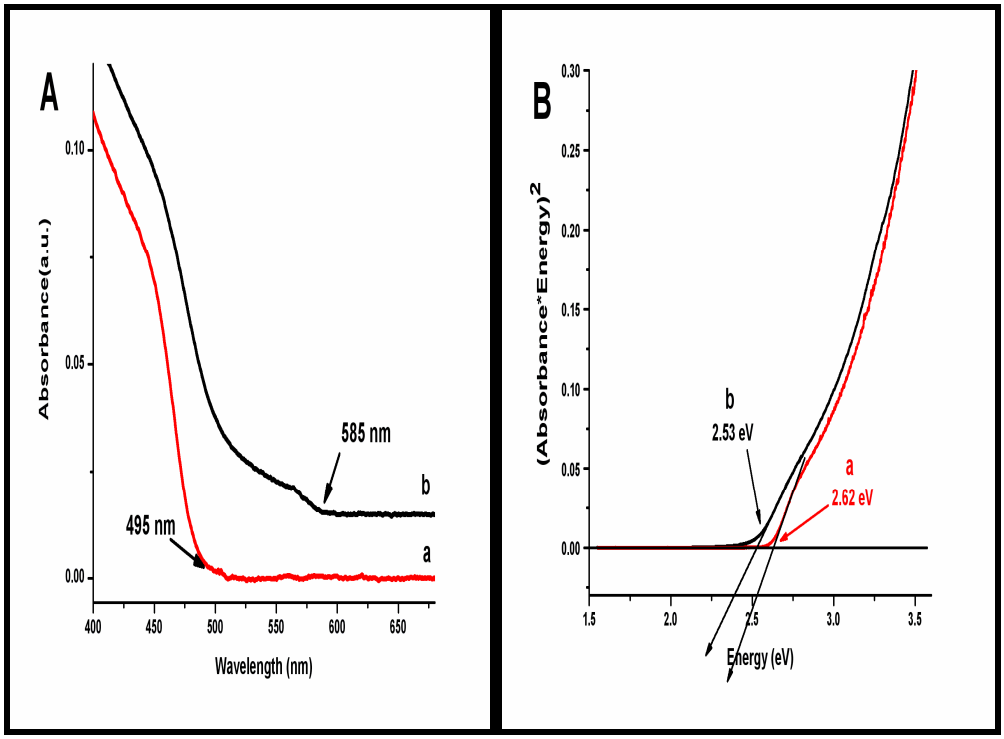

Figure 3.3.4: A, B) UV-Vis absorption spectra of **a)** the normal thin film of the mesostructured CdS, **b)** the cracked thin film of the mesostructured CdS. Synthesized from $[Cd(H_2O)_4](NO_3)_2$:P85 at 7:1 mole ratio.

It was also observed that both the cracked and normal thin films of those mesostructured metal sulfides (MS) formed dendritic structures in time. SEM images of fresh and old CdS thin films are given in Figure 3.3.5. Figure 3.3.5.A is the SEM image of a fresh CdS thin film with 1 µm scale bar. This CdS sample was prepared by exposing the LC thin film to 350 torrs H_2S gas for 15 minutes. This sample is quite a homogenous film and there is no formation of domains of surfactant or CdS nanocrystals whatsoever. However, dendritic structures form at different sides of the film sample over time and grow further until they cover almost the entire film sample, as seen in Figure 3.3.5.B and C. In the older films such as those around 10 days old, dendritic structures start gathering and large domains form over the entire sample (see Figure 3.3.5.D). These domains are still homogenous. However, when the LC thin films are exposed to H_2S gas at a very low pressure such as 10 torr for a longer time such as 2 hours in the closed

evacuated reaction chamber and if the film sample is thin enough and if the LC is prepared by a volatile solvent such as acetone, ethanol or methanol, formation and growth of dendritic structures become much faster so that they can even cover all the entire sample during 2 hours H_2S reaction. Hence, by changing H_2S gas pressure and the reaction time, the thickness of the film, type of solvent, and rate of formation, the growth of dendritic structures can be controlled.

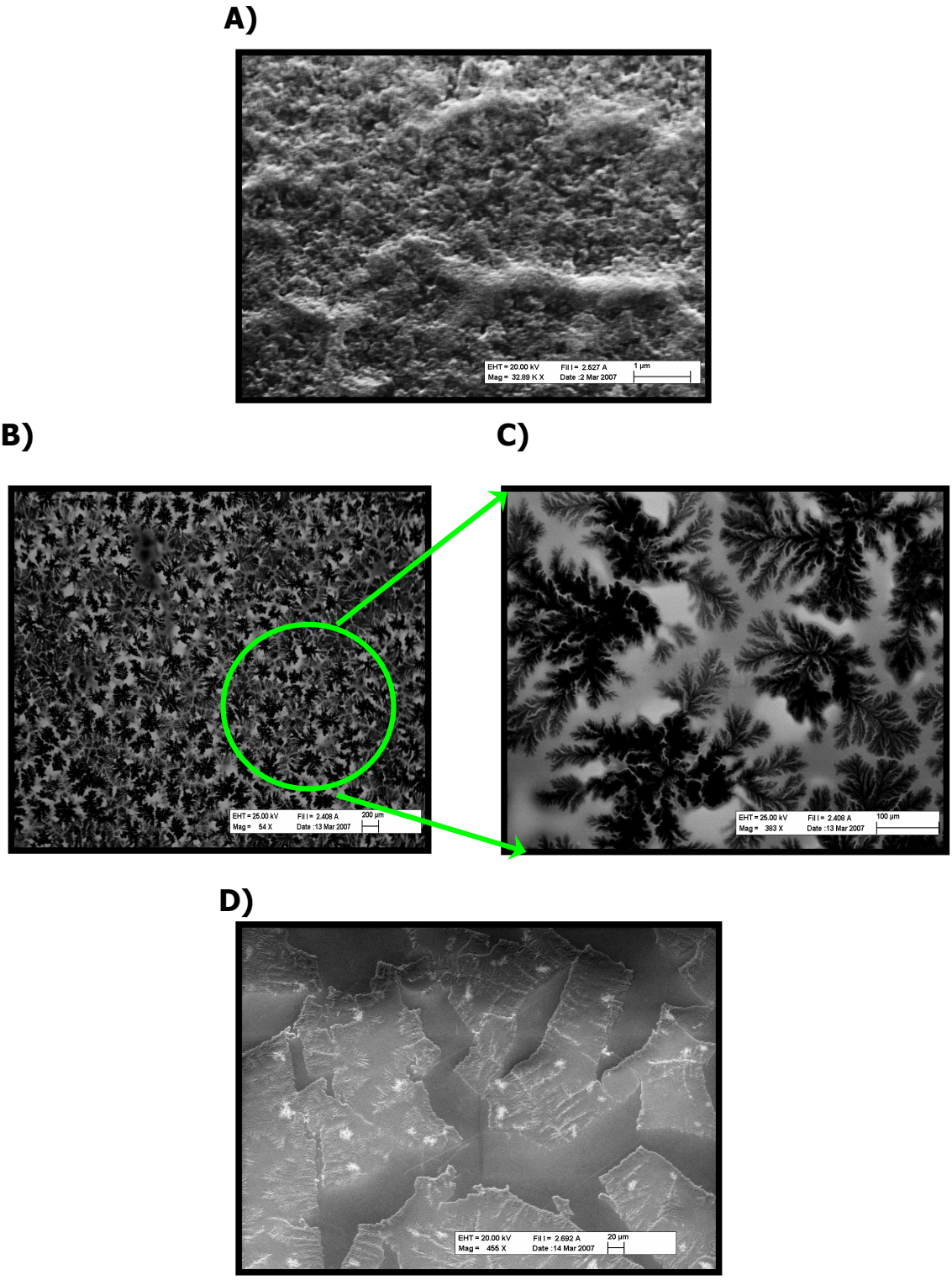

Figure 3.3.5) The SEM images of **A)** fresh with a 1 µm scale bar , **B)** with 200 µm scale bar **& C)** 5 days old with 100 µm scale bar, and **D)** 2 weeks old with 20 µm scale bar CdS thin films.

The FT-IR spectra of 7:1 mole ratio $[Cd(H_2O)_4](NO_3)_2$: P85 thin film sample before and after H_2S gas exposure, old CdS thin films, P85 and $[Cd(H_2O)_4](NO_3)_2$ dissolved in acetone are given in Figure 3.3.6. When the IR signals around 1300-1500 cm^{-1} and 800-1050 cm^{-1} are compared, the IR spectrum of the old CdS samples, in which the dendritic structures formed and covered almost all over the sample as seen in Figure 3.3.5.B, differ from the IR spectrum of the fresh CdS and become similar to the IR spectrum of P85. Besides, when compared to IR spectrum of $[Cd(H_2O)_4](NO_3)_2$, it can be said that those dendritic structures are not due to $[Cd(H_2O)_4](NO_3)_2$ crystals.

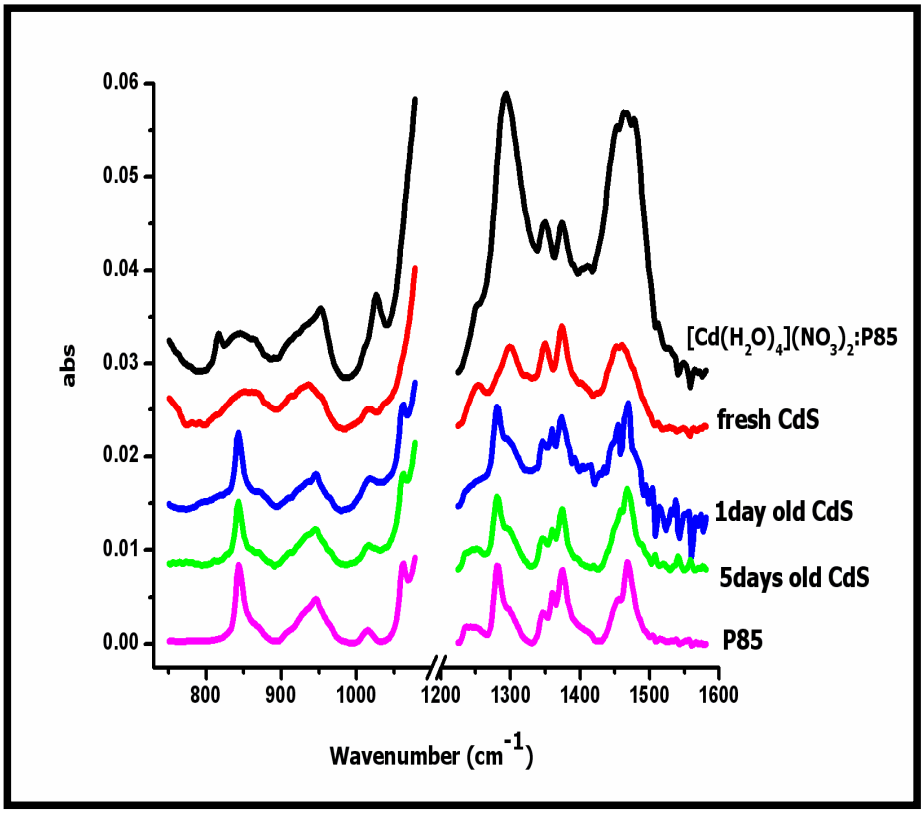

Figure 3.3.6) FT-IR spectra of 7:1 mole ratio $[Cd(H_2O)_4](NO_3)_2$:P85 thin film sample before and after H_2S gas exposure, old CdS thin films, P85 and $Cd(H_2O)_4](NO_3)_2$ dissolved in acetone.

The EDS mapping of the CdS thin film, synthesized using 7:1 mole ratio $[Cd(H_2O)_4](NO_3)_2$:P85 LC mesophase, collected for CdS, Cd, S and C are given in Figure 3.3.7. Figure 3.3.7.A indicates distribution of CdS nanoparticles as yellow colored in regions outside the dendritic structure. Figure 3.3.7.C and D are the images collected using X-rays originated from Cd and S, respectively. The color intensities and EDS intensities are almost the same indicating that the Cd and S source is CdS showing that all Cd(II) ions are reacted with H_2S gas forming the CdS nanocrystals. In Figure 3.3.7.E, yellow colored domains are due to excess of C species (most likely free P85 molecules). The yellow part forms the dendritic structure confirming the fact that the dendritic structures are formed by the free surfactant molecules. Therefore, the EDS maps are consistent with the FT-IR spectra given in Figure 3.3.6. The dendritic structures are formed by the separation of the free P85 molecules in the sample. At 7:1 mole ratio of TMS:P85, there is 3-4 times more P85 than required to form the mesostructured CdS. Note that the CdS samples synthesized from 20:1 or above mole ratios of $[Cd(H_2O)_4](NO_3)_2$:P85 do not form the dendritic structures. Since the samples, obtained from low metal concentration, are not rigid enough to prevent the flow of surfactant molecules or CdS nanocrystals, the free surfactant molecules phase separate into mesostructured CdS domains and dendritic domains (free P85). The defects in the LC samples seem like the proper nucleation sites to grow the dendrites further until they cover the entire sample, Figure 3.3.5.B. In time, those dendrites also combine and form the bigger domains as seen in Figure 3.3.5.D. Hence, the darker domains in Figure 3.3.5.D are due to those free surfactants and the lighter domains are due to the mesostructured CdS thin films. Those thin films are not continuous all over the sample; however, they are the first synthesized example of an ordered mesostructured (MS) thin films in the literature. Even though, the MS film samples have intense XRD diffraction at around 1.5º, 2Θ which is a good proof of the order in the mesostructure, the TEM or SEM images are needed to define clearly the structures of those MS thin films.

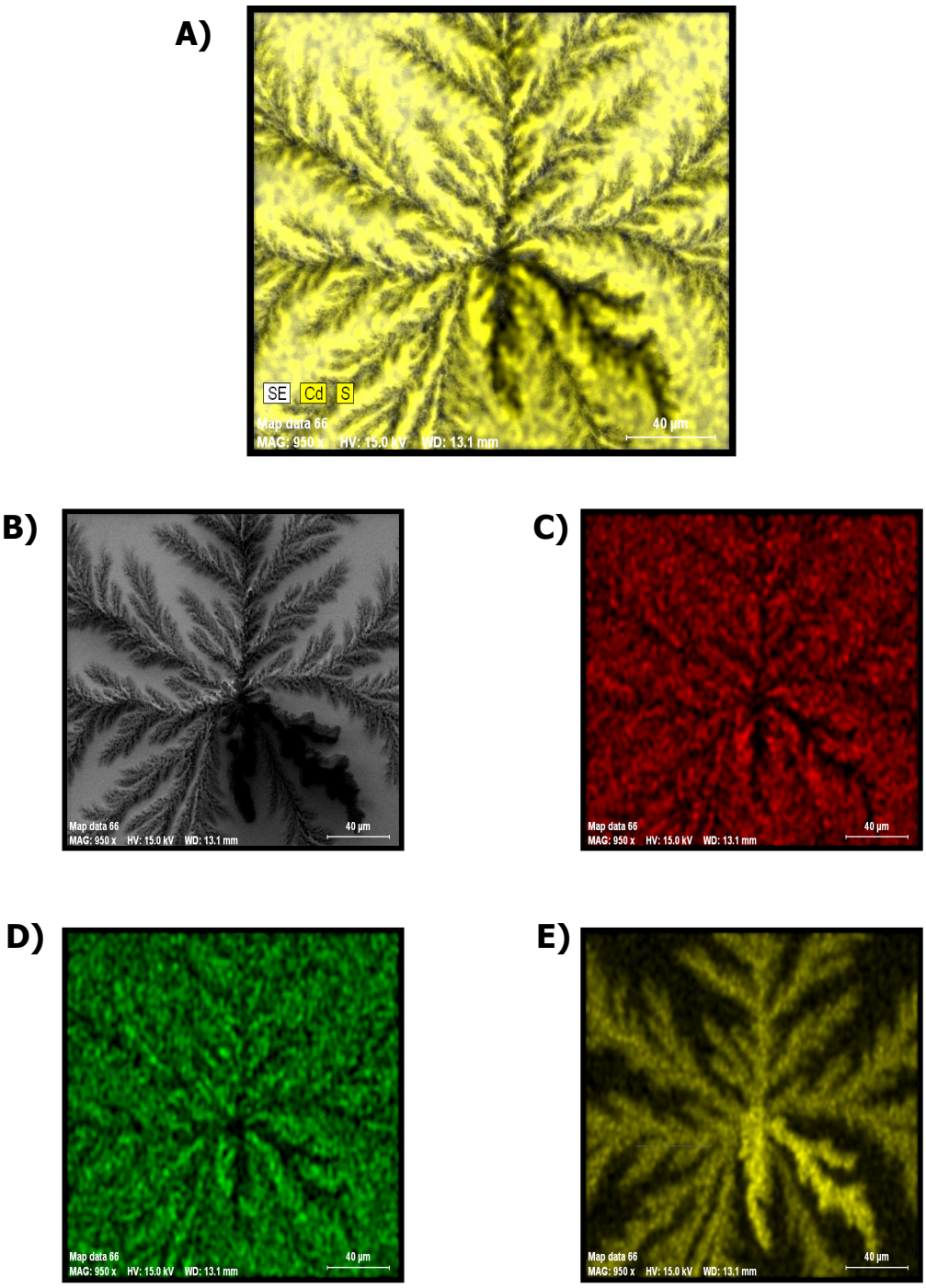

Figure 3.3.7) The EDX mapping of CdS thin film sample. **A)** yellow color demonstrates the CdS, **B)** SEM image, **C)** red color demonstrates Cd, **D)** green color demonstrates S, and **E)** yellow color demonstrates the C. CdS thin film synthesized from 7:1 mole ratio $[Cd(H_2O)_4](NO_3)_2$:P85 mesophase.

The CdS thin film sample, which had the dendritic structures as in Figure 3.3.5.B, was washed gently with acetone. The SEM image of the washed sample is given in Figure 3.3.8.A. Upon washing, the dendritic parts, free surfactants, were gone completely and the CdS thin film parts remained on the sample without any damage. Figures 3.3.8.B, C and D are the EDX mappings collected by Cd, S and C, respectively. All mappings give the same image as their SEM image. The red and green colors in Figure 3.3.8.B and C respectively are almost with the same intensity. This indicates that all Cd ions are reacted with H_2S gas forming the CdS nanocrystals. C mapping in Figure 3.3.8.D represent for the surfactant molecules used in the mesostructured CdS and they are part of the structure.

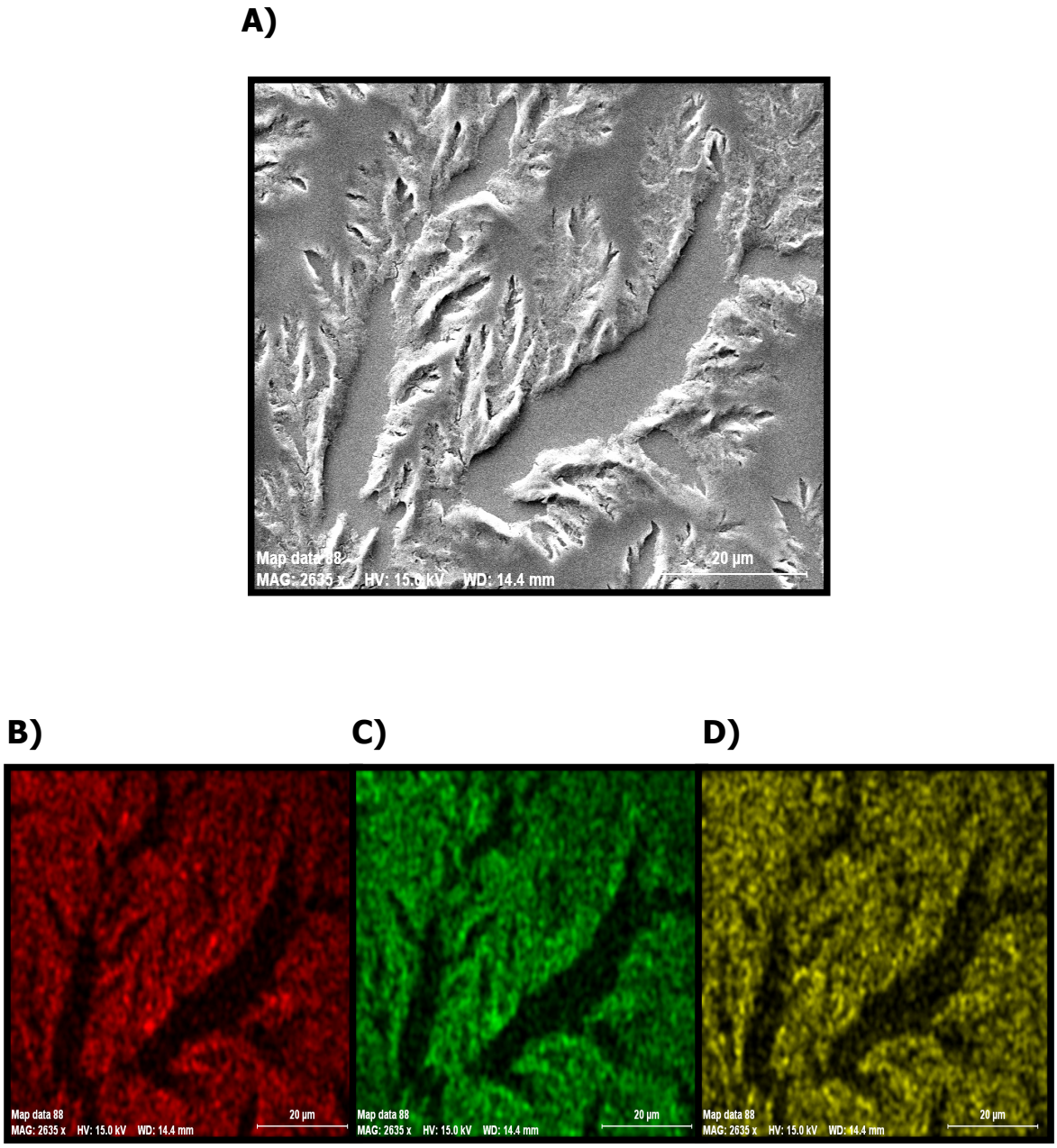

Figure 3.3.8: A) The SEM image of the washed CdS thin film sample and the EDS mappings of **B)** red color demonstrates Cd, **C)** green color demonstrates S, and **D)** yellow color demonstrates the C. LC mesophase synthesized from 7:1 mole ratio of $[Cd(H_2O)_4](NO_3)_2$:P85 mesophase.

Figure 3.3.9.A and B are the SEM images of washed CdS thin film sample. The pores in figure 3.3.9.A are due to the domains of free surfactant molecules, which were removed upon washing the sample with acetone. The parts other than porous parts are the mesostructured CdS. The sample is formed upon aggregation of the mesostructured CdS domains given in Figure 3.3.9.B. In Figure 3.3.9.B, the mesostructured CdS domains are in the shape of spheres with various sizes at around 60-80 nm. Upon washing the sample with acetone, CdS domains are gathered as in the shape of sphere and spread over the sample. Those mesostructured CdS domains can be represented as in the schema, given in Figure 3.3.9.C.

In order to identify the mesostructure of CdS in more detail, those mesostructured CdS domains with 60-80 nm sizes are required to be further analyzed with high resolution microscopy techniques, such as high resolution SEM or TEM.

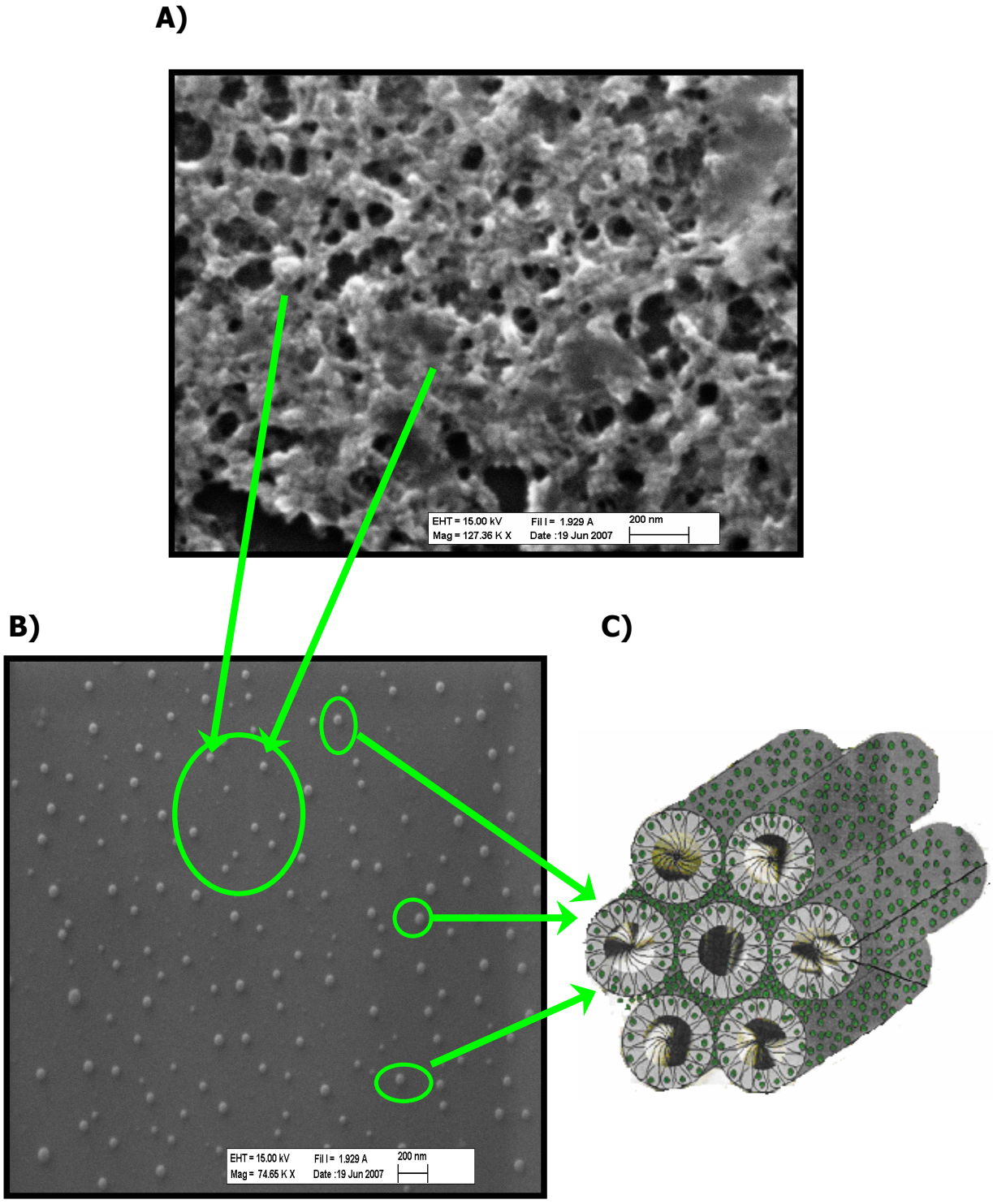

Figure 3.3.9: The SEM images of the washed CdS thin film samples and a model indicating the mesostructures. Note that green dots on the model represents for the CdS nanocrystals.

Here, even though the synthesis of the thin films of mesostructured MS is a great contribution to the literature, further work is required for the synthesis of better structured mesoporous metal sulfides.

3.4. Synthesis of Mesostructured Solid-Solutions of $Cd_{1-x}Zn_xS$

In Figure 3.4.1, the small angle XRD patterns of the $([Cd(H_2O)_4](NO_3)_2)_{1-x}([Zn(H_2O)_6](NO_3)_2)_x$: P85 (x = 0.0- 1.0) LC thin film samples show that adding $[Zn(H_2O)_6]^{2+}$ ions in the range of amount x = 0.0- 1.0 didn't destroy the mesostructure. Hence, relatively high ordered LC mesophase can be used as a template to produce mesostructured solid-solutions of $Cd_{1-x}Zn_xS$ films.

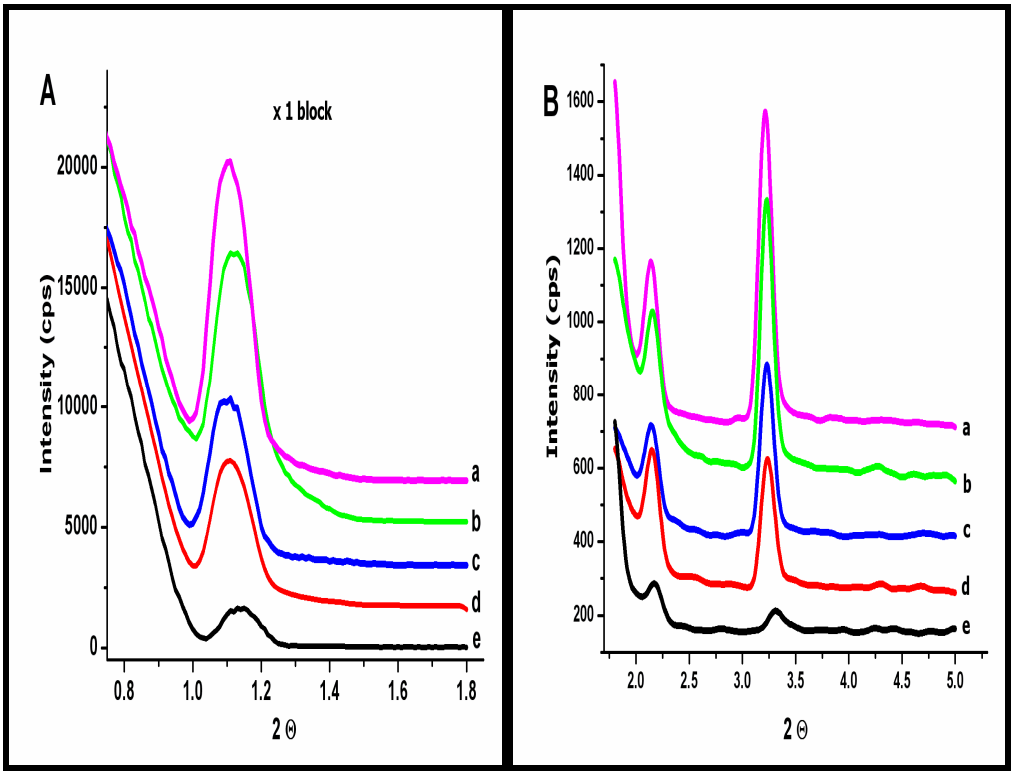

Figure 3.4.1: A) The small angle XRD patterns (with ~10 times reduced intensity), **B)** The small angle XRD pattern of **a)** $[Cd(H_2O)_4](NO_3)_2$:P85, and $([Cd(H_2O)_4](NO_3)_2)_{1-x}([Zn(H_2O)_6](NO_3)_2)_x$:P85 LC mesophase at a 7:1 mole ratio of TMS:pluronic where x is **b)** 0.3, **c)** 0.5, **d)** 0.7 and **e)** 1.0.

The mesostructured $([Cd(H_2O)_4](NO_3)_2)_{1-x}([Zn(H_2O)_6](NO_3)_2)_x$: P85 (x = 0.0- 1.0) LC thin film samples were reacted with H_2S gas in an evacuated reaction chamber under 350- 400 torr pressure for 15 minutes. Figure 3.4.2 gives the small angle XRD pattern of the mesostructured $Cd_{1-x}Zn_xS$ (x = 0.0- 1.0) materials. The patterns consist of weak and broad diffraction line at around 1.0-1.5°, 2Θ angle. The reason might be that the film samples are very thin and not well ordered or made up of small domains that cannot display intense diffraction lines. However, as the amount of zinc component, x increased in the $Cd_{1-x}Zn_xS$, the diffraction line became more intense showing that $[Zn(H_2O)_6]^{2+}$ ions provided advantage to better maintain the LC mesostructure during H_2S reaction. The $Cd_{1-x}Zn_xS$ films are crack free, giving a better resolved small angle XRD line.

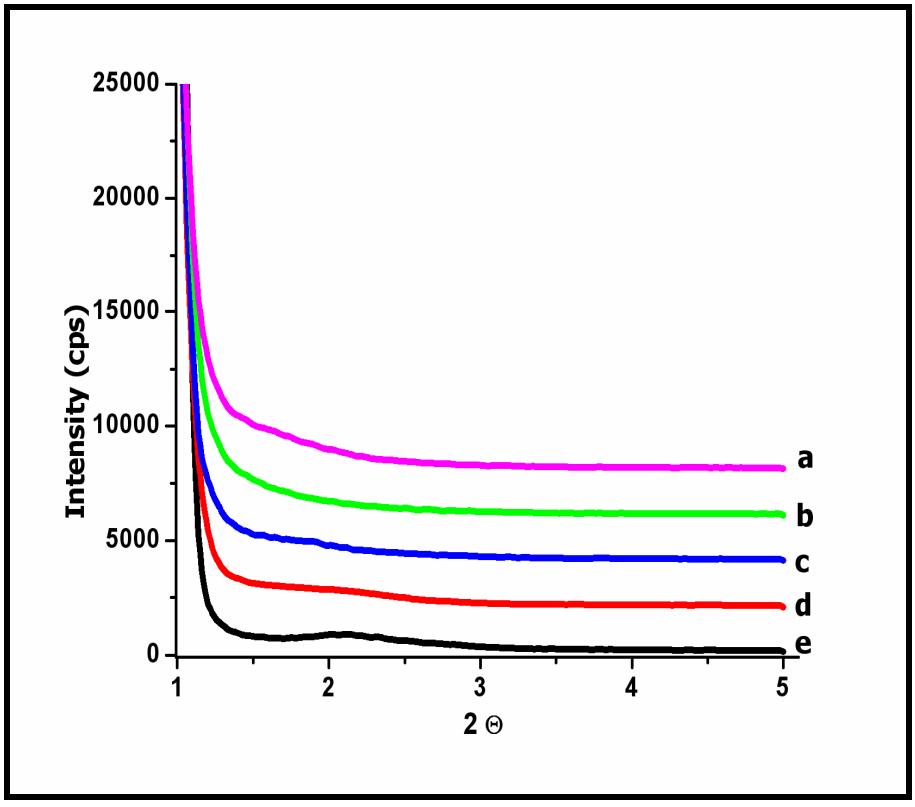

Figure 3.4.2: The XRD pattern of mesostructured **a)** CdS, **b)** $Cd_{0.7}Zn_{0.3}S$, **c)** $Cd_{0.5}Zn_{0.5}S$, **d)** $Cd_{0.3}Zn_{0.7}S$, **e)** ZnS thin films. Synthesized from 7 mole ratio $([Cd(H_2O)_4](NO_3)_2)_{1-x}([Zn(H_2O)_6](NO_3)_2)_x$:P85.

The UV-Vis absorption spectra were recorded in transmittance mode for all $Cd_{1-x}Zn_xS$ materials, Figure 3.4.3. The absorption edge gradually blue shifts going from mesostructured CdS thin film sample to ZnS sample. The absorption edges of the mesostructured CdS and ZnS start at 495 nm and 314 nm, respectively.

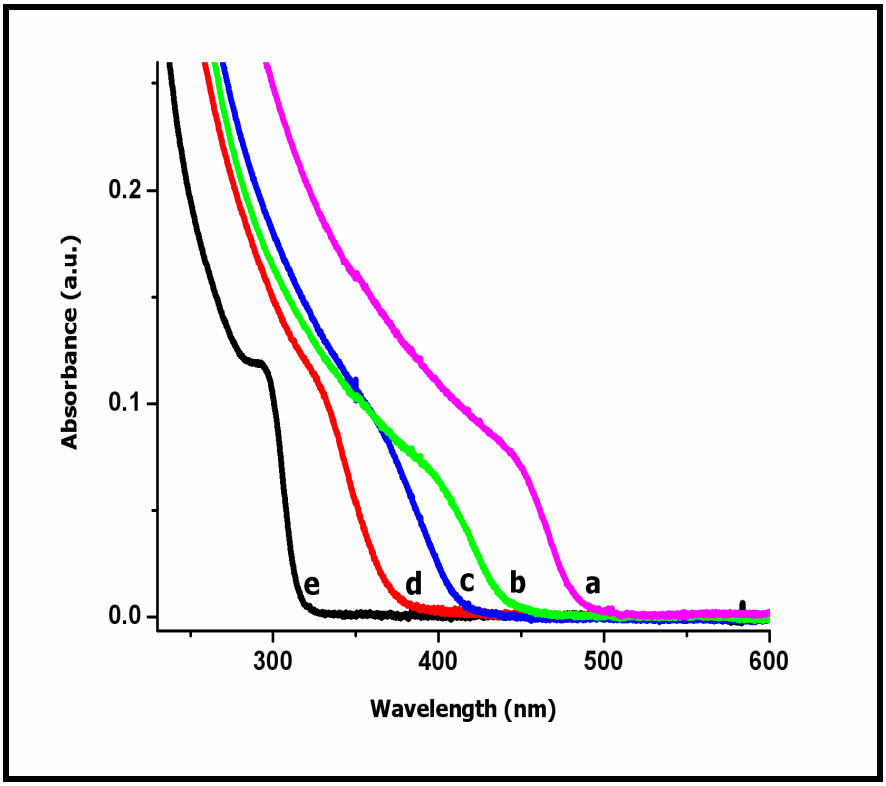

Figure 3.4.3: The UV-Vis absorption spectra of mesostructured **a)** CdS, **b)** $Cd_{0.7}Zn_{0.3}S$, **c)** $Cd_{0.5}Zn_{0.5}S$, **d)** $Cd_{0.3}Zn_{0.7}S$, **e)** ZnS thin films. Synthesized from 7:1 mole ratio $([Cd(H_2O)_4](NO_3)_2)_{1-x}([Zn(H_2O)_6](NO_3)_2)_x$:P85.

The band gaps of each sample were evaluated using the linear fit of the absorption edge after plotting the spectra against the direct gap relationship, $(Absorbance*energy)^2$ versus *energy* in eV, given in Figure 3.4.4. The band gaps of $Cd_{1-x}Zn_xS$ gradually varies from 2.62 eV in x = 0.0 to 4.00 eV in x = 1.0. The band gap values of $Cd_{1-x}Zn_xS$ are 2.91 eV in x = 0.3, 3.16 eV in x = 0.5 and 3.51 eV in

x = 0.7. The bulk band gap values of CdS and ZnS are 2.42 eV and 3.68 eV, respectively. [95] The blue shift from the bulk E_g values by 0.20 eV for CdS and 0.32 eV for ZnS indicating that the particles are smaller at the Zn(II) rich end of the $Cd_{1-x}Zn_xS$ nanocrystals.

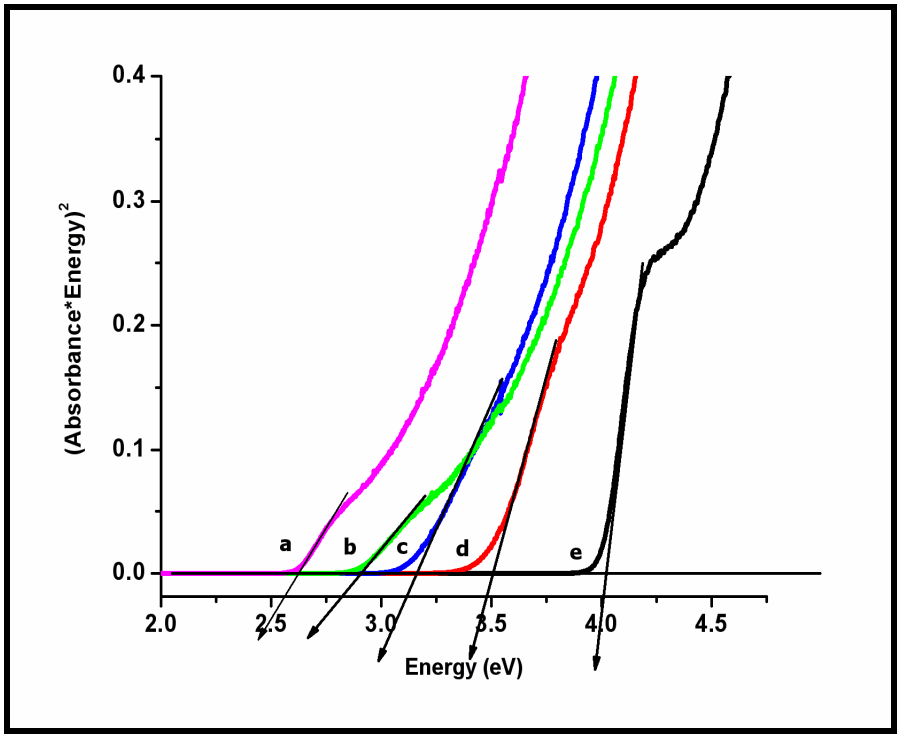

Figure 3.4.4: Plot of (Absorbance*Energy)^2 versus Energy of mesostructured **a)** CdS, **b)** $Cd_{0.7}Zn_{0.3}S$, **c)** $Cd_{0.5}Zn_{0.5}S$, **d)** $Cd_{0.3}Zn_{0.7}S$, **e)** ZnS thin films. Synthesized from 7 mole ratio $([Cd(H_2O)_4](NO_3)_2)_{1-x}([Zn(H_2O)_6](NO_3)_2)_x$:P85.

The plot of the band-gap shift given in Figure 3.4.5 was drawn by using equation 3.2.2 according to parameters given in Table 3.2.1 for CdS and ZnS. It should be recognized that the variations in the band gap with respect to the particle size in both CdS and ZnS, are very similar. Hence, we can assume that the variation in the $Cd_{1-x}Zn_xS$ nanocrystals should also follow the same trend given in Figure 3.4.5. The size of the $Cd_{1-x}Zn_xS$ nanocrystals was calculated using Figure 3.4.5. The particle size of the $Cd_{1-x}Zn_xS$ nanocrystals calculated from the band gap shifts are

given in Table 3.4.1. The gradual blue shift of the band-gaps going from CdS to ZnS and sharp absorption edges shows that the small sized $Cd_{1-x}Zn_xS$ nanoparticles form with a uniform size distribution.

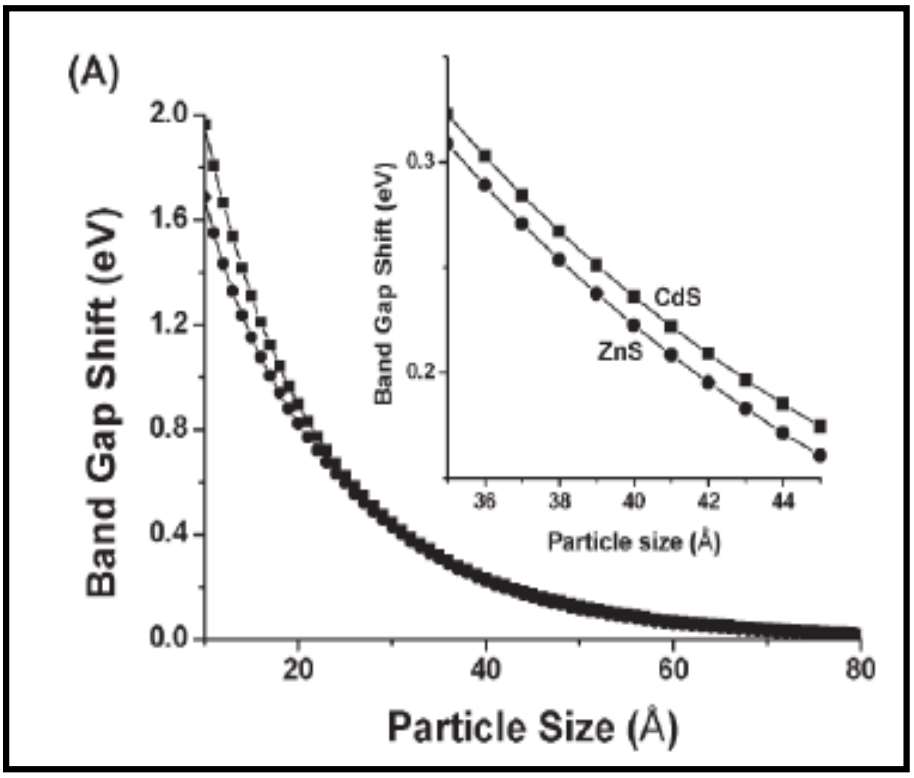

Figure 3.4.5: Plot of band-gap shift (ΔE_g) of CdS and ZnS obtained from empirical formula of equation (3.2.1) versus particle size (Å). The inset is the same plot showing the regions used in this work.

Table 3.4.1: The band gap values and particles sizes of $Cd_{(1-x)}Zn_xS$ samples.

Composition	Band Gap (eV)	Particle Size (nm)
ZnS	4.00	3.4
$Zn_{0.7}Cd_{0.3}S$	3.51	4.21
$Zn_{0.5}Cd_{0.5}S$	3.16	5.16
$Zn_{0.3}Cd_{0.7}S$	2.91	5.10
CdS	2.62	4.30

Here, we showed that a solid-solution of nanocrystalline mesostructured $Cd_{1-x}Zn_xS$ can be synthesized by letting the LC mesophase of $1\text{-}x[Cd(H_2O)_4](NO_3)_2/x[Zn(H_2O)_6](NO_3)_2$/P85 react with H_2S gas. It was already shown that, the Cd(II) and Zn(II) ions could be homogenously incorporated into the channels of mesostructured silica using the true liquid crystalline (TLC) approach with the help of metal containing liquid crystalline (MLC) mesophase and then reacted with H_2S gas. [71] Both methods can be used to fine tune both the composition (between x=0.0 and 1.0) and the optical band-gap of $Cd_{1-x}Zn_xS$ nanocrystallites between 2.60 eV and 4.00 eV. However, the nanocrystallites, synthesized by using the approach in our work, are slightly larger in every composition compared to the particles produced in the mesostructured silica.

3.5. $Cd_{1-x}Co_xS$ and $Cd_{1-x}Mn_xS$ Synthesis

Since the LC system of the $Cd(H_2O)_4](NO_3)_2$: P85 at 7:1 mole ratio forms a mesostructure, the TMS to surfactant mole ratio was kept at 7:1 while adding $[Co(H_2O)_4]^{2+}$ or $[Mn(H_2O)_4]^{2+}$ ions into the system. The solutions of 7:1 mole ratio $([Cd(H_2O)_4](NO_3)_2)_{1-x}/([Co(H_2O)_6](NO_3)_2)_x$:P85 with x from 0 to 1 were prepared by stirring the mixture in 8.0 mL ethanol and magnetic stirring for one day. The thin film samples were prepared using above solution by spin coating at 2000 rpm over glass and quartz substrates and silicon wafers for different purposes. Figure 3.5.1 shows the XRD pattern of Co(II) added fresh samples with x = 0.0 to 1.0. Adding Co(II) do not destroy the mesostructure, rather they provided to form relatively more ordered structures. The additional diffraction line at angle 4.0, 2 Θ appears as the mole ratio of $[Co(H_2O)_4]^{2+}$ ions increase in the LC film samples. Note that the diffraction lines observed at around 1.1°, 2Θ were recorded by blocking the detector with two thin Cu plates that reduce the intensity by 2 orders of magnitude (100 times).

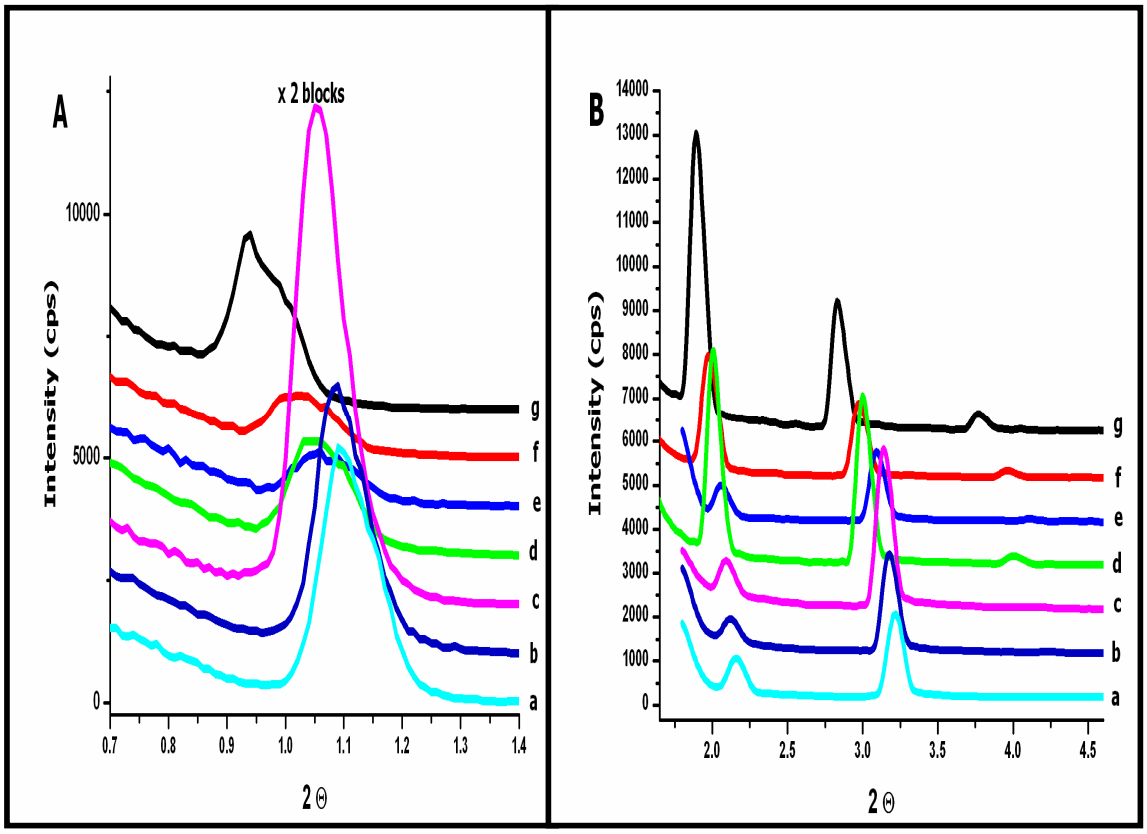

Figure 3.5.1: A) The small angle XRD pattern (with ~ 100 times lower intensity), **B)** The small XRD pattern of **a)** $[Cd(H_2O)_4](NO_3)_2$:P85 and $([Cd(H_2O)_4](NO_3)_2\ )_{1-x}([Co(H_2O)_6](NO_3)_2\ )_x$:P85 LC mesophase thin film samples at 7: 1 mole ratio TMS: surfactant where x is **b)** 0.01, **c)** 0.05, **d)** 0.10, **e)** 0.15, **f)** 0.20 and **g)** 1.00.

The thin film samples of $([Cd(H_2O)_4](NO_3)_2\ )_{1-x}([Co(H_2O)_6](NO_3)_2\ )_x$: P85 with x = 0.0-1.0 were exposed to H_2S gas in the evacuated reaction chamber under 350-400 torr H_2S pressure for 15 minutes. The color of $[Co(H_2O)_4]^{2+}$ ions rich samples turned to black upon exposed to H_2S. Figure 3.5.2 gives the small angle XRD pattern of fresh $Cd_{1-x}Co_xS$ samples with x = 0.0-1.0. The XRD pattern of fresh $Cd_{1-x}Co_xS$ samples behaved similar to mesostructured CdS up to x = 0.20, but samples with x above 0.20 gave diffraction line like their LC mesophase.

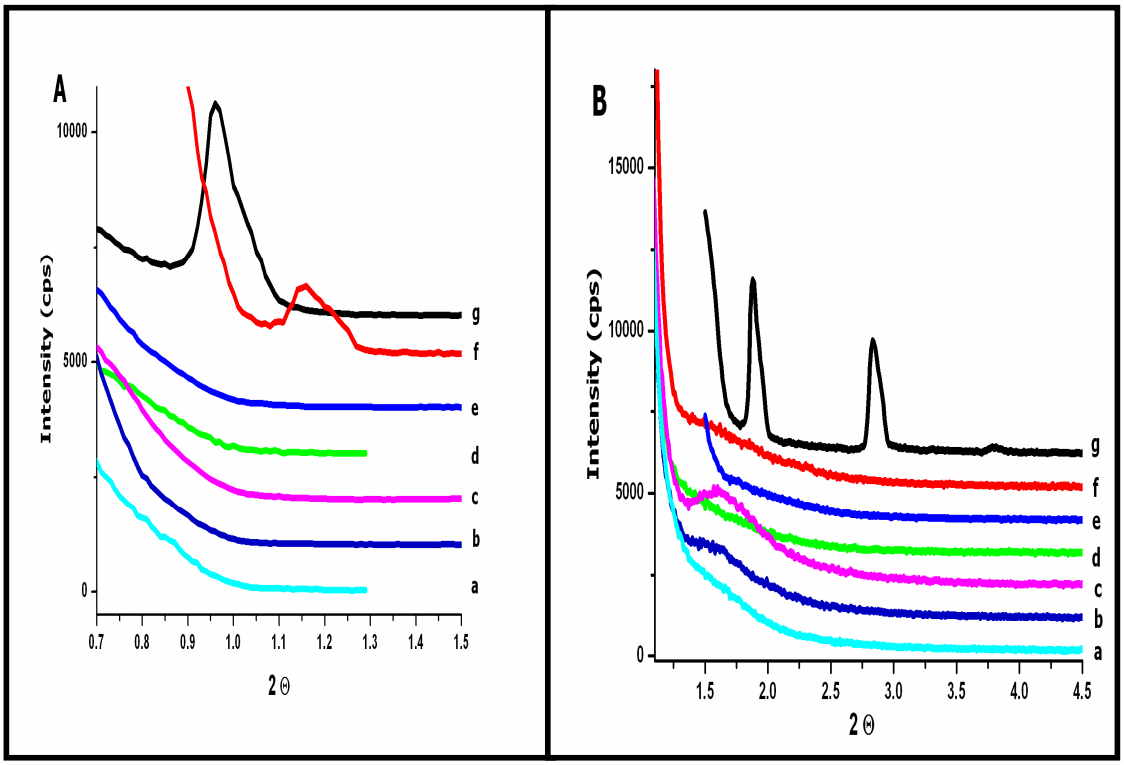

Figure 3.5.2: A) The small angle XRD pattern (with ~ 100 times reduced intensity), **B)** The small angle XRD pattern of fresh **a)** CdS, **b)** $Cd_{0.99}Co_{0.01}S$, **c)** $Cd_{0.95}Co_{0.05}S$, **d)** $Cd_{0.9}Co_{0.1}S$, **e)** $Cd_{0.85}Co_{0.15}S$, **f)** $Cd_{0.8}Co_{0.2}S$, **g)** CoS samples. The samples were synthesized from 7: 1 mole ratio $([Cd(H_2O)_4](NO_3)_2)_{1-x}([Co(H_2O)_6](NO_3)_2)_x$:P85 LC system.

The FT – IR and micro –Raman spectra were recorded in order to further analyze the samples before and after H_2S gas exposure. As explained in the previous section, the splitted coordinated NO_3^- signals at around 1300 – 1460 cm^{-1} loses its intensity. This indicates that during the reaction of the Cd(II) salt with H_2S gas, the NO_3^- counter ion becomes free and solvated due to the free water produced. The changes in those signals during H_2S gas exposure to $[Co(H_2O)_6](NO_3)_2$: P85 LC thin film were also recorded. Figure 3.5.3 shows that those nitrate signals lose intensity upon exposed to H_2S but regain intensity immediately. This means that the CoS formed degrade back to the Co(II). That is why X-ray diffraction pattern has similar pattern to that of LC mesophase. The CoS particles are not stable probably

due to the reason that its solubility product(Ksp) is higher than that of the CdS. Note that the K_{sp} values of the CdS and CoS in water at RT are $1x10^{-27}$ and $5x10^{-22}$, respectively. The K_{sp} values of those materials in LC systems were not found out yet but they can be assumed to behave more or less the same as in water.

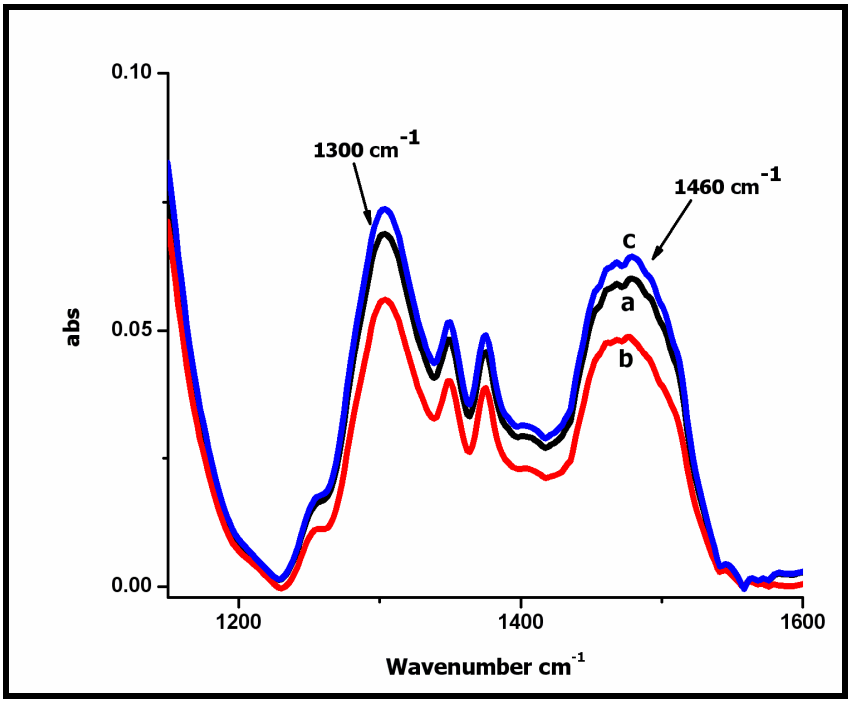

Figure 3.5.3: FT-IR spectra showing structural changes upon exposure of H_2S reaction on a 7 mole ratio $[Co(H_2O)_6](NO_3)_2$:P85 LC thin film. **a)** Before H_2S reaction, **b)** just after H_2S reaction, **c)** 6 hours after H_2S reaction

The CoS in $Cd_{1-x}Co_xS$ samples with x = 0.2 and 0.15 were stable only for one day. The lost small angle X-ray diffraction lines upon H_2S reaction reformed in one day, Figure 3.5.4 and 3.5.5.A. The FT-IR spectra in Figure 3.5.5.B proved that the reformed diffraction lines belong to regenerated LC phase not to mesostructured CoS. Hence, Co^{2+} incorporation don't occur in the $Cd_{1-x}Co_xS$ samples with $x \geq 0.15$.

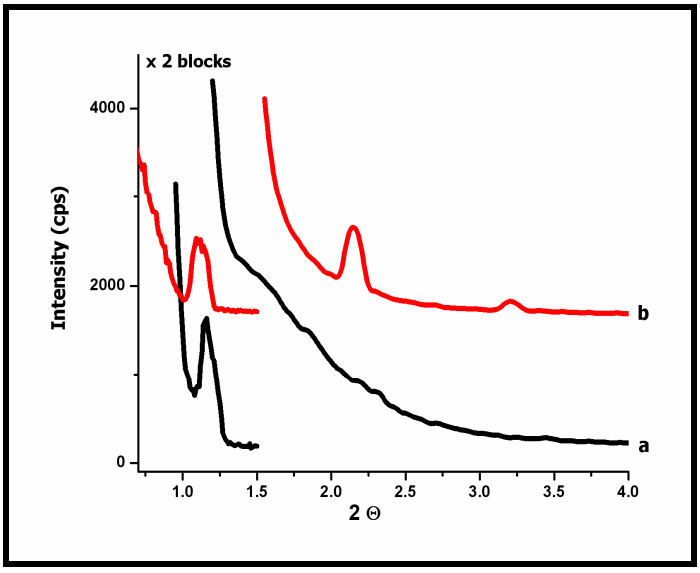

Figure 3.5.4: The XRD pattern of **a)** fresh, **b)** 1 day old $Cd_{0.8}Co_{0.2}S$. Synthesized from 7: 1 mole ratio $([Cd(H_2O)_4](NO_3)_2)_{0.8}([Co(H_2O)_6](NO_3)_2)_{0.2}$: P85 LC system.

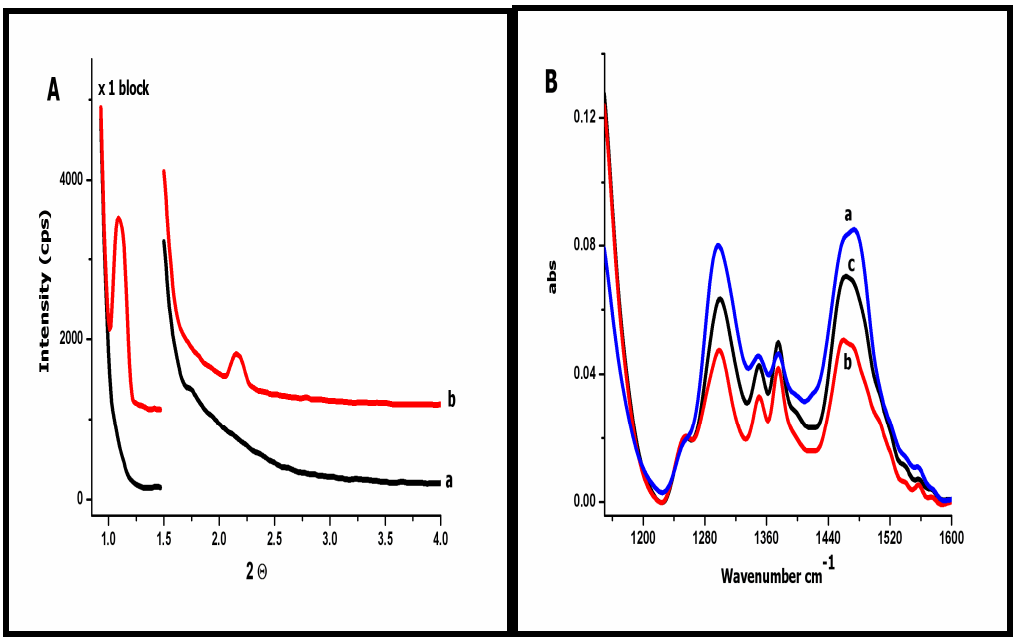

Figure 3.5.5: A) The XRD pattern of **a)** fresh, **b)** 1 day old $Cd_{0.85}Co_{0.15}S$, synthesized from 7: 1 mole ratio $([Cd(H_2O)_4](NO_3)_2)_{0.85}([Co(H_2O)_6](NO_3)_2)_{0.15}$: P85 LC system. **B)** The FT-IR spectra of the sample **a)** before H_2S reaction, **b)** just after H_2S reaction and **c)** 1 day after H_2S reaction.

Figure 3.5.6.A shows that the XRD pattern of $Cd_{1-x}Co_xS$ samples with x = 0.1 and also for x = 0.0 to 0.1 (not shown here) did not change for 10 days. The FT-IR spectra provided that the LC mesophase didn't reform (Figure 3.5.6.B). This means that $Cd_{1-x}Co_xS$ samples with x = 0.0 to 0.1 are stable.

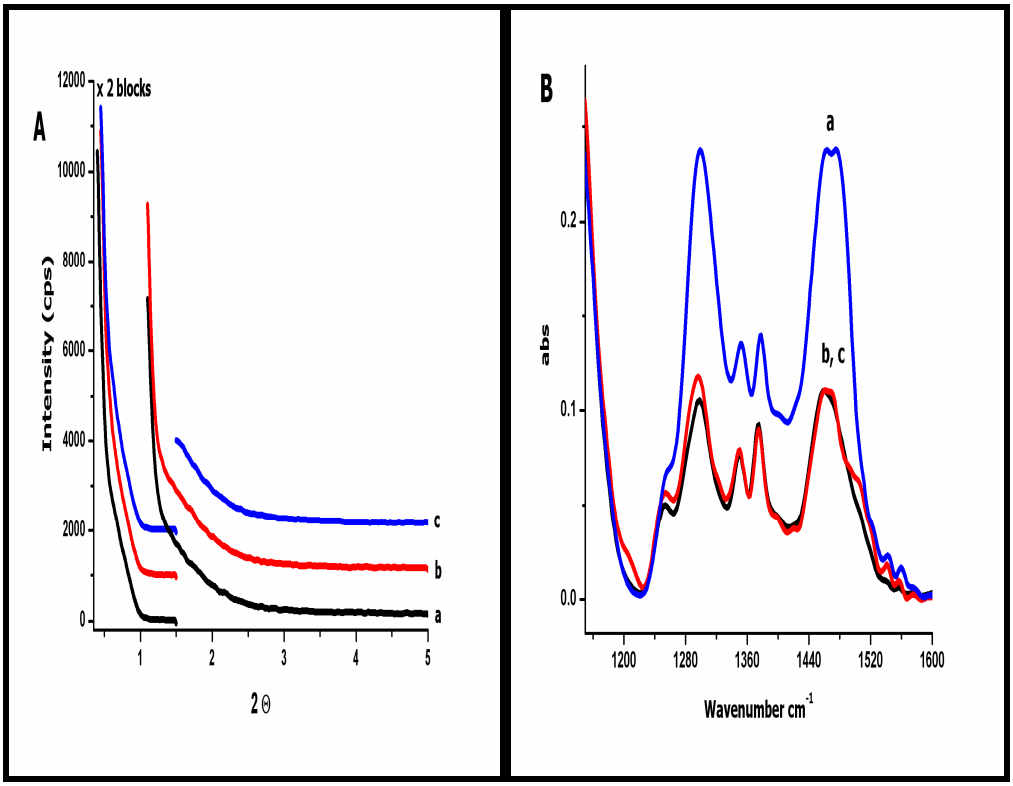

Figure 3.5.6: A) The XRD pattern of **a)** fresh, **b)** 1 day old, **c)** 10 days old $Cd_{0.9}Co_{0.1}S$. Synthesized from 7: 1 mole ratio $([Cd(H_2O)_4](NO_3)_2)_{0.9}([Co(H_2O)_6](NO_3)_2)_{0.1}$:P85 LC system. **B)** FT-IR spectra of the sample **a)** before H_2S reaction, **b)** just after H_2S reaction and **c)** 10 days after H_2S reaction.

The UV-Vis absorption spectra of the fresh $Cd_{1-x}Co_xS$ samples with x = 0.0 to 0.2 were recorded (Figure 3.5.7). The absorption edges of the samples are the same. However, there is almost linear decrease in the absorption intensity up to around x = 0.15. The relatively thicker $Cd_{1-x}Co_xS$ samples have absorption features

in 600-800 nm, which was readily identified as the $^4A_2$ (F) $\rightarrow$ $^4T_1$ (P) ligand-field transition of Co^{2+} substitutionally doped in CdS (Fig. 3.5.8.A). It is well known that the ligand-field transition energy and intensity pattern are sensitive to the Co^{2+} coordination environment as described by ligand-field theory. The weak signals were the significant evidences of that Co^{2+} ions occupy the isolated tetrahedral holes in CdS until x = 0.15 in the fresh samples. There is a linear dependence of absorbance at 730 nm on the amount of Co^{2+} for x =0.0 to 0.15 (Figure 3.5.8.B). Those results confirm that the Co^{2+} ions are homogenously doped as a substitutional dopant within the zinc-blend structured of CdS lattice.

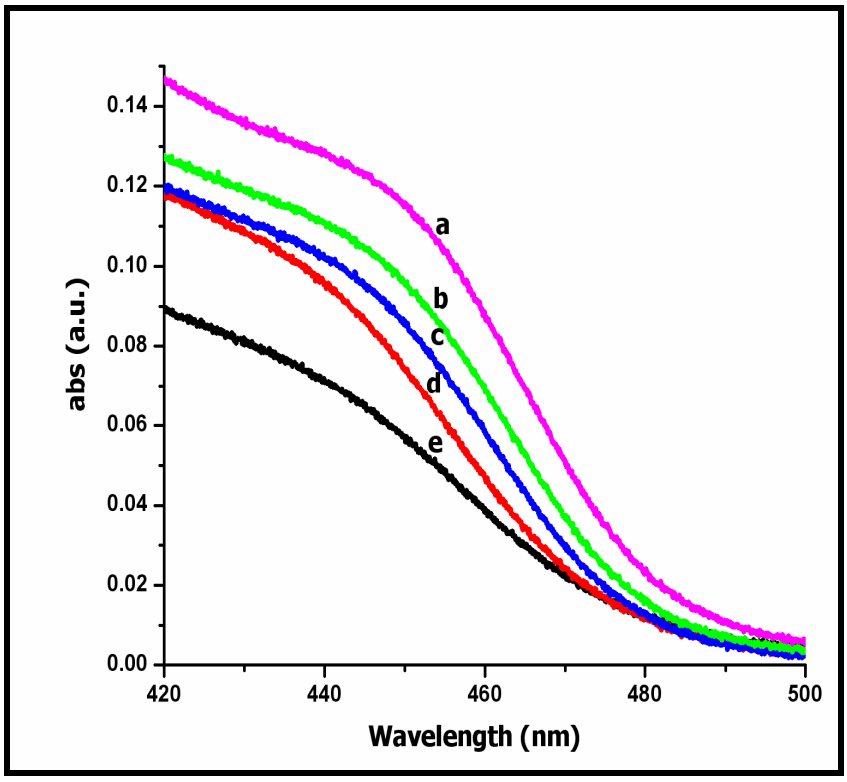

Figure 3.5.7: The UV-Vis absorption spectra of **a)** CdS, **b)** $Co_{0.01}Cd_{0.99}S$, **c)** $Cd_{0.95}Co_{0.05}S$, **d)** $Cd_{0.85}Co_{0.15}S$, **e)** $Cd_{0.8}Co_{0.2}S$ samples. Synthesized from 7: 1 mole ratio $([Cd(H_2O)_4](NO_3)_2)_{1-x}([Co(H_2O)_6](NO_3)_2)_x$:P85 LC system.

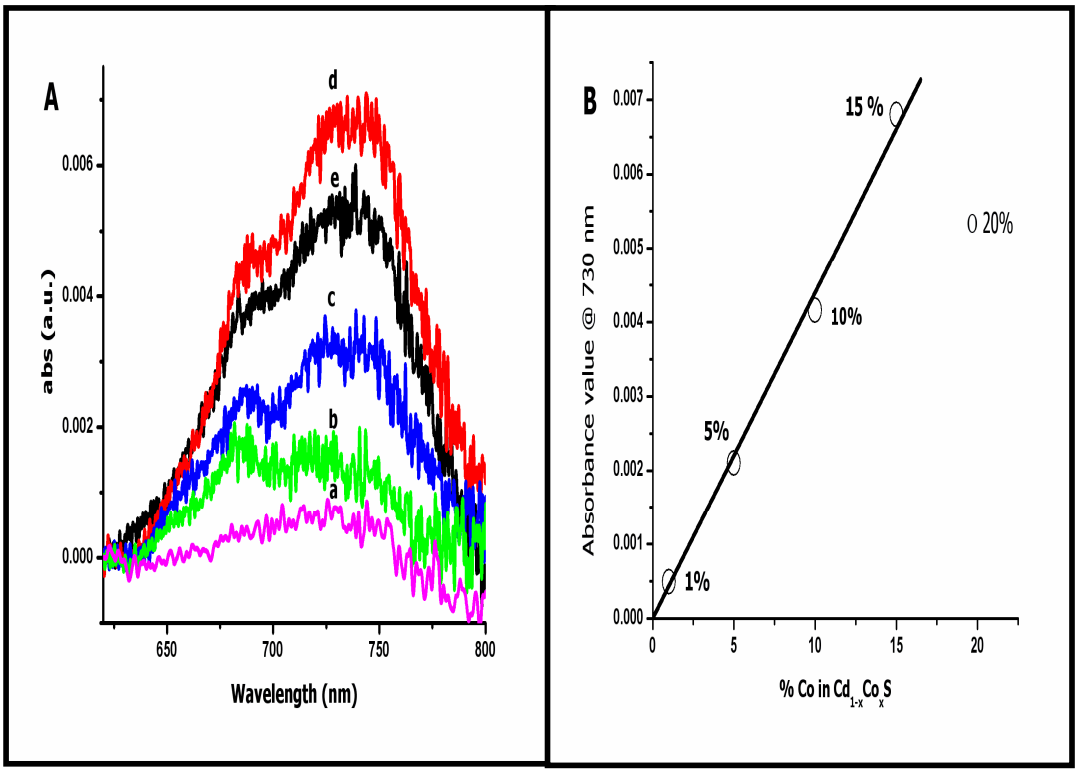

Figure 3.5.8: A) UV-Vis absorption spectra of **a)** $Cd_{0.99}Co_{0.01}S$, **b)** $Cd_{0.95}Co_{0.05}S$, **c)** $Cd_{0.9}Co_{0.1}S$, **d)** $Cd_{0.85}Co_{0.15}S$ and **e)** $Cd_{0.8}Co_{0.2}S$ samples. **B)** Plot of absorbance dependence on %Co amount in $Cd_{1-x}Co_xS$. Synthesized from 7: 1 mole ratio $([Cd(H_2O)_4](NO_3)_2)_{1-x}([Co(H_2O)_6](NO_3)_2)_x$: P85 LC system.

The line mapping of the washed $Cd_{0.9}Co_{0.1}S$ thin film sample is given in Figure 3.5.9. The Cd, S, C and Co lines in the spectrum have the same intensities at all points through the line. In the dendritic parts, which were empty upon washing with acetone, all the intensities including C intensity decrease to zero intensity. Notice that the spectra are collected along the line shown in the SEM image given below the spectra. The Cd and S intensities have 1:1 ratio and 3 times of C intensity. Therefore, EDX line spectrum confirms the EDX mapping given in Figure 3.3.8.

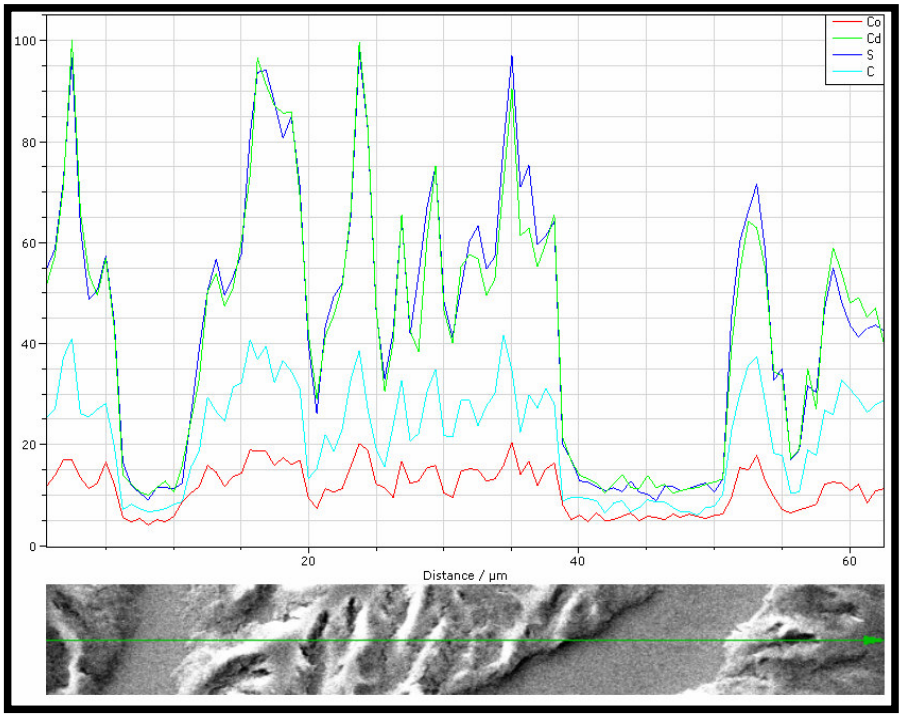

Figure 3.5.9: EDX line mapping of $Cd_{0.1}Co_{0.9}S$ thin film sample.

The TMS:surfactant ratio was kept to be 7:1 in the $([Cd(H_2O)_4](NO_3)_2)_{1-x}([Mn(H_2O)_4](NO_3)_2)_x$:P85 samples with x = 0.0 to 1.0 by simple mixing the ingredients one day in 8.0 mL ethanol. The thin film samples were prepared by spin coating at 2000 rpm over glass, quartz substrates and silicon wafers for various purposes. Figure 3.5.10 shows that adding $[Mn(H_2O)_4]^{2+}$ ions with x = 0.0 to 1.0 didn't destroy the mesostructures, rather they provided to form relatively more ordered mesostructure. The additional diffraction line at angle 4.0, 2Θ appears as the ratio of $[Mn(H_2O)_4]^{2+}$ ions increase above x = 0.3 in the system and those LC samples are very stable.

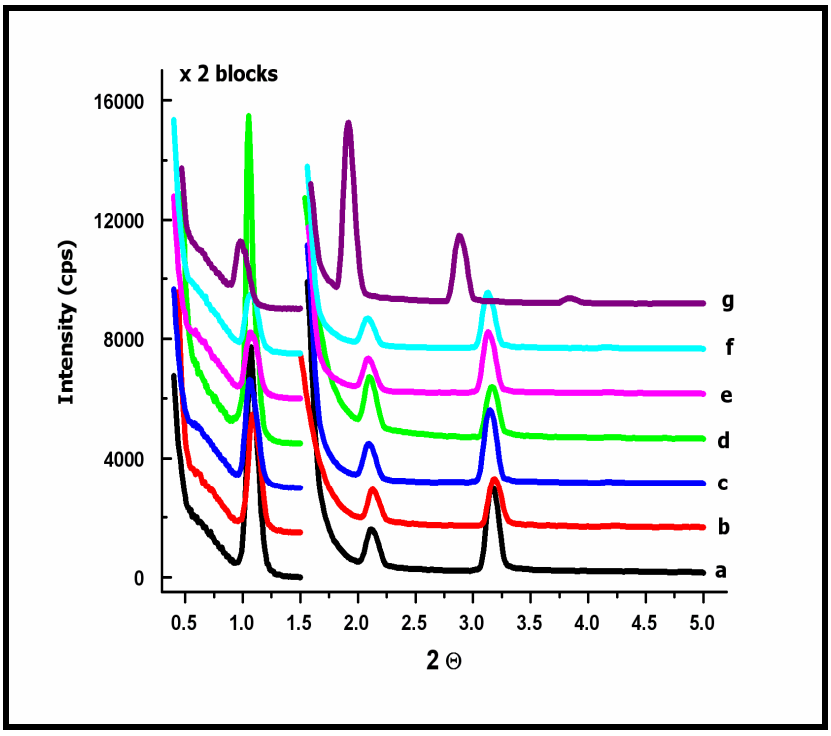

Figure 3.5.10: XRD pattern of $[Cd_{1-x}Mn_x(H_2O)_4](NO_3)_2$ with a 7:1 mole ratio of $[Cd_{1-x}Mn_x(H_2O)_4](NO_3)_2$:P85 where x is **a)** 0.01, **b)** 0.05, **c)** 0.10, **d)** 0.15, **e)** 0.2, **f)** 0.3 and **g)** 1.00.

The thin film samples of the $([Cd(H_2O)_4](NO_3)_2)_{1-x}([Mn(H_2O)_4](NO_3)_2)_x$:P85 with x = 0.0-1.0 were exposed to H_2S gas in an evacuated reaction chamber under 350-400 torr H_2S pressure for 15 minutes. The $[Mn(H_2O)_4]^{2+}$ rich samples were colorless after exposed to H_2S. Figure 3.5.11 gives the small angle XRD pattern of fresh $Cd_{1-x}Mn_xS$ samples with x = 0.0-1.0. The XRD pattern of fresh $Cd_{1-x}Mn_xS$ samples behaved similar to mesostructured CdS up to x = 0.2, but the samples with x above 0.2 gave diffraction lines similar to their LC mesophases.

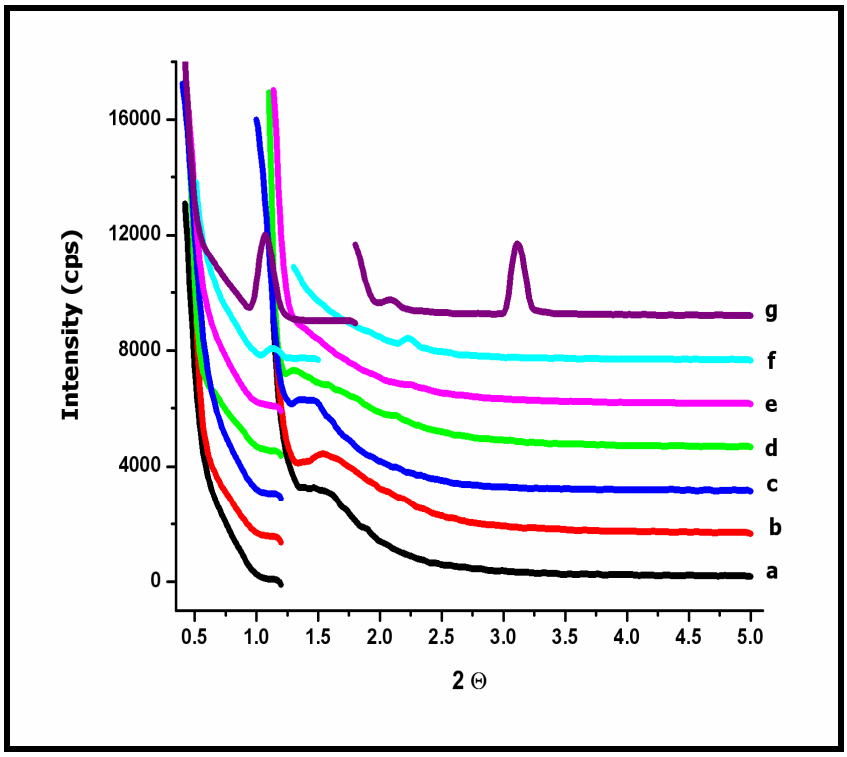

Figure 3.5.11: XRD pattern of fresh **a)**$Cd_{0.99}Mn_{0.01}S$, **b)**$Cd_{0.95}Mn_{0.05}S$, **c)**$Cd_{0.9}Mn_{0.1}S$, **d)**$Cd_{0.85}Mn_{0.15}S$, **e)**$Cd_{0.8}Mn_{0.2}S$, **f)**$Cd_{0.7}Mn_{0.3}S$ and **g)**MnS. Synthesized from $([Cd(H_2O)_4](NO_3)_2)_{1-x}([Mn(H_2O)_4](NO_3)_2)_x$:P85 with 7:1 mole ratio.

The MnS in the $Cd_{1-x}Mn_xS$ samples with x above 0.2 were stable only for one day. The FT-IR spectra in Figure 3.5.12 proved that XRD lines of $[Mn(H_2O)_4](NO_3)_2$:P85 thin film sample recorded just after exposed to H_2S were due to the reformed $[Mn(H_2O)_4](NO_3)_2$:P85 LC phase, not to mesostructured MnS. The small angle X-ray diffraction lines gained intensity one day after exposed to H_2S. Figure 3.5.13.A and the FT-IR spectra in Figure 3.5.13.B showed the reformation of coordinated nitrate species. Hence, Mn^{2+} incorporation don't occur in the $Cd_{1-x}Mn_xS$ samples with $x \geq 0.2$.

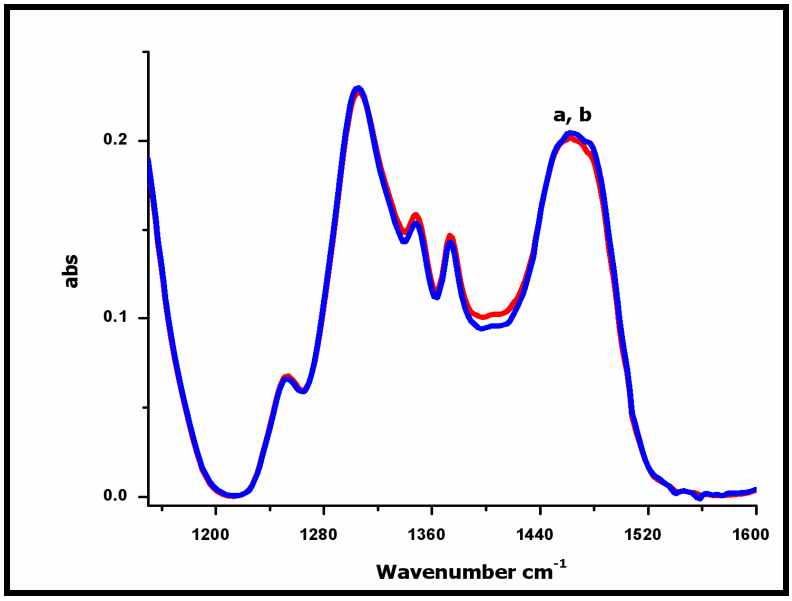

Figure 3.5.12: FT-IR spectra of 7:1 mole ratio $[Mn(H_2O)_4](NO_3)_2$:P85 **a)** before and **b)** after exposed to H_2S gas.

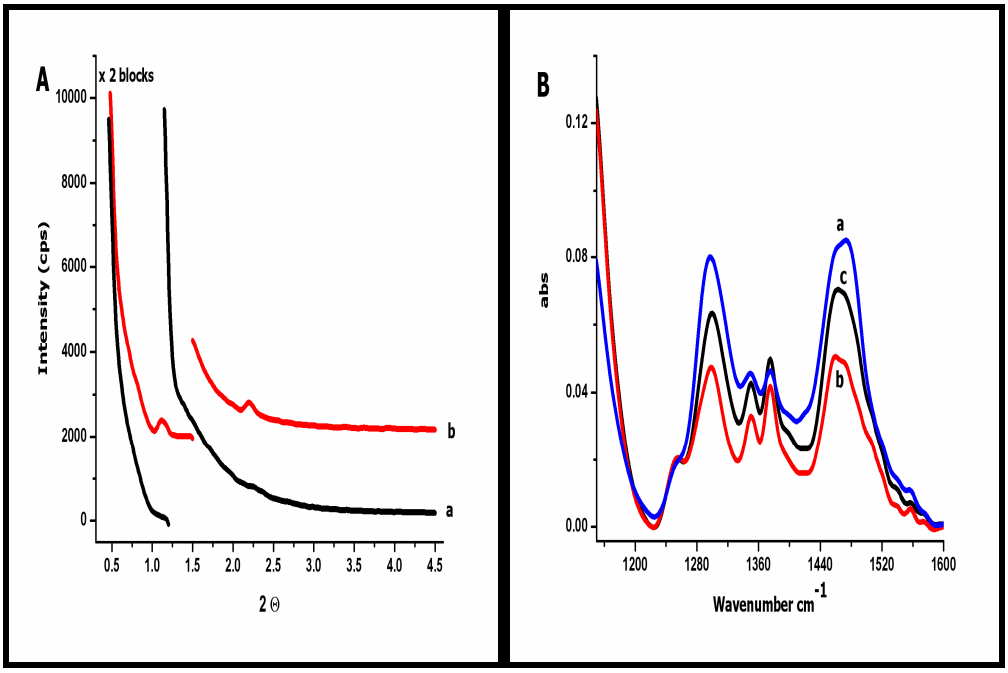

Figure 3.5.13: A) The XRD pattern of **a)** fresh, **b)** 1 day old $Cd_{0.8}Mn_{0.2}S$. Synthesized from 7: 1 mole ratio $[Cd_{0.8}Mn_{0.2}(H_2O)_4](NO_3)_2$,:P85 LC system.
B) FT-IR spectra of the sample **a)** before H_2S reaction, **b)** just after H_2S reaction and **c)** 1 day after H_2S reaction.

The XRD pattern of the $Cd_{1-x}Mn_xS$ samples with x = 0.1 (Figure 3.5.14.A) and also for x = 0.0 to 0.15 (not shown here) did not change for 10 days. The FT-IR spectra provided that the coordinated nitrate signals don't reform (Figure 3.5.14.B). This means that $Cd_{1-x}Mn_xS$ samples with x = 0.0 to 0.15 are stable.

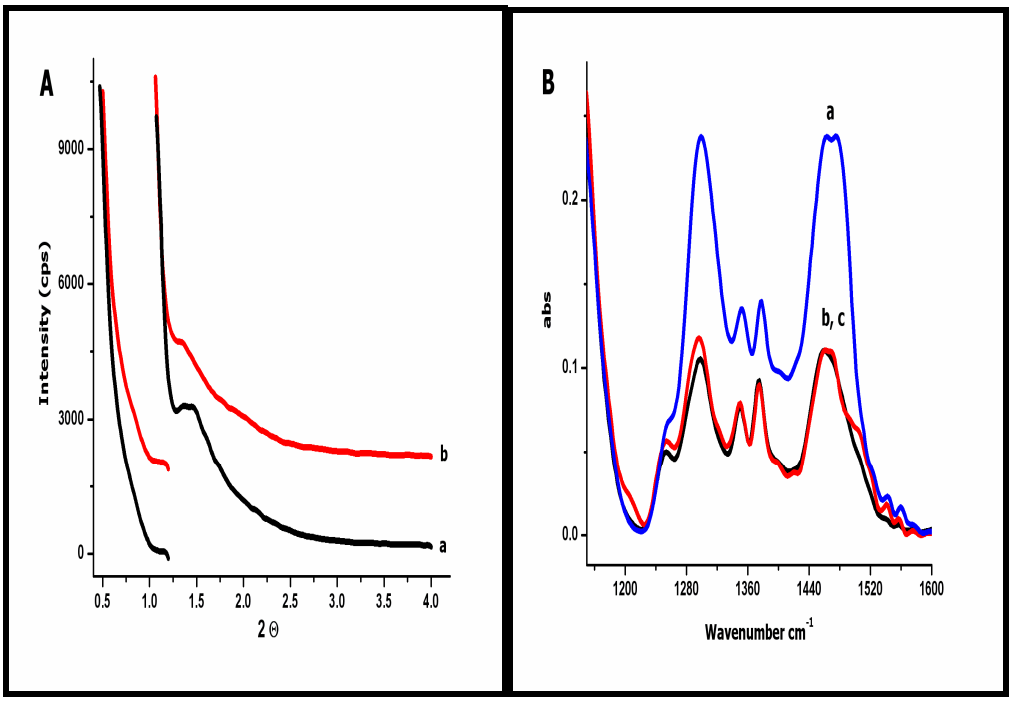

Figure 3.5.14: A) The XRD pattern of **a)** fresh and **b)** 10 days old $Cd_{0.85}Mn_{0.15}S$. Synthesized from 7: 1 mole ratio $[Cd_{0.85}Mn_{0.15}(H_2O)_4](NO_3)_2$,:P85 LC system.
B) FT-IR spectra of the sample **a)** before H_2S reaction, **b)** just after H_2S reaction, and **c)** 10 days after H_2S reaction.

The UV-Vis absorption spectra of fresh $Cd_{1-x}Mn_xS$ samples with x=0.0 to 0.3 were also recorded (Figure 3.5.15). There is a blue shift in the absorbance edges of the samples going from Cd(II) to Mn(II) rich samples. However, the blue shift is almost linear until around x=0.15 in the fresh samples but then, it seems to deviate from linearity for fresh samples $x \geq 0.3$, Figure 3.5.16. The plot of band gap versus x in $Cd_{1-x}Mn_xS$ is shown in Figure 3.5.17. The band gap values of fresh samples are linearly dependent on the composition for x = 0.01-0.2. However, the $Cd_{0.8}Mn_{0.2}S$ sample is not stable. From these results, it can be concluded that the Mn^{2+} ions could be doped to the CdS lattice within x = 0.0 to 0.15 range for stable $Cd_{1-x}Mn_xS$ samples. The linear dependence of the absorption edge to x means that there is a solid-solution behavior of MnS in CdS in the x = 0.0 to 0.15 range, Figure 3.5.17.

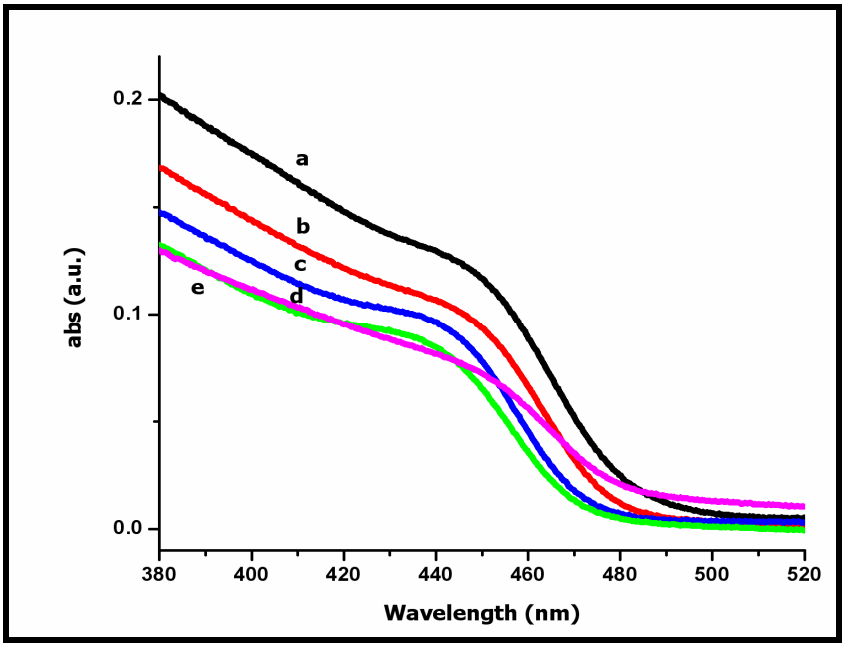

Figure 3.5.15: The UV-Vis absorption spectra of fresh **a)** CdS, **b)** $Cd_{0.95}Mn_{0.05}S$, **c)** $Cd_{0.9}Mn_{0.1}S$, **d)** $Cd_{0.8}Mn_{0.2}S$, and **e)** $Cd_{0.7}Mn_{0.3}S$ samples. Synthesized from $([Cd(H_2O)_4](NO_3)_2)_{1-x}([Mn(H_2O)_4](NO_3)_2)_x$:P85 with 7:1 mole ratio.

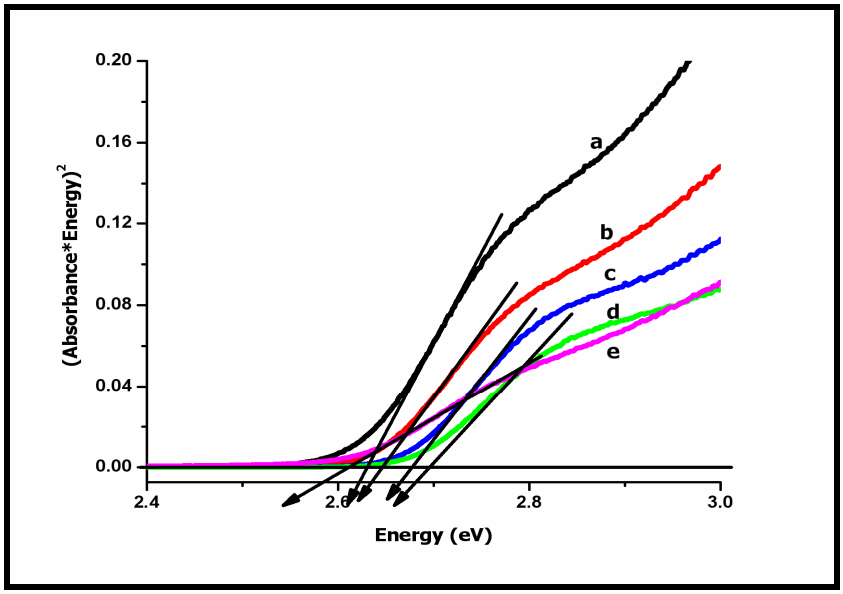

Figure 3.5.16: Band gap spectra of fresh **a)** CdS, **b)** $Cd_{0.95}Mn_{0.05}S$, **c)** $Cd_{0.9}Mn_{0.1}S$, **d)**$Cd_{0.8}Mn_{0.2}S$, and **e)**$Cd_{0.7}Mn_{0.3}S$ samples. Synthesized from $([Cd(H_2O)_4](NO_3)_2)_{1-x}([Mn(H_2O)_4](NO_3)_2)_x$:P85 with 7:1 mole ratio.

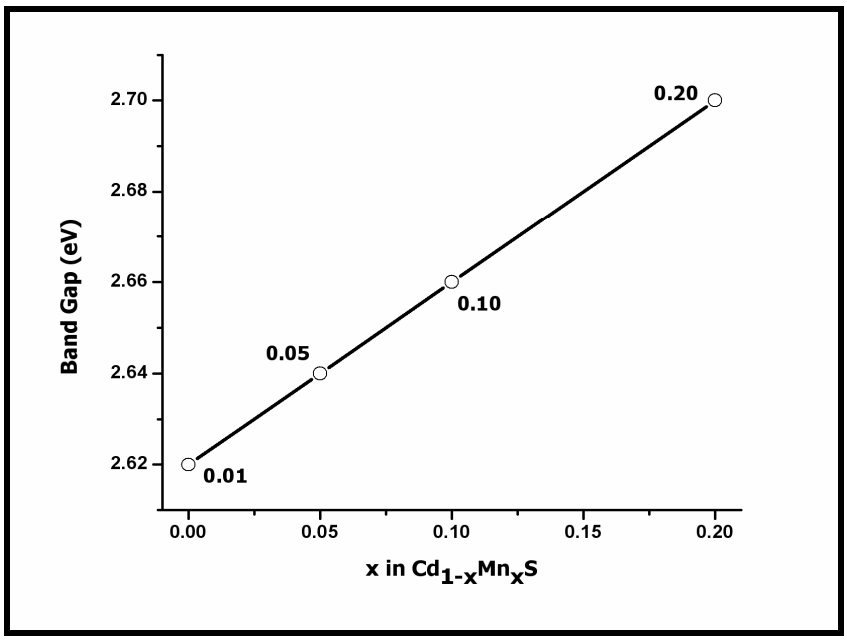

Figure 3.5.17: The plot of band gap versus x in the $Cd_{1-x}Mn_xS$ film samples.

Here, further works are needed to clarify if the Co(II) and Mn(II) ions doped $Cd_{1-x}Co_xS$ and $Cd_{1-x}Mn_xS$ samples have magnetic properties. They do not show magnetism at room temperature. However, they might show magnetic properties at low temperatures.

3.6. FUTURE PROJECT

The mesoporous silica spheres have significant features such as high specific surface area, regular and adjustable pores, presence of silanol groups.[69] Hence, they are used in several applications as packing materials and in cosmetic industry, [113-114] etc. Several mechanisms [115-117] have been introduced for the formation of these self assembled silica spheres. Figure 3.6.1 shows the schematic description of the all possible mechanisms.[115] The silica/surfactant ratio, type of surfactant, amount of solvent, stirring and aging of the reaction mixture, temperature of the reaction are the major factors affecting the size and morphology of the spheres. Synthesizing the silica spheres mainly by using nonionic surfactants enables some advantages such as easy removal, non-toxic, biodegradable and cheap. [117]

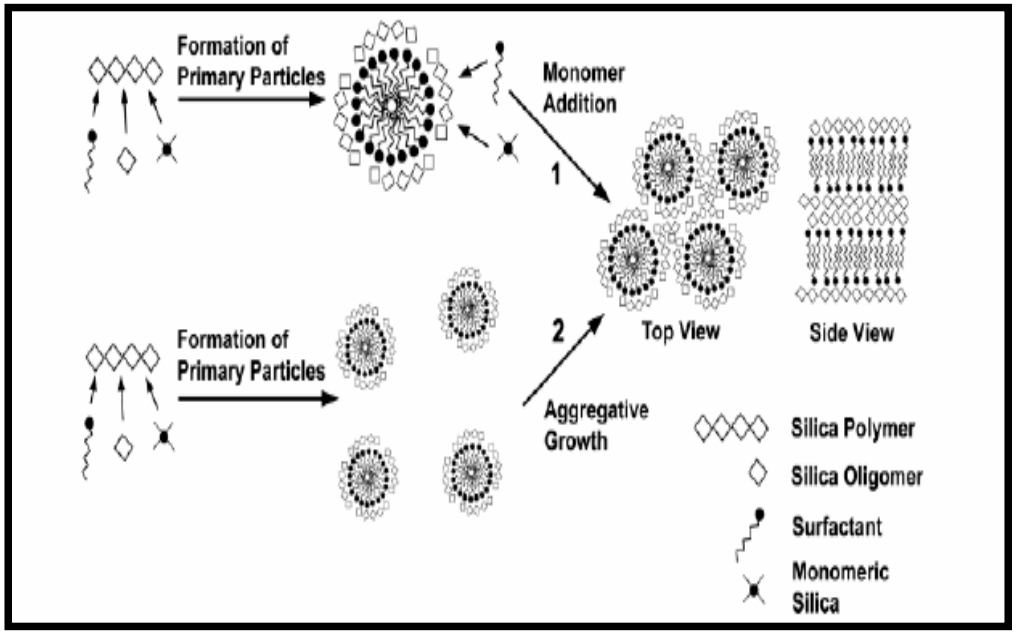

Figure 3.6.1: The schematic description of the all possible mechanisms of silica spheres.

Here the silica spheres were synthesized by using pluronic, P85 and a little CTMABr, a cationic surfactant which is used to provide the perfect spherical morphology, and tetraethylorthosilicate (TEOS) as a silica source, and heated at 95ºC. The particle sizes of the silica spheres are in the range of 1-10 μm. It was investigated that those silica spheres can be covered with LC mesophases synthesized in this thesis. Then, upon exposure to H_2S reaction, the thin films of mesostructured MS can be synthesized over those silica spheres as in the case of silicon wafer substrates. Figure 3.6.2 gives the SEM image of one of those silica spheres which is covered with thin film of mesostructured CdS. The LC mesophase is $[Cd(H_2O)_4](NO_3)_2$:P85 with 7:1 mole ratio, dissolved in 10.0 mL ethanol. The silica microspheres were added into this solution and stirred for around 3.0 minutes and then filtrated. The LC mesophase covered silica microspheres were reacted with 350 torr H_2S gas in an evacuated reaction chamber for 15 minutes. The microspheres turned into yellow color during H_2S reaction indicating the formation of CdS. Figure 3.6.2.B, C and D are the EDS mapping of this silica microsphere collected using Si (red color), Cd (yellow color) and S (green color) X-rays, respectively. They all display the same features as the SEM image. Hence, it shows that those silica microspheres can be covered with LC mesophase and the thin films of mesostructured MS can be synthesized over those microspheres. Those CdS covered silica microspheres strongly emit orange light under UV irradiation at low temperatures.

A)

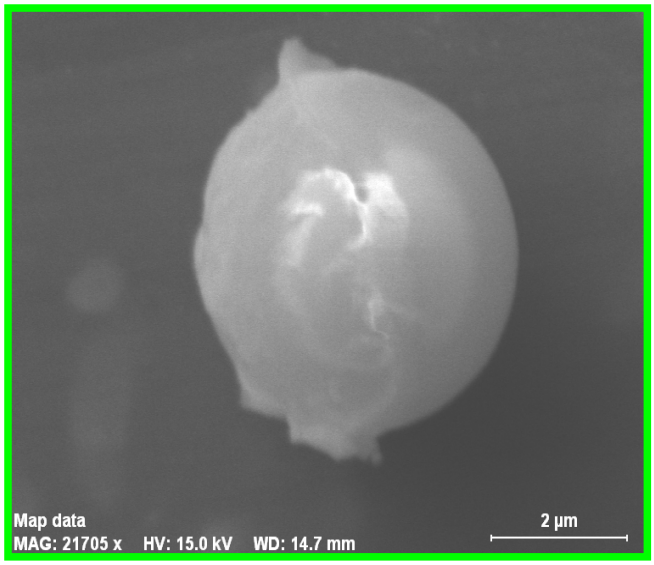

B) C) D)

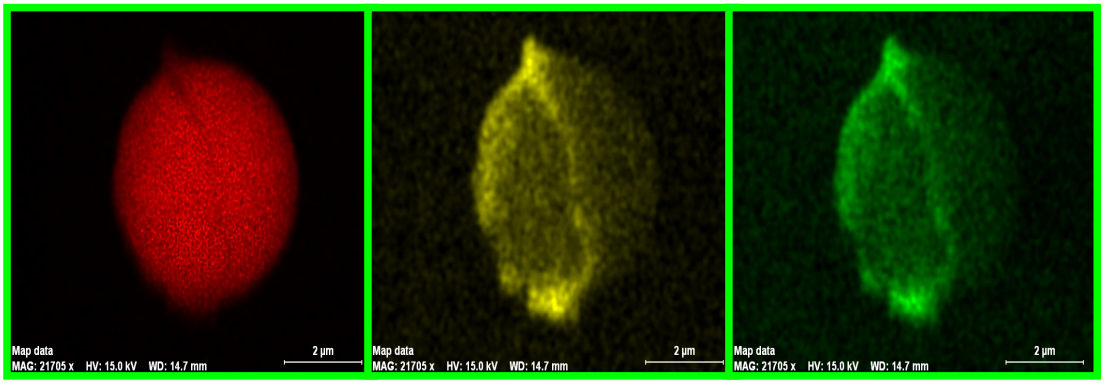

Figure 3.6.2: The thin film of the mesostructured CdS covered mesoporous silica spheres **A)** SEM image and EDS mapping **B)** red color demonstrates silica, **C)** yellow color demonstrates Cd, and **D)** green color demonstrates S. The thin film is synthesized from LC mesophase at $[Cd(H_2O)_4](NO_3)_2$:P85 7:1 mole ratio.

Figure 3.6.3.A gives the EDS line mapping of the surface of a silica microsphere, covered by the thin film of the mesostructured CdS, collected for Cd and S. The intensities of Cd and S lines on the spectra of line mapping confirms the SEM image given below that spectra. Also, Cd and S intensities are close to 1:1 indicating that all Cd ions are reacted with H_2S gas. The SEM image given in Figure 3.6.3.B shows that the film thickness of the mesostructured CdS over the silica spheres is around 80-90 nm.

The silica microspheres can be covered by other MS thin films (M = $Cd_{1-x}Co_x$, $Cd_{1-x}Mn_x$, $Cd_{1-x}Zn_x$) synthesized in this thesis. This may enable the spheres to have a magnetic and optical property. The silica spheres with other size and morphologies can be investigated to cover with these LC mesophases as well.

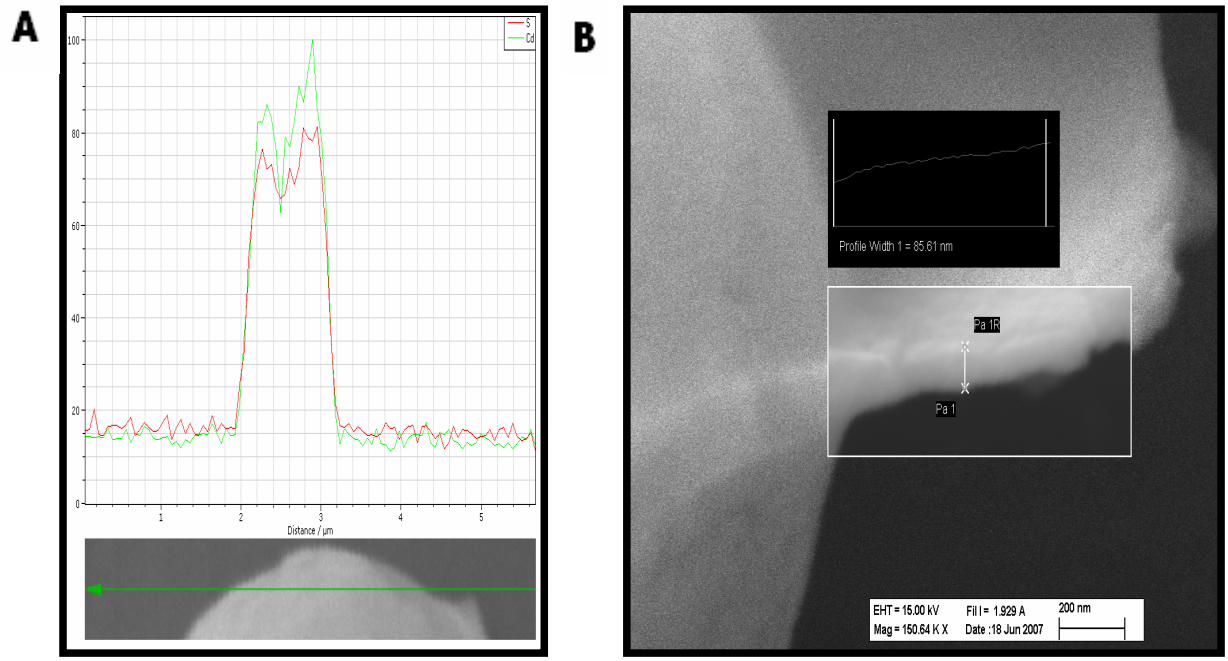

Figure 3.6.3: A) The EDX line mapping, **B)** SEM image of profile width of silica microspheres covered by the thin film of the mesostructured CdS.

4. CONCLUSION

In this thesis, a new synthesis method for the mesostructured metal sulfides (MS) (M = Cd, Zn, $Cd_{1-x}Zn_x$, $Cd_{1-x}Cd_{1-x}$, $Cd_{1-x}Mn_x$) has been developed by using LC mesophases of the salt:P85 systems. The most appropriate conditions to prepare the homogenized solutions were obtained by mixing the TMS, $[M(H_2O)_4](NO_3)_2$, with 1.0 g P85 in 10.0 mL ethanol or acetone through stirring overnight at RT. The mixture of salt:surfactant:solvent has advantage to increase the salt to pluronic mole ratio up to 30:1. However, the LC mesophase is stable and ordered in the salt:P85 mole ratio range of 3:1 to 11:1 with a 3D hexagonal structure in *P6₃/mmc* space group having unit cell parameters of ***a*** = 99.5 Å and ***c*** = 162.5 Å with a ***c/a*** ratio of 1.633.

The CdS thin film samples synthesized by using the LCT approach could somehow retain the mesostructure of the LC mesophase in the mole ratio range of 3:1 to 11:1. The blue shifts of the UV-Vis absorption edges of those CdS thin film samples compared to the bulk CdS absorption edge indicate that the mesostructured CdS is made of nanoparticles. The particle size of the CdS nanocrystals were calculated to be around 4.3 nm by using XRD data, evaluated using Scherrer`s formula and also by using the UV-Vis data, using Sarma`s TB model. The mesostructured CdS films are made of nanoparticles with almost the same size at all mole ratios in the mole ratio range of 3:1 to 11:1 and those nanoparticles are uniformly organized into mesostructured MS, except at mole ratios higher than 13:1. The linear dependence of absorbance versus salt to P85 mole ratio between 3:1 and 11:1 and similar XRD pattern before H_2S reaction indicate that the mesostructures are retained after H_2S reaction. The CdS film samples are photoluminescent under UV light. Under 320 nm wavelength, the films emit weakly orange at mole ratios 1, 3, 5, 11, 13, 20 and strongly orange at mole ratios 7, 9. Under 280 nm wavelength, they emit weakly white at mole ratios; 1, 3, 5, 11, 13,

20 and strongly orange at mole ratios 7 and 9. Therefore, the luminescent behavior of the samples obtained at mole ratios of 7 and 9 must be further investigated.

It has been investigated that it is possible to synthesize the thin films of mesostructured MS by using the LCT approach prepared from the aqua complexes of TMS and the pluronic P85. The formation of cracks over the film samples upon being exposed to H_2S gas and high order XRD pattern of those MS samples are the strong evidences for the formation of the thin films of the mesostructured MS. The thin film samples that form dendritic structures over time undergo phase separation into mesostructured MS and free surfactant molecules. Those dendritic structures form upon agglomeration of the free surfactant molecules in the sample. When the free surfactant molecules are completely separated in time, the large domains of thin films of mesostructured MS form all over the sample. Even though the MS thin film samples are not continuous, they are the first synthesized well ordered mesostructured MS thin films using LCT approach in the literature. The main factors that are effective in the formation of thin film of mesostructured MS might be the existence of the LC mesophase. Use of ethanol or acetone as a solvent, and pluronic P85 as the surfactant allowed to prepare high TMS:P85 mole ratio LC films by spin coating method so that the thin film samples could be prepared in the form of well ordered materials.

The LCT method developed in this thesis was also used to synthesize the solid-solution of nanocrystalline mesostructured $Cd_{1-x}Zn_xS$ by reacting the LC mesophase of $(1-x)[Cd(H_2O)_4](NO_3)_2/x[Zn(H_2O)_6](NO_3)_2$/P85 with H_2S gas. It was shown that this method can be used to fine tune both the composition (between $x = 0.0$ and 1.0) and the optical band-gap of $Cd_{1-x}Zn_xS$ nanocrystallites between 2.60 eV and 4.00 eV. The Zn(II) and Cd(II) ions are homogenously incorporated throughout the structure of the nanocrystallites. The nanocrystallites synthesized by this approach, are slightly larger in every composition compared to the ones synthesized in the channels of mesostructured silica materials.

The LCT method was also used to synthesize the mesostructured $Cd_{1-x}Co_xS$ and $Cd_{1-x}Mn_xS$ by letting the LC mesophase of $(1-x)[Cd(H_2O)_4](NO_3)_2/x[Co(H_2O)_6](NO_3)_2$/P85 and

(1-x)[$Cd(H_2O)_4$](NO_3)$_2$/x[$Mn(H_2O)_4$](NO_3)$_2$/P85 react with H_2S gas, respectively. Both Co(II) and Mn(II) ions could be doped into the CdS lattice up to x = 0.15 for stable $Cd_{1-x}Co_xS$ and $Cd_{1-x}Mn_xS$ samples, respectively. The Co(II) ions occupy the tetrahedral holes in the CdS lattice up to x = 0.15 for stable samples. Further studies are required to elucidate the photoluminescent and magnetic properties of these materials.

5. REFERENCES

[1] Diddams, P. *Inorganic Supports and Catalysts*; Smith, K. Ed.; Ellis Horwood: New York, 1992.

[2] Sarrade, S. J.; Rios, G. M.; Carles, M. *Sep. Purif. Techol.* **1998**, *14*, 19.

[3] Nakanishi, K.; Minakuchi, H.; Soga, N.; Tanaka, N. *J. Sol-Gel Sci. Technol.* **1998**, *13*, 163.

[4] Thomas, J. M.; Catlow, C. R. A.; Sankar, G. *Chem. Commun.* **2002**, *2002*, 2921.

[5] Ferey, G. *Science **2001**, 291*, 994.

[6] Rouquerol, J. *Pure and Appl. Chem*, **1994,** *66*, 1739.

[7] Behrens, P. *Adv. Mater.* **1993**, *5*, 127.

[8] Wilson, S. T.; Lok, B. M.; Messina, C. A.; Cannan, T. R.; Flanigen, E. M. *J. Am. Chem. Soc.* **1982**, *104*, 1146.

[9] Wilson, S. T.; Lok, B. M.; Flanigen, E. M. U.S. Patent 4,320,440; 1982.

[10] Cheetham, A. K.; Ferey, G.; Loiseau, T. *Angew. Chem., Int. Ed.* **1999**, *38*, 3268.

[11] Gavalas, G. R.; Megiris, C. E.; Nam, S. W. *Chem. Eng. Sci.* **1989**, *44*, 1827.

[12] Tsapatsis, M.; Kim, S.; Nam, S. W.; Gabalas, G. *Ind. Eng. Chem. Res.* **1991**, *30*, 2152.

[13] Park, D. H.; Nishiyama, N.; Egashira, Y.; Ueyama, K. *Ind. Eng. Chem. Res.* **2001**, *26*, 6105.

[14] Velev, O. D.; Jede, T. A.; Lobo, R. F.; Lenhoff, A. M. *Nature* **1997**, *389*, 448.

[15] Holland, B. T.; Blanford, C. F.; Stein, A. *Science* **1998**, *281*, 538.

[16] Imhof, A.; Pine, J. *Nature* **1997**, *389*, 948.

[17] Breulmann, M.; Davis, S. A.; Mann, S.; Hentze, H. P.; Antonietti, M. *Adv. Mater.* **2000**, *12,* 502.

[18] Antonelli, D. M. *Microporous and Mesoporous Mater.* **1999**, *33*, 209.

[19] Sepulveda, P.; Binner, G. P. *J. Eur. Ceram. Soc.* **1999**, *19*, 2059.

[20] Davis, S. A.; Burkett, S. L.; Mendelson, N. H.; Mann, S. *Nature* **1997**, *385*, 420.

[21] Li, D. L.; Zhou, H. S.; Honma, I. *Nat. Mater.* **2004**, *3,* 65.

[22] Huang, L. M.; Wang, Z. B.; Sun, J. Y.; Miao, L.; Li, Q. Z.; Yan, Y. S.; Zhao, D. Y. *J. Am. Chem. Soc.* **2000**, *122*, 3530.

[23] Kresge, C.T.; Leonowicz, M.E.; Roth, W.J.; Vartuli, J.C.; Beck, J.S. *Nature* **1992**,*359*,710.

[24] Feng, X.; Fryxell, G.E.; Wang, L.Q.; Kim, A.Y.; Liu, J.; kemner, K.M. *Science* **1997**, *276*,923.

[25] Dag, Ö.; Ozin, G.A.; Yang, H.; Reber, C.;Guillaume, B. *Adv. Ater.* **1999**, *6*,474.

[26] Scott, B.J.; Wirnsberger, G.; Stucky, G.D. *Chem. Mater.* **2001**, *13*, 3140.

[27] Scott, B.J.; Wirnsberger, G.; McGehee, M.D.; Chmelka, B.F.; Stucky, G.D. *Adv. Mater.* **2001**, *13,*1231.

[28] Roggenbuck, J.; Tiemann, M. *J. Am. Chem. Soc.* **2005**, *127*, 1096.

[29] Zhou, X. D.; Conradsson, T.; Klingstedt, M.; Dadachov, M. S.; O`Keeffe, M. *Nature* **2005**, *437*, 716.

[30] Lu, Q.; Gao, F.;Li, Y.; Zhou, Y.; Zhao, D. *Micropor. Mesopor. Mater.* **2002**, *56*, 219.

[31] Baiker, A. *Curr. Opin. Solid State Mater. Sci.* **1998**, *3*, 86.

[32] Attard, G.S.; Glyde, J.C.; Göltner, C. G. *Nature* **1995**,*378*,366.

[33] Yang, H.; Kuperman, A.; Coombs, N.; Mamiche-Afara, S.; Ozin, G.A. *Nature* **1996***,379,*703.

[34] Besson, S.; Gacoin, T.; Ricolleau, C.; Boilot, J.P. *Nano Let.* **2002**, *2*, 409.

[35] Zhang, W.H.; Shi, J.L.; Chen, H.R.; Yan, D.S. *Chem. Mater.* **2001**, *13,* 648.

[36] Tura, C.; Coombs, N.; Dag, Ö. *Chem. Mater.* **2005**, *17,* 573.

[37] Akdogan, Y.; Üzüm, Ç.; Dag, Ö.; Coombs, N. *J. Mater. Chem.* **2006**, *16*, 2048.

[38] Braun, P. V.; Osenar, P.; Stupp, S.I. *Nature* **1996**, *380*, 325.

[39] Eftekharzadeh, S.; Stupp, S.I. *Chem. Mater.* **1997**,*9*, 2059.

[40] Tohver, V.; Braun, P.V.; Pralle, M.U.; stupp, S.I. *Chem. Mater.* **1997**, *9*, 1495.

[41] Braun, P. V.; Osenar, P.; Tohver, V.; Kennedy, S.B.; Stupp, S.I. *J. Am. Chem. Soc.* **1999**, *121,* 7302.

[42] Dag, Ö.; Alayoğlu, S.; Tura, C.; Çelik, Ö. *Chem. Mater.* **2003**, *15*, 2711

[43] Collings, J. *Liquid Crystals*, Princeton University Press, 1990.

[44] Collings, P.J.; Hired, M. *Introduction to Liquid Crystals*, Taylor&Francis, 1997.

[45] Myers, D. *Surfactant Science and Technology,* 2nd ed.; VCH: New York, 1992.

[46] Raman, N.K.; Anderson, M.T.; Brinker, C.F. *Chem. Matter* **1996**, *8*, 1682.

[47] Soler-Illia, G.; Crepaldi, E.; Grosso, D.; Sanchez, C. *Current Opinion in Colloid and Interface Science* **2003**, *8*, 109.

[48] Alivisatos, A.P. *J. Phys. Chem.* **1996**, *100,* 13226.

[49] Nishizawa, M.; Saito, K.; Sorai, M. *J. Phys. Chem. B.* **2001**, *105,* 2987.

[50] Mitchell, D. J.; Tiddy, G. J. T.; Waring, L.; Bostock, T.; McDonald, M. P. *J. Chem. Soc., Faraday Trans. 1* **1983**, *79*, 975.

[51] Pileni, M.; Ninham, B. W.; Tanori, J.; Lisievcki, I.; Filankembo, A. *Adv. Mat.* **1999**, *11,* 1358.

[52] Yang, H.; Kuperman, A.; Coombs, N.; Mamiche-Afara, S.; Ozin, G.A. *Nature* **1996***,379,*703.

[53] Göltner, C.G.; Henke, S.; Weissenberger, M.C., Antonietti, M. *Angew. Chem. Int. Ed.* **1998**, *37*, 613.

[54] Alexandridis, P.; Olsson, U.; Lindman, B. *Langmuir* **1998,** *14*, 2627.

[55] Zhao, D.; Yang, P.; Chmelka, B. F.; Stucky, G. D. *Chem. Mater.* **1998,** *10,* 2033.

[56] Zhao, D.; Yang, P.; Melosh, N.; Feng, J.; Chmelka, B. F.; Stucky, G. D. *Adv. Mater.* **1998,** *10,* 1380

[57] Zhao, D.; Feng, J.; Huo, Q.; Melosh, N.; Chmelka, B. F.; Stucky, G. D. *Science,* **1998,** *279,* 548.

[58] Zhao, D.; Feng, J.; Huo, Q.; Chmelka, B. F.; Stucky, G. D. *J. Am. Chem. Soc.* **1998,** *120,* 6024.

[59] Attard, G. S.; Göltner, C. G.; Corker, J. M.; Henke, S.; Templer, R. H. *Angew. Chem., Intl. Ed. Engl.* **1997**, *36*, 1315.

[60] Attard, G. S.; Bartlett, P. N.; Coleman, N. R. B.; Elliott, J. M.;Owen, J. R.; Wang, J. H. *Science* **1997**, *278*, 838.

[61] Whitehead, A. H.; Elliott, J. M.; Owen, J. R.; Attard, G. S. *J.Chem. Soc., Chem. Commun.* **1999**, 331.

[62] Attard, G. S.; Leclerc, S. A. A.; Maniguet, S.; Russell, A. E.; Nandhakumar, I.; Bartlett, P. N. *Chem. Mater.* **2001**, *13*, 1444.

[63] Yamauchi, Y.; Momma, T.; Yokoshima, T.; Kuroda, K.; Osaka, T. *J. Mater. Chem.* **2005**, *15*, 1987.

[64] Yamauchi, Y.; Yokoshima, T.; Momma, T.; Osaka, T.; Kuroda, K. *J. Mater. Chem.* **2004**, *14*, 2935.

[65] Yang, P.; Zhao, D.; Margolese, D. I.; Chmelka, B. F.; Stucky, G. D. *Nature,***1998** *,396,*152.

[66] Osenar, P.; Braun, P.V.; Stupp, S.I. *Adv. Mater.* **1996**, *8*, 1022

[67] Çelik, Ö.; Dağ, Ö. *Angew. Chem. Int. Ed.* **2001**, *40*,3800.

[68] Dag, Ö.; Samarskaya, O.; Tura, C.; Günay, A.; Çelik, Ö. *Langmuir*, **2003**, *19*, 3671.

[69] Demirörs, A.F.; Eser, B.E.; Dağ, Ö. *Langmuir* **2005**, *21*, 4156.

[70] Albayrak, C.; Gulten, G.; Dag, Ö. *Langmuir* **2007**, *23*, 855.

[71] Schoot, H. *J. Colloid Interface Sci.* **1997**, *192*, 458.

[72] Attard, G. S.; Bartlett, P.N.; Coleman, N. R.B.; Elliot, J. M. *Langmuir* **1998**, *14*, 7340.

[73] Iwanaga, T.; Suzuki, M.; Kuineda, H. *Langmuir* **1998**, *14*, 5775.

[74] Dag, Ö.; Alayoğlu, S.; Uysal, I. *J. Phys. Chem. B.* **2004**, *108*, 8439

[75] Steigerwald, M. L.;Brus, L. E. *Acc. Chem. Res*. **1990**, *23*, 183.

[76] Wang, Y.; Herron, N. *J. Phys. Chem*. **1991,** *95,* 525.

[77] Weller, H. *Adv. Mater*. **1993**, *5,* 88.

[78] Alivisatos, A. P. *Science* **1996**, *271,* 933.

[79] Eychmuller, A. *J. Phys. Chem. B* **2000**, *104***,** 6514.

[80] Bawendi, M. G.;Wilson, W. L.; Rothberg, L.; Carrol, P. J.; Jedju, T. M.;Steigerwald, M. L.; Brus, L. E. *Phys. Rev. Lett*. **1990**, *65*, *1623.*

[81] Bawendi, M. G.; Carroll, P. J.; Wilson, W.; Brus, L. *J. Chem. Phys*. **1992,** *96*, 1335.

[82] Hoheisel, W.; Volvin, V. L.; Johnson, C. S.; Alivisatos, A. P. *J. Chem. Phys*. **1994,** *101***,** 8455.

[83] Murry, C. B.; Kagan, C. R.; Bawendi, *Science* **1995,** *270*, 1335.

[84] Rossetti, R.; Hill, R.; Gibson, J. M.; Brus, L. E. *J. Chem. Phys*. **1995,** *82*, 522.

[85] Weller, H. *Angew. Chem. Int. Ed. Engl.* **1993,** *32*, 41.

[86] Mann, S. *Nature* **1988,** *322***,** 119.

[87] Dabbousi, B. O.; Bawendi, M. G.; Onitsuka, O.; Rubner, M. F. *Appl. Phys. Lett.* **1995,** *66*, 1316.

[88] Greenham, N. C.; Peng, X. G.; Alivisatos, A. G. *Phys. Rev. B* **1996,** *54*, 17628.

[89] Gorer, S.; Ganske, J. A.; Hemminger, J. C.; Penner, R. M. *J. Am. Chem. Soc.* **1998,** *120*, 9584.

[90] Britt, J.; Ferekides, C. *Appl. Phys. Lett*. **1993,** *62*, 2851.

[91] Tsai, C. T.; Chuu, D. S.; Chen, G. L.;Yang, S. L. *J. Appl. Phys*. **1996,** *79***,** 9105.

[92] Taguchi, T.; Endoh, Y.; Nozue, Y. *Appl. Phys. Lett.* **1991***, 56*, 342.

[93] Guha, S.; Wu, B. J.; Cheng, H.; Depuydt, J. M. *Appl. Phys. Lett.***1993**, *63*, 2129.

[94] Bhattacharjee, B.; Mandal, S.K.; Chakrabarti, K.; Ganguli, D.; Chaudhuri, S. *J. Phys.* D:*Appl. Phys.* **2002***, 35,* 2636.

[95] Cizeron, J.; Pileni, M.P. *J. Phys. Chem.* **1995**, *99*, 17410.

[96] Ohno, H.; Chiba, D.; Matsukura, F.; Omiya, T.; Abe, E.; Dietl, T.; Ohno, Y.; Ohtani, K. *Nature* **2000***, 408,* 944.

[97] Fiederling, R.; Keim, M.; Reuscher, G.; Ossau, W.; Schmidt, G.; Waag, A.; Molenkamp, L. W. *Nature* **1999,** *402,* 787.

[98] Wolf, S. A.; Awschalom, D. D.; Buhrman, R. A.; Daughton, J. M.; von Molnar, S.; Roukes, M. L.; Chtchelkanova, A. Y.; Treger, D. M. *Science* **2001,** *294,* 1488.

[99] Jun, Y.; Jung, Y.; Cheon, J. *J. Am. Chem. Soc.* **2002**, *124*, 615.

[100] Yang, H.; Holloway, P. H.; Santra, S. *J. Chem. Phys.* **2004**, *121*, 7421.

[101] Brieler, F. J.; Grundmann, P.; Fröba, M.; Chen, L.; Klar, P. J.; Heimbrodt, W.; von Nidda, H.-A.K.; Kurz, T.; Loidl, A. *Chem. Mater.* **2005**, *17*, 795.

[102] Kouzema, A. V.; Fröba, M.; Chen, L.; Klar, P. J.; Heimbrodt, W. *Adv. Func. Mater.* **2005**, *15*, 168.

[103] Norberg, N. S.; Dalpian, G. M.; Chelikowsky, J.R.; Gamelin, D.R. *Nano Lett.* **2006,** *0,* A.

[104] Norberg, N. S.; Parks, G. L. Salley, G. M.; Gamelin, D. R. *J. Am. Chem. Soc.* **2006**, *128,* 13195.

[105] Furdyna, J. K. *J. Appl. Phys.* **1988**, *64*, R29.

[106] Sakya, P.; Seddon, J.M.; Templer, R.H.; Mirkin, R.J.; Tiddy, G.J.T. *Langmuir* **1997**,*13*,3706

[107] Lee, M. ; Cho, M. K. *Chem. Mater.* **1998**, *10*, 1894

[108] Ohtake, T. ; Ogasawara, M. ; Ito – Akita, K.; Nishina, N. ; Ujiie, S. ; Ohno, H. ; Kato, T. *Chem. Mater.* **2000**, *12*, 782

[109] Kittel, C., *Introduction to Solid State Physics* **1996**, John Wiley & Sons:New York.

[110] Brus , L. E. *J. Chem. Phys.* **1983**, *79*, 5566.

[111] Sapra, S.; Sarma, D. D. *Phys. Rev. B* **2004,** *69*, 125304.

[112] Sapra , S.; Shanthi , N.; Sarma , D. D. *Phys. Rev. B* **2002,** *66*, 205202.

[113] Qi, L.; Ma, J.; Cheng, H.; Zhao, Z. *Chem.Mater.* **1998**, *10*, 1623.

[114] Lee, M. H.; Oh, S-G.; Moon, S-K.; Bae, S. Y. *J.Colloid Interface Sci.* **2001**, *83*, 240.

[115] Stevens,W.J.J.; Lebeau,K.; Mertens,M.; Tendeloo,G.V.; Cool, P.; Vansant,E.F. *J.Phys.Chem.B* **2006**, *110*, 9183.

[116] Ocana, M.; Rodriguez-Clemente, R.; Serena, C. J. *Adv. Mater.* **1995**, **7**, 212.

[117] Zhao, D.; Feng, J.; Huo, Q.; Melosh, N.; Frederickson, G. H.; Chemelka, B.F.; Stucky,G.D. *Science* **1998**, *279*, 548.